ANTIOXIDANTS & REDOX SIGNALING
Volume 21, Number 10, 2014

DOI: 10.1089/ars.2013.5378

COMPREHENSIVE INVITED REVIEW

The Clinical Importance of Assessing Tumor Hypoxia: Relationship of Tumor Hypoxia to Prognosis and Therapeutic Opportunities

Joseph C. Walsh,[1] Artem Lebedev,[1] Edward Aten,[2] Kathleen Madsen,[3] Liane Marciano,[2] and Hartmuth C. Kolb[1]

Abstract

Tumor hypoxia is a well-established biological phenomenon that affects the curability of solid tumors, regardless of treatment modality. Especially for head and neck cancer patients, tumor hypoxia is linked to poor patient outcomes. Given the biological problems associated with tumor hypoxia, the goal for clinicians has been to identify moderately to severely hypoxic tumors for differential treatment strategies. The ''gold standard'' for detecting and characterizing of tumor hypoxia are the invasive polarographic electrodes. Several less invasive hypoxia assessment techniques have also shown promise for hypoxia assessment. The widespread incorporation of hypoxia information in clinical tumor assessment is severely impeded by several factors, including regulatory hurdles and unclear correlation with potential treatment decisions. There is now an acute need for approved diagnostic technologies for determining the hypoxia status of cancer lesions, as it would enable clinical development of personalized, hypoxia-based therapies, which will ultimately improve outcomes. A number of different techniques for assessing tumor hypoxia have evolved to replace polarographic pO_2 measurements for assessing tumor hypoxia. Several of these modalities, either individually or in combination with other imaging techniques, provide functional and physiological information of tumor hypoxia that can significantly improve the course of treatment. The assessment of tumor hypoxia will be valuable to radiation oncologists, surgeons, and biotechnology and pharmaceutical companies who are engaged in developing hypoxia-based therapies or treatment strategies. *Antioxid. Redox Signal.* 21, 1516–1554.

I. Introduction 1517
II. The Clinical Importance of Tumor Hypoxia 1517
A. Pathophysiology of hypoxia 1517
B. Hypoxia's negative impact on the effectiveness of curative treatment 1519
1. Hypoxic tumors accumulate and propagate cancer stem cells 1519
2. Hypoxia reduces the effectiveness of radiotherapy 1519
3. Hypoxia increases metastasis risk and reduces the effectiveness of surgery 1520
4. Hypoxic tumors are resistant to the effects of chemotherapy and chemoradiation 1521
C. Hypoxia is prognostic for poor patient outcomes 1521
III. Diagnosis of Tumor Hypoxia 1521
A. Direct methods 1523
1. Oxygen electrode—direct pO_2 measurement most used in cancer research 1523
2. Phosphorescence quenching—alternative direct pO_2 measurement 1524
3. Electron paramagnetic resonance 1524
4. ^{19}F-magnetic resonance spectroscopy 1525
5. Overhauser-enhanced MRI 1526

Reviewing Editors: *Claudine Kieda, Periannan Kuppusamy, Ken-Ichiro Matsumoto, Suzanne Monte, Des Richardson, Matteo A. Russo, Gregg Semenza, Chandan K. Sen, Jolanta Tarasuik, Michel Toledano, Laura Vera-Ramirez*

[1]Siemens Molecular Imaging, Inc., Culver City, California.
[2]Certus International, Inc., Bedford, New Hampshire.
[3]Certus International, Inc., Chesterfield, Missouri.

B. Endogenous markers of hypoxia 1526
1. Hypoxia-inducible factor-1α 1526
2. Carbonic anhydrase IX 1526
3. Glucose transporter 1 1527
4. Osteopontin 1527
5. A combined IHC panel of protein markers for hypoxia 1527
6. Comet assay 1527
C. Physiologic methods 1527
1. Near-infrared spectroscopy/tomography—widely used for pulse oximetry 1527
2. Photoacoustic tomography 1527
3. Contrast-enhanced color duplex sonography 1528
4. MRI-based measurements 1528
5. Blood oxygen level-dependent MRI 1528
6. Pimonidazole 1529
7. EF5 (pentafluorinated etanidazole) 1529
8. Hypoxia PET imaging—physiologic hypoxia measurement providing tomographic information 1529
a. ^{18}F-fluoromisonidazole 1530
b. ^{18}F-fluoroazomycinarabinofuranoside 1531
c. ^{18}F-EF5 (pentafluorinated etanidazole) 1532
d. ^{18}F-flortanidazole 1532
e. Copper (II) (diacetyl-bis (N4-methylthiosemicarbazone)) 1532
f. ^{18}F-FDG imaging of hypoxia 1533
IV. Modifying Hypoxia to Improve Therapeutic Outcomes 1533
A. Use of hypoxia information in radiation therapy planning 1534
B. Use of hypoxia assessment for selection of patients responsive to nimorazole 1534
C. Use of hypoxia assessment for selection of patients responsive to tirapazamine 1539
D. Use of hypoxia assessment for selection of patients responsive to oxygen delivery therapies 1539
V. Concluding Remarks 1541

I. Introduction

Tissue hypoxia is a biological condition that is characterized by deficient tissue oxygenation compromising normal biological function. The aberrant growth of tumors exacerbates their susceptibility to hypoxia, especially for malignant solid tumors. The resultant compensatory mechanisms utilized by tumors in response to hypoxia negatively influence the delivery of curative treatment, regardless of the treatment modality employed. Especially for head and neck cancer (H&NC) patients, tumor hypoxia is linked to poor overall survival (OS), disease-free survival (DFS), and locoregional control (LRC). Given the biological problems associated with tumor hypoxia, the goal for clinicians has been to identify moderately to severely hypoxic tumors for differential treatment strategies. The ''gold standard'' for the detection and characterization of tumor hypoxia are invasive polarographic electrodes. However, their clinical use is severely impeded by several factors, and newer methods for accurately assessing tumor hypoxia are needed for both hypoxia diagnosis and therapy development. Several modalities exist for assessing tumor hypoxia by utilizing various mechanisms, yet no single modality is approved for assessing tumor hypoxia in routine clinical practice.

The detection and assessment of tumor hypoxia now plays a critical role in both the validation and development of hypoxia modification therapies for their eventual adoption into routine clinical practice. Recent clinical trial data appear to demonstrate how patients identified by their hypoxic tumor status have beneficial treatment responses to hypoxia-modified therapies compared with standard therapies, while high-risk patients with hypoxic tumors receiving the control therapies performed poorly. However, despite current research into hypoxia-modification therapies, measurement of tumor hypoxia within lesions is not performed routinely and, consequently, has hindered the development of these therapies. Therefore, there is an acute need to identify tumor hypoxia, to enable appropriate patient classification, and to determine the extent of hypoxia within each lesion, enabling clinicians to make decisions regarding the therapy management for the patient. The hypoxia assessment may aid not only radiation oncologists and surgeons, but also biotechnology and pharmaceutical companies in developing tumor hypoxia therapies or other new treatment strategies for hypoxic tumors.

II. The Clinical Importance of Tumor Hypoxia

A. Pathophysiology of hypoxia

Hypoxia is a pathophysiological property that is defined as a state of depressed oxygen tension. Hypoxia can be present in tissues, including tumors, causing the impairment of cellular or organ functions once critical oxygen levels are breached. Localized tissue hypoxia, as it relates to tumors, can be the result of two general types of oxygen starvation. Hypoxia can be perfusion limited (''acute hypoxia''), caused by a temporary reduction in blood supply. Alternatively, hypoxia can be diffusion limited (''chronic hypoxia''), caused by insufficient vascularization impairing the metabolic needs of the growing tumor. The presence of hypoxia in cancerous tissue was first reported by Thomlinson and Gray,

who observed that hypoxic, yet viable, lung carcinoma rods were surrounded by a necrotic core caused by a tissue oxygen gradient (263). All types of solid tumors, especially malignant solid tumors, are subject to hypoxia, often exhibiting oxygenation levels measurably lower than their tissue of origin (Table 1) (7, 27, 124). Recurring tumors often exhibit a higher hypoxic fraction than primary tumors (258, 280). A tumor's hypoxic status cannot be accurately determined anatomically, as the presence of tumor hypoxia is independent of a tumor's size, stage, grade, or histology. Intratumoral oxygenation often disperses heterogeneously, and, therefore, an accurate characterization of tumor hypoxia is possible only from composite measurements.

The physiology and biochemistry of hypoxic tumors adapts to oxygen starvation to preserve both tumor growth and propagation. For example, in depressed oxygen environments, hypoxic cells readily revert from aerobic respiration to anaerobic glycolysis, which increases both glucose consumption and the production of pyruvate. These cells can continue to function using this metabolic pathway even in the presence of oxygen (the Warburg effect) (247). This survival mechanism is common among hypoxic tumors, resulting in a twofold increase in glucose uptake (determined *in vitro*) (29), elevated tissue acidity (44), and an evolutionary selection for a progressively more malignant phenotype (102, 122).

The proteomic and genomic transformations of tumor cells in response to hypoxia lead to permanent alterations in their cellular composition that is regulated predominantly by hypoxia-inducible factors (HIFs). HIFs are a family of heterodimeric transcription factors that are critically up-regulated in response to hypoxia. HIF-1α is a member of this family and it plays an integrative role in the cellular response to hypoxia (245, 274). HIF-1α contains two transactivation domains known as the N-terminal activation domain (N-TAD) and the C-terminal activation domain (C-TAD). C-TAD regulates HIF-1α transcriptional activation under hypoxia, while N-TAD modulates stability of HIF-1α. Under normoxic conditions, amino-acid-specific hydroxylations deactivate HIF-1α activity. Prolyl hydroxylase domain protein (PHD) hydroxylates proline residues on HIF-1α in an oxygen-dependent fashion, enabling von Hippel-Lindau (VHL) tumor suppressor protein to bind HIF-1α for subsequent ubiquitylation and targeted degradation by 26S proteasome (Fig. 1). HIF-1α can also undergo hydroxylation by factor inhibiting HIF1 (FIH-1), which inhibits the recruitment of HIF-1α coactivators and the expression of downstream HIF-1α target genes. However, when intracellular levels of oxygen decrease, the rate of HIF-1α hydroxylation by PHD and FIH-1 also decreases. Consequently, VHL fails to bind to HIF-1α, leading to an accumulation of HIF-1α in the cell. This enables HIF-1α to interact with CREB-binding protein/E1A-binding protein p300 (CBP/p300), a transcriptional co-factor, followed by heterodimerization with HIF-1β. The heterodimer readily binds to the HIF-responsive element (HRE) of DNA, leading to the transcriptional activation and up-regulation of multiple HIF-1α target genes. Other factors affecting HIF-1α activation will be discussed in a subsequent section.

Through the onset of hypoxia, HIF-1α initiates multiple hypoxia-derived molecular processes that drive tumor growth, proliferation, and metastatic potential. Growth and survival mechanisms such as angiogenesis *via* vascular endothelial growth factor (VEGF), pH regulation *via* involving

TABLE 1. TYPICAL OXYGEN TENSIONS IN TUMORS AND THE RESPECTIVE HEALTHY TISSUES

Cancer type	*Median tumor pO_2, mmHg (# of patients) (277)*	*Median pO_2 of tissue of origin, mmHg*	*Fraction of hypoxic tumors among all tumors of this type (hypoxia threshold)*	*Clinical outcomes for hypoxic vs. normoxic tumors*
Head and neck	10 ($n=592$)	40–51	70% (median $pO_2<10$ mm) (21) 51% ($HP_5>25\%$) (162)	Decreased 3 year survival rate (28% *vs.* 38%, $2P=0.006$) (201)
Lung	16 ($n=26$)	39	38% ($HP_{2.5}>20\%$) (108)	Decreased 2-year OS rate (17% *vs.* 79%, $P=0.02$) (160)
Breast	10 ($n=212$)	65 (279)	63% ($pO_2\leq 2.5$ mm Hg) (278)	Not determined
Pancreatic	2 ($n=7$)	52	100% ($HP_{2.5}>20\%$) (152)	Not determined
Cervix	9 ($n=730$)	51	48% (median $pO_2<10$ mm) (120)	Decreased 6 year OS rate (29% *vs.* 87%, $P=0.0004$) (181)
Prostate	7 ($n=190$)	20,31 (198)	19% (270) $\frac{pO_2(prostate)}{pO_2(muscle)}\leq 0.1$	Decreased 8 year freedom from biochemical failure (46% *vs.* 78% $P=0.027$) (270)
Soft tissue sarcoma	14 ($n=283$)	—	45% ($HP_{2.5}>20\%$) (14)	Decreased 18 month DFS rates (35% *vs.* 70%, $P=0.01$) (23)
Brain tumors	13 ($n=104$)	54 (139)	64% ($HP_{2.5}>20\%$) (51) 38% ($pO_2<10$ mm) (139)	Decreased 3 year OS (25% *vs.* 53%, $P=0.13$) (157)

HP_x—the percent frequency of pO_2 measurements below a given mmHg value, see Figure 3 for further explanation.
DFS, disease-free survival; HIF, hypoxia-inducible factor; OS, overall survival.

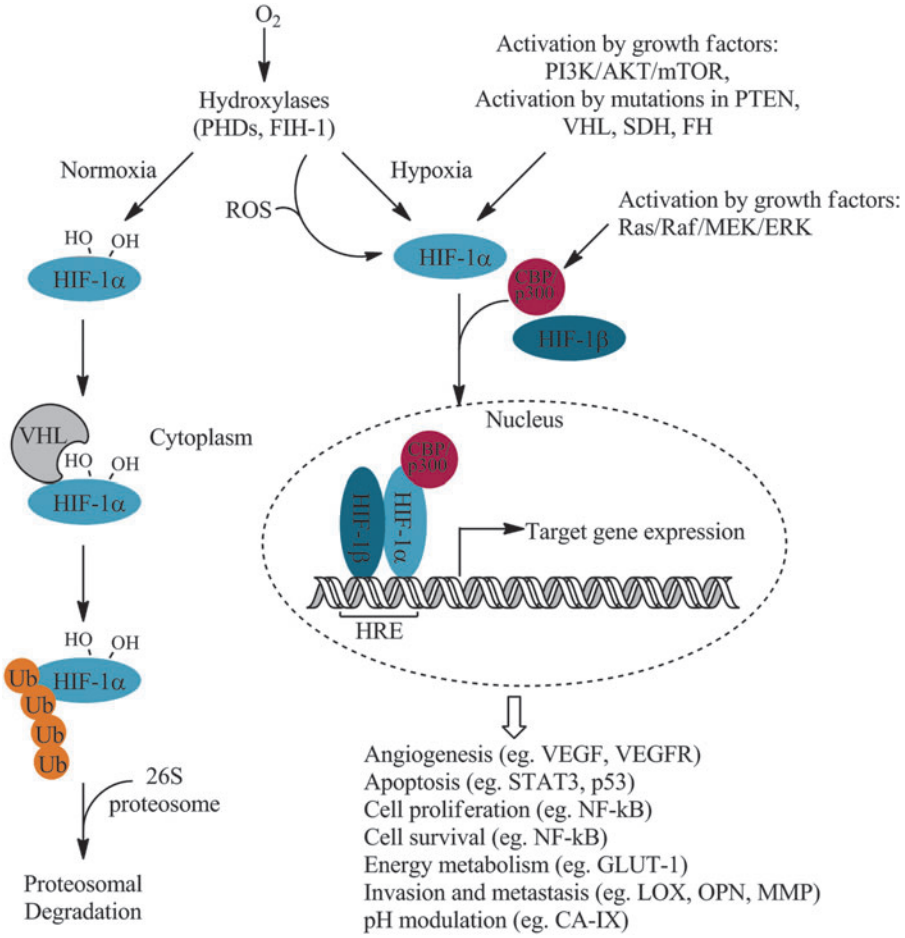

FIG. 1. Regulation of HIF-1α and protein signaling under normoxic and hypoxic conditions. Adapted from Xia *et al.* (294) and Collet *et al.* (50). AKT, protein kinase B; CBP/p300, CREB-binding protein/E1A binding protein p300; ERK, extracellular signal-regulated kinase; FH, fumarate hydratase; FIH-1, factor inhibiting HIF1; GLUT-1, glucose transporter 1; HIF-1α, hypoxia-inducible factor 1α; HIF-1β, hypoxia-inducible factor-1β; HRE, HIF-responsive element; LOX, lysyl oxidase; MEK, MAPK/ERK kinase; MMP, matrix metalloproteinase; mTOR, mammalian target of rapamycin; NF-kB, nuclear factor kappa-light-chain-enhancer of activated B cells; OPN, osteopontin; p53, tumor protein 53; PHD, prolyl hydroxylase domain containing protein; PI3K, phosphoinositide 3 kinase; PTEN, phosphatase and tensin homolog; Raf, serine/threonin-specific protein kinase; RAS, rat sarcoma; ROS, reactive oxygen species; SDH, succinate dehydrogenase; STAT3, signal transducer and activator of transcription 3; VEGF, vascular endothelial growth factor; VEGFR, vascular endothelial growth factor receptor; VHL, von Hippel-Lindau tumor suppressor; Ub, ubiquitylation.

carbonic anhydrase IX (CA-IX), metabolism *via* glucose transporter 1 (GLUT-1), and oxygen management are up-regulated in response to hypoxia (130). Transcription factors that control cell proliferation, cell survival *via* nuclear factor kappa-light-chain-enhancer of activated B cells (NF-kB), and apoptosis *via* signal transducer and activator of transcription 3 (STAT3, p53) are also up-regulated in hypoxic tumor cells. The up-regulation of these proteins directly influences the malignancy of hypoxic tumors (102, 275, 276), including a propensity for the development of metastatic disease (23, 255, 297) by propagating cells that have lost their apoptotic potential through decreased p53 expression, increased mutant p53 or bcl-2 protein expression (105, 155), increased angiogenesis (254), and overall increases in proteinase activity (31, 106). Over-expression of several of the protein markers mentioned earlier and linked to hypoxia, each one alone or in conjunction with other markers, has been found to be prognostic for 10-year OS and cancer-specific survival in head and neck patients (161).

B. Hypoxia's negative impact on the effectiveness of curative treatment

1. Hypoxic tumors accumulate and propagate cancer stem cells. Tumor-initiating cells, also known as cancer stem cells (CSC), have phenotypic characteristics that include differentiation, self-renewal, apoptotic resistance, pluripotency, and sufficient motility to initiate new tumor growth at distant sites. Unsurprisingly, the presence of CSC in tumors correlates strongly with both treatment failure and tumor recurrence, despite being a smaller subset of the overall tumor cell population (58). Hypoxic regions within solid tumors harbor CSC in an area known as the hypoxic niche (173), which enriches the CSC population through accumulation and selective propagation. In breast tumors, CSC populations increase within hypoxic zones that are modulated by protein kinase B (Akt)/β-catenin signaling, a pathway which is reported to enable self-renewal of breast CSC (52). Tumor hypoxia reprograms cell dedifferentiation in ductal breast carcinomas that are characterized by a down-regulation of estrogen receptor-α and an increase in the epithelial breast stem cell marker cytokeratin 19, creating a more aggressive, stem cell-like phenotype (118).

2. Hypoxia reduces the effectiveness of radiotherapy. Evidence that depressed oxygen levels compromise the effects of radiation was established more than 75 years ago. Mottram and co-workers observed that poorly oxygenated normal and malignant tissues were resistant to the effects of both X- and γ-irradiation because of a lack of long-lived reactive oxygen radicals (197). Thomlinson and Gray demonstrated that hypoxic tumor cells were thrice more resistant to radiation than well-oxygenated ones, thus forming the basis of understanding that hypoxia impairs the effectiveness

of radiotherapy (109, 122). In addition to the physical aspects of radio-resistance imparted by hypoxia, the acquired genetic traits of hypoxic tumor cells during their malignant progression also actively contribute to mechanisms of radioresistance. Hypoxic cells with decreased apoptotic potential and deregulated cell cycle arrest mechanisms still undergo cellular proliferation despite damaged DNA. In addition, the expression of proteins downstream from HIF1-α, such as VEGF and basic fibroblast growth factor (bFGF), were also found to confer radioresistant effects (193, 245). CSC are reported to have reduced amounts of endogenous reactive oxygen species (ROS) relative to both tumorogenic and nontumorogenic cells of the same type, which may prolonged survival of CSC, especially during treatment cycles (66). In addition, mitochondrial dysfunction in a subset of head and neck squamous cell carcinoma CSC is associated with a decrease in levels of endogenous ROS within the cell (98). In the clinical setting, both head and neck and prostate cancer patients with hypoxic tumors undergoing radiotherapy have been reported to be at elevated risk for poor LRC, OS, and biochemical failure (21, 270).

3. Hypoxia increases metastasis risk and reduces the effectiveness of surgery. Hypoxia has been linked to the formation of metastatic disease and, thus, provides important prognostic information (255). The downstream expression of hypoxia proteins initiates and supports metastatic spread *via* tumor cell motility and invasion, intravasation, extravasation, and metastatic colonization (Fig. 2) (179). Hypoxia-mediated activation of snail family zinc finger 1 (SNAIL1) and class A basic helix-loop-helix protein 38 (TWIST) induces epithelial to mesenchymal transition in tumor cells enhancing cell motility by diminishing cell–cell adhesion properties and inducing a loss of cell polarity. Cellular motility is further supported by the expression of lysyl oxidase (LOX), an extracellular matrix remodeling enzyme. Both matrix metalloproteinase (MMP) and cathepsin D compromise the basement membrane, facilitating tumor invasion. Subsequent pericyte detachment from the basement membrane exacerbates vascular structure and function. The overexpression of VEGF leads to leaky vasculature and high vessel permeability, facilitating both intravasation and extravasation of circulating tumor cells and even CSC. Lastly, secreted chemokines facilitate the localization of tumor cells, leading to the formation of metastatic colonies (133).

The effects of hypoxic-mediated metastasis have also been reported in the clinic. In a study of H&NC patients undergoing planned neck dissection after primary radiotherapy treatment, pathology analysis of the neck dissection specimens confirmed the presence of viable tumor from patients having hypoxic lesions, yet no residual disease was found in patients with normoxic lesions (21). In addition, clinical reports have cited an increased propensity for distant metastases in patients with hypoxic soft tissue sarcomas (STS) and cervix cancer undergoing surgery (23, 121). Patients with hypoxic prostate tumors treated by radical prostatectomy were at high risk for biochemical failure over a period of 8 years independent of pathological tumor stage, Gleason

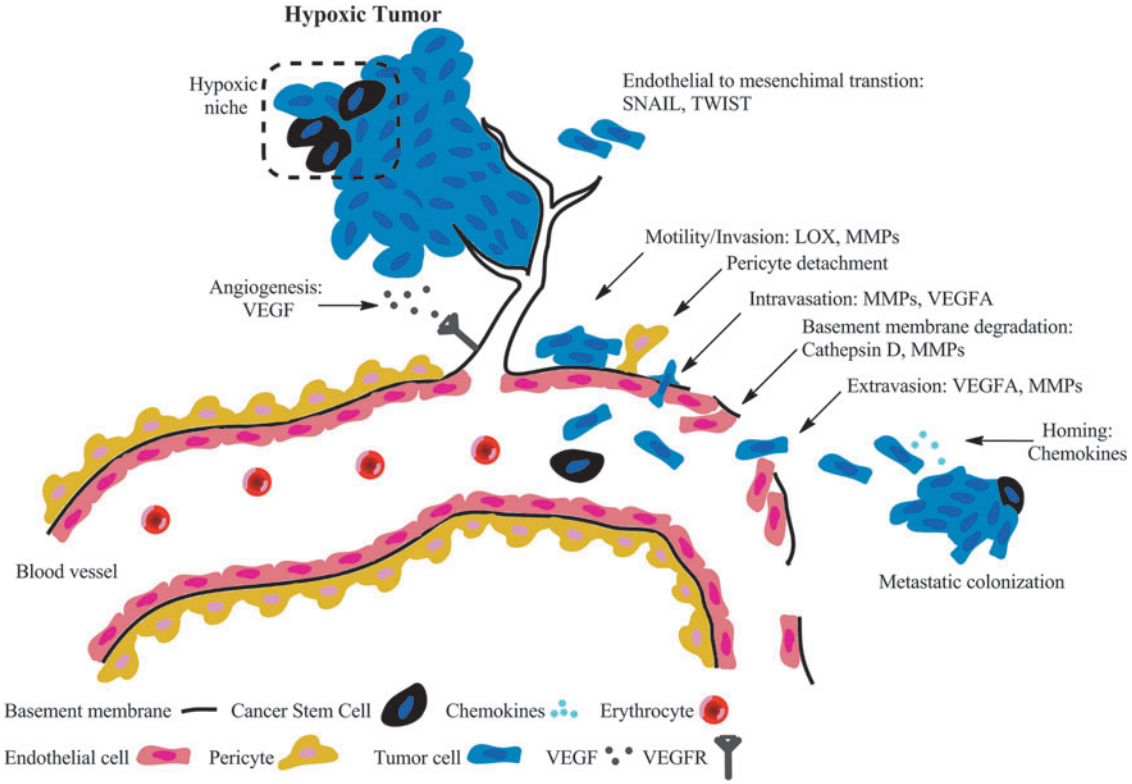

FIG. 2. The downstream expression of hypoxia proteins supporting the various stages of metastatic spread. VEGFA, vascular endothelial growth factor A; SNAIL, snail family zinc finger 1; TWIST, class A basic helix-loop-helix protein 38.

score, serum prostate-specific antigen (PSA) concentration, and margin status (281).

4. Hypoxic tumors are resistant to the effects of chemotherapy and chemoradiation. Tumor hypoxia exacerbates chemotherapy resistance through both physiological and genomic mechanisms (257, 260). From a physiological perspective, hypoxia potentiates the growth abnormal vascular networks that support cancer progression. Deregulated vasculature consists of vessels with pathologic size, inconsistent dilation, tortuousness networks, and hyper-permeability. In these conditions, the delivery of agents that are beneficial for cancer treatment is both irregular and inefficient, increasing the immune tolerance of cancer. Hypoxic tumors continually up-regulate angiogenic factors, such as VEGF, to meet metabolic demands; however, this neovascularization fails to support adequate blood supply that further worsens local hypoxia, ensuring a vicious cycle. Prolonged treatment of anti-angiogenic therapies has been known to exacerbate hypoxia, resulting in subsequent treatment failures (32, 101).

On the genomic level, reduced proliferation rates, up-regulation of multidrug resistance, and increased cellular acidification can diminish drug toxicity (44). Consequently, angiogenic factors are up-regulated, furthering the cycle of hypoxia. Hypoxic cells are known to be more resistant toward fluorouracil (251), doxorubicin (92), bleomycin (233), and platinum-based drugs (261) than normoxic cells. Combined therapeutic modalities have also demonstrated a diminished performance in hypoxic tumors (229, 287). Despite the overall improvement in locoregional control (LRC) and OS, treatment strategies, including concurrent chemoradiotherapy, have had higher failure rates with hypoxic tumors than normoxic ones (214). Patients with hypoxic tumors undergoing chemoradiation therapy often exhibit both poor treatment response (22) and survival rates (201). Hypoxia compensation is, therefore, a critical aspect in treating cancer.

C. Hypoxia is prognostic for poor patient outcomes

Multiple clinical studies have concluded that hypoxia is associated with poor prognosis across multiple tumor types as evidenced by adverse outcomes, including poor OS, DFS, and LRC (Table 1). While there are likely multiple factors influencing a patient's poor outcome and response to therapy, tumor hypoxia is established as one of the strongest prognostic indicators, especially for patients with H&NC. Key clinical studies are highlighted next.

In a study reported by Rudat *et al.* (Table 2- Study F), for patients with Stage IV H&NC treated with radiation with or without chemotherapy, the hypoxic fraction ($HP_{2.5}$) was shown to have a predictive value for OS, with the hypoxic subgroup having lower probability of survival ($P = 0.05$). A subsequent analysis by Rudat *et al.* (236), using pooled data from very advanced H&NC patients with inoperable tumors, also found that tumor oxygenation above the median ($HP_{2.5} < 9\%$) was associated with longer survival, confirming the influence of tumor oxygenation on the prognosis of patients with H&NC. The authors also concluded that the sensitivity for predicting patient survival status using a $\leq 10\%$ threshold for $HP_{2.5}$ was 75% (1 year survival) and 65% (2-year survival); the corresponding specificity was 41% (1 year survival) and 27% (2 year survival). While the negative predictive value (NPV) was low (25%), the positive predictive value (PPV) was high (81% for 2 years), which is desirable for selecting patients for treatment alternatives. A separate study determined that the NPV of pO_2 in predicting pathological clinical response in normoxic patients was 80%, and the PPV to predict persistent disease in hypoxic tumors was 62% (Fig. 3) (22).

Nordsmark *et al.* (201) reported the results of a joint analysis of the data from all of the studies in Table 3, except Study A and Study H, as well as some previously unpublished data. Based on the pooled tumor hypoxia data, Nordsmark concluded that pretreatment tumor hypoxia defined by $HP_{2.5}$ was a significant prognostic factor for survival after treatment with radiation alone or in combination with surgery, chemotherapy, or a radiation sensitizer (201). Based on the univariate analysis, the relationship between 3 year survival and tumor hypoxia ($HP_{2.5}$) was found to be significant. In multivariate models, only pretherapy $HP_{2.5}$ was prognostic for 3 year OS ($P = 0.006$) using a hypoxia threshold of $HP_{2.5} > 19\%$. Nordsmark also concluded that a change in $HP_{2.5}$ from 30% to 40% in two otherwise identical tumors increased the relative risk of death by 13%. The authors concluded that the international, multi-center study firmly established the prognostic significance of hypoxia in H&NC patients after radiotherapy. In conclusion, while there are likely multiple factors influencing a patient's response to therapy, tumor hypoxia has been established as one of the strongest prognostic indicators, and, thus, pretreatment measurements of tumor oxygenation will be useful in the search for therapeutic strategies for overcoming hypoxia in H&NC.

III. Diagnosis of Tumor Hypoxia

Given the numerous treatment complications related to hypoxia, researchers have investigated various ways to assess hypoxia within tumors. Interestingly, the emerging field of hypoxia modification therapies has been largely ongoing without a convenient means for assessing tumor hypoxia, severely restricting the ability to stratify patients based on their tumor's hypoxia status. To continue the development of hypoxia modification therapies, there should be an accurate, composite, and noninvasive means for tumor hypoxia assessment that enables both appropriate patient selection and, ultimately, a change in therapy management.

Methods for assessing tumor hypoxia can be separated into three major groups: methods directly related to assessing the oxygen concentration, methods reporting on the physiologic processes involving oxygen molecules, and methods evaluating the expression of endogenous markers as a response to hypoxia (Fig. 4). Table 4 summarizes the existing methods used to evaluate tissue hypoxia status.

Direct methods for detecting tissue hypoxia rely on the explicit interaction of oxygen with a selective sensor providing oxygen concentration data within the vicinity of the probe. Physiologic methods report on processes also directly involving oxygen molecules. While these methods do not directly measure oxygen concentrations in tissues, their response is proportional to the concentration of oxygen. Endogenous markers of hypoxia comprise proteins that are overexpressed in response to diminished oxygen supply.

Table 2. Studies Investigating the Prognostic Value of Tumor Oxygenation in Head and Neck Cancer

Study ID	N	*pO_2 (mmHg) median [Range]*	*Tx*	*Follow-up (months) median [range]*	*Findings*	P-*value*
(A) Gatenby *et al.* (100)	31	NA [0–30] (Mean = 13.6)	R	3 [Not available]	Mean pO_2 was 20.6 ± 4.4 mmHg in the complete responders group and 4.7 ± 3.0 mmHg in the nonresponders group. (Tumor volume 90 days after therapy)	< 0.001
(B) Nordsmark *et al.* (206)	35	14 [1–35]	R	17 [11–46]	2-year LRC 33% ↔ $HP_{2.5}$ > 15% 2-year LRC 77% ↔ $HP_{2.5}$ < 15%	0.01
(C) Nordsmark and Overgaard (204)	31	12 [0–54]	R	28 [12–47]	2-year LRC 45% ↔ $HP_{2.5}$ > 15% 2-year LRC 90% ↔ $HP_{2.5}$ < 15%	0.04
(D) Brizel *et al.* (21)	63	5 [0–60]	R or R + C w/wo S	20 [3–50]	2-year LRC 73% ↔ median pO_2 > 10 mmHg 2-year LRC 30% ↔ median pO_2 < 10 mmHg 2-year DFS 73% ↔ median pO_2 > 10 mmHg 2-year DFS 26% ↔ median pO_2 < 10 mmHg 2-year OS 83% ↔ median pO_2 > 10 mmHg 2-year OS 35% ↔ median pO_2 < 10 mmHg	0.01 0.005 0.02
(E) Stadler *et al.* (251)	59	13 [0–59]	R or R + C	8 [< 6–42]	Patients with HSV > 6 ml have 2.5-shorter survival time than patients with HSV below this threshold.	0.01
(F) Rudat *et al.* (237)	41	10 [0–62] (based on 60 pts)	R or R + C	12 [2–37]	$HP_{2.5}$ 2.1 HR in univariate analysis HP_5 1.2 HR Median pO_2 0.8 HR	0.05 0.68 0.61
(G) Adam *et al.* (1) and Terris (262)	25	20 [0–51]	R or R + C w/wo S	16 [1–81]	No statistically significant correlation between $HP_{2.5}$; HP_5; HP_{10}; Median pO_2 and OS	
(H) Dietz *et al.* (67)	37	3 [NA]	R or R + C	Not available	3-year OS 14% ↔ median ΔpO_2 > 0.8 mmHg 3-year OS 26% ↔ median ΔpO_2 < 0.8 mmHg	0.036

DFS, disease free survival; HR, hazard ratio; HSV, hypoxia subvolume; LRC, locoregional control; R, radiation; R + C, radiation plus chemotherapy; w/wo S, with or without surgery.

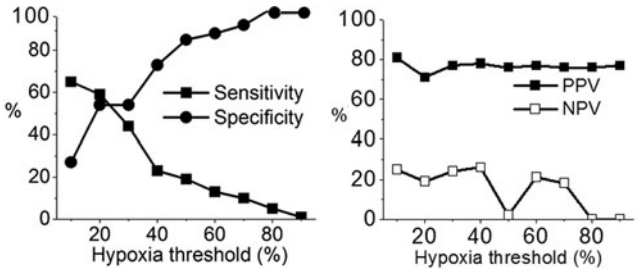

FIG. 3. Predictive power of Eppendorf Histograph for 1 year survival after beginning of the radiotherapy (236). See Figure 5 for the definition of hypoxia threshold. PPV, positive predictive value; NPV, negative predictive value.

Considerable effort has been invested into the development of simple, reliable, and accurate methods for determining hypoxia using immunohistochemical (IHC) staining (*via* biopsy or tumor sectioning) or plasma protein assays (7, 283).

A. Direct methods

1. Oxygen electrode—direct pO_2 measurement most used in cancer research. The polarographic electrode is an invasive, yet direct method for measuring tissue oxygen concentration based on the electrochemical reduction of oxygen molecules. Between 1988 and 2005, more than 70 research articles quantified data on the oxygenation status of solid tumors (277), and the method is often cited as the ''gold standard'' for hypoxia determination (93, 253). The procedure is considered safe, and no major adverse effects in using the probes for hypoxia assessment have been reported so far (277). Similar oxygen electrodes are currently used clinically for brain oxygenation assessment during neurocritical procedures.

The oxygen measurements involve inserting an electrode into a tumor or metastatic lymph node and measuring oxygen from several points per needle track in sub-millimeter steps. The more regular the lesion shape results in a more representative sampling of pO_2 measurements (100). Typically, more than a hundred measurements are generated over the accessible areas of the lesion, providing a composite overview of the lesion's hypoxia status. The probes are reported to sample a tissue volume of about 50–100 cells (253). The polarographic probes have limited sampling capabilities, accessible only to surface lesions including metastatic lymph nodes. The distribution of pO_2 tension between primary tumors and lymph node metastases have shown little difference, suggesting that node measurements can be surrogates for the hypoxic status of the primary tumor, (277) although later positron emission tomography (PET) imaging studies have reported a discordance in uptake between lesions (*vide infra*) (229).

Data obtained from all tracks form a histogram: a graph plotting the oxygen pressure *versus* the frequency of this particular pressure within the tumor (Fig. 5A) (158). In order to facilitate the assignment of hypoxic *versus* normoxic tumors across patient populations, several descriptive parameters of the histogram have been reported, including the frequency of measurements below a given mmHg value, referred to as the hypoxic fraction. An example using 2.5 mmHg ($HP_{2.5}$) as the hypoxic cut-off is shown in Figure 5A. Other descriptive statistical parameters include HP_5,

TABLE 3. PUBLICATIONS PRESENTING POOLED ANALYSES OF INDEPENDENT STUDIES

Author (studies included)	N	*pO_2 (mmHg), median [range]*	*Tx*	*Outcome endpoint(s)*	*Follow up (months), median [range]*	*Independent prognostic factors for survival*	*Statistical significance*
Rudat *et al.* (236) (studies E and F)	134[a]	9 [0–60]	R or R+C	OS	21 [1–55]	$HP_{2.5}$ stratified by median	$P=0.004$ (95% CI (1.226–2.892))
Dunst *et al.* (77) (studies E and F)	125[b]	9 [0–59]	R or R+C	OS	21 [1–55]	HSV_5	$P=0.001$
Nordsmark and Overgaard (205) (studies B and C)	67	13 [0–54]	R	LRC	29 [2–131]	$HP_{2.5}$ (>22% *vs.* ≤22%) $HP_{2.5}$ (continuous)	$P<0.054$ (95% CI 0.09–1.02) $P<0.0001$ (95% CI 1.02–1.06)
Nordsmark *et al.* (201) (studies B, C, D, E, F, and G)	397[c]	3 [NA]	R or R+C w/wo S	OS	28 [0–120]	$HP_{2.5}$ (%) squared $HP_{2.5}$ increase from 30% to 40%	$P=3.8\times10^{-5}$ Relative risk = 1.13 (95% CI 1.07–1.19)

[a]Includes additional patients not reported in Studies E and F.
[b]Presumed to be a subset of patients in Rudat *et al.* (236).
[c]397 is total number of patients across studies and centers; however, one or more prognostic factor was missing for many patients; the final regression model was based on data from 253 patients.
Tx, treatment; R, radiation; R+C, radiation plus chemotherapy; w/wo S, with or without surgery.

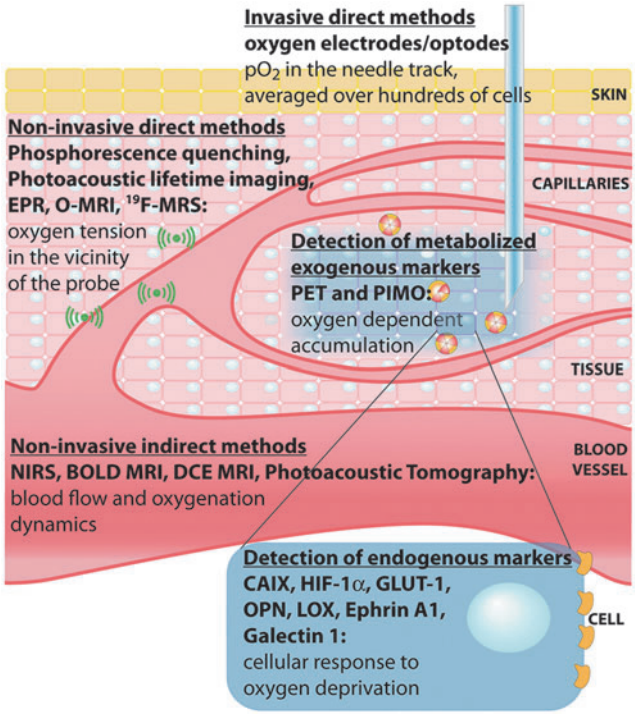

FIG. 4. Hypoxia imaging methods and the type of information provided by each modality. BOLD MRI, blood oxygen level-dependent magnetic resonance imaging; DCE-MRI, dynamic contrast-enhanced magnetic resonance imaging; EPR, electron paramagnetic resonance; HIF-1α, hypoxia-inducible factor 1α; NIRS, near-infrared spectroscopy; OMRI, Overhauser-enhanced MRI; PALI, photoacoustic lifetime imaging; PAT, photoacoustic tomography; PET, positron emission tomography; PIMO, pimonidazole.

HP_{10}, and median pO_2. Hypoxia subvolume is another metric for hypoxia quantification defined as the total tumor volume multiplied by the hypoxic fraction. The stratification of patients into hypoxic or normoxic subgroups requires defining a hypoxic threshold. Figure 5B illustrates a defined hypoxia threshold of a large patient population (262). While there is no standard threshold commonly accepted for defining hypoxia, researchers reported using median $HP_{2.5}$ (236) or $HP_{2.5} > 19\%$ (108, 201) as hypoxic cut-offs to identify patient groups, as these values are linked to poor treatment outcomes.

Oxygen electrodes have several limitations that impede their routine use in clinical practice. Most notably, the method is highly invasive, making repeated measurements extremely rare. The machine itself requires a technically skilled user, and inter-operator variability can be significant. The construction of three-dimensional (3D) oxygen maps is using electrodes difficult, despite a spatial resolution of 50–100 cells, preventing electrode-based therapy planning. The probe does not discriminate between viable and necrotic tissue; thus, it overestimates hypoxia when necrotic areas are sampled (277). Polarographic electrodes function poorly when patients are administered halogenated anesthetics (such as halothane), giving rise to inaccurate oxygen measurements (64, 248).

2. Phosphorescence quenching—alternative direct pO_2 measurement. Phosphorescence quenching relies on the interaction of oxygen molecules with phosphorescent dyes. When illuminated with a short flash of light, the dyes emit their own light and the intensity of this emission decays exponentially at a rate proportional to the local oxygen concentration. Using precalibrated parameters that include the rate of decay in the absence of oxygen and the Stern–Volmer constant, the rate of decay translates into tissue oxygenation. Unlike other oxygen-sensing techniques, the oxygen feedback is independent of tracer concentration, because phosphorescence lifetime is analyzed rather than signal intensity. Another key advantage of this methodology is its high temporal resolution that provides a real-time tissue oxygenation profile which is not easily obtainable with other methods.

The two basic phosphorescent quenching methods employed for the *in vivo* assessment of oxygen concentration rely on either molecular reporters or physical needle probes. Molecular reporters are largely based on various palladium-containing porphyrins with preclinical investigations starting in 1986 (238, 273). An early *in vivo* investigation of phosphorescence quenching examined the behavior of an intravenously administered porphyrin solution in a perfused rat liver subjected to either normoxic or anoxic conditions. The phosphorescence quenching in the liver increased fourfold under anoxic conditions with a response time of approximately milliseconds, indicating that the discrimination of oxygen levels was possible using this modality.

Dendrimerized palladium porphyrins, Oxyphor R2 and G2, were later developed for mapping oxygen concentrations in murine tumor models at oxygen levels below 10 mmHg (76) using either basic oxygen contour plots or reconstructed oxygen histograms (301). From a preclinical validation study, the Oxyphor G2 signal differentiated well-oxygenated malignant melanomas (37.8 ± 5.1 mmHg) from both moderately oxygenated renal cell carcinomas (24.8 ± 17.9 mmHg) and hypoxic Lewis lung carcinomas (1.8 ± 1.1 mmHg). The assessment of hypoxia was confirmed by tumor histology, pentafluorinated etanidazole (EF5) binding, and tumor blood flow by contrast-enhanced ultrasound suggesting that Oyxphor G2 provides critical tissue oxygenation information in tumors. Recently, new Oxyphor derivatives were developed to tolerate a variety physiological environments (289). This new generation of the ''protected'' dendritic probes operate in either albumin-rich (blood plasma) or albumin-free (interstitial space) environments over a range of physiological oxygen concentrations with excellent submillimeter spatial and subsecond temporal resolution (85).

Recently, phosphorescent molecules embedded into a solid support within physical needle probes enable tissue oxygen measurements, albeit invasively. These instruments monitor regional pO_2 concentrations in brain tissue (63) and surface accessible tumors (110).

3. Electron paramagnetic resonance. The method requires an injection of an exogenous probe bearing an unpaired electron that is selective in its interaction with oxygen (97). Recently, implantable and metabolically inert paramagnetic lithium phthalocyanine crystals have been utilized as oxygen-sensitive electron paramagnetic resonance (EPR) probes to monitor changes in tissue hypoxia (140). The width of the spectral band corresponding to the probe signal correlates with oxygen concentration. Similar to oxygen electrodes, EPR imaging data provide quantitative pO_2 values. With EPR, repeated measurements of absolute pO_2 from the

Table 4. Existing Techniques for *In Vivo* Assessment of Tissue Oxygenation

Method	*Direct*	*Physiologic*	*Endogenous*	*Approved clinical procedure*
Polarographic oxygen electrode	•			+
Phosphorescence quenching	•			Europe only
EPR oximetry	•			−
^{19}F-MRI relaxometry	•			−
Overhauser-enhanced MRI	•			−
Immunohistochemical staining				
CA-IX; HIF; Glut-1; OPN; protein panels			•	
Comet assay			•	−
Near-infrared spectroscopy (multiple modalities)		•		+
Photoacoustic tomography		•		−
Photoacoustic lifetime imaging	•			−
Contrast-enhanced color duplex sonography		•		−
MRI/MRS techniques				
DCE-MRI		•		Not for tumors
BOLD		•		Not for tumors
O_2-MRI	•			−
Lactate MRS			•	−
Pimonidazole, EF5		•		−
PET				
^{18}F tracers: FMISO, EF5, FAZA, HX4, *etc.*		•		−
^{64}CuATSM		•		−
Miscellaneous perfusion measurements				
PET with [^{15}O]H_2O		•		−
Contrast-enhanced CT		•		+
Ultrasound Doppler methods		•		+

BOLD, blood oxygen level dependent; CA-IX, carbonic anhydrase IX; CT, computed tomography; EPR, electron paramagnetic resonance; PET, positron emission tomography; •, method of hypoxia assessment; +, approved clinical procedure; −, not approved clinical procedure.

same tissue spanning a few minutes to days or even months enables the sensitive detection of fluctuating hypoxia, which is an advantage over other imaging methods.

Oxygen levels determined by EPR imaging closely mirror oxygen levels assessed by Oxylite measurements in fibrosarcoma (FSa) xenografts (79). A significant correlation in the median pO_2 levels was observed between the modalities ($R = 0.64$), indicating that EPR imaging provides relevant *in vivo* oxygen tension data.

Although stand-alone EPR imaging intrinsically provides no anatomical details, recent studies have obtained anatomical magnetic resonance imaging (MRI) imaging data with functional EPR pO_2 measurements in a sequential imaging system yielding co-registered composite images of hypoxia (240). This dual imaging modality relies on a resonator tuned to a frequency of 300 MHz, which is optimal for detecting OX63, a paramagnetic oxygen-sensitive triaryl methyl radical used as the *in vivo* oxygen probe. Both instruments detect the probe's signal, enabling facile image co-registration. Using this dual-modality imaging approach, multiple 3D pO_2 imaging maps were generated over 30 min, detecting rapid fluctuations in oxygen tension (187, 295). Rodents bearing SCCVII (murine squamous cell carcinoma) or HT29 (human colorectal carcinoma) tumors subjected to breathing cycles of air/carbogen (95% oxygen:5% carbon dioxide)/air led to observable modulations in intratumoral pO_2. Although relatively minor changes in oxygen tension were observed during the air breathing phase (0–12 min, pO_2 median = 7.2 mmHg), larger changes in oxygen tension were evident during the carbogen breathing phase (12–24 min, pO_2 median = 13.1 mmHg), consistent with the pharmacologic effect that carbogen breathing reduces tissue hypoxia.

EPR imaging can monitor the effects of radiation and chemoradiation in preclinical tumor models using co-registered MRI and EPR imaging data (80). The curative effect of radiation doses (21.1 to 52 Gy) administered to mice bearing FSa tumors was correlated against several descriptors for pO_2 obtained by EPR imaging. Based on survival data, HP_{10} was most strongly correlated with curative treatment (pseudo-$R^2 = 0.59$) and identifying tumors at risk for treatment failure, consistent with clinical data obtained from oxygen-sensitive electrodes. In a follow-up radiation treatment study, $HP_{10} > 10\%$ and $HP_{10} > 15\%$ were predictive for treatment failure in FSa tumors and MCa4 (mammary carcinoma) tumors, respectively (81). The hypoxic treatment outcomes cut-offs observed in this study are similar to hypoxic cut-offs observed in human patients.

EPR imaging has been clinically used, but on a limited basis. Several reports disclosed the use of this method in humans, including melanoma and H&NC patients as well as healthy volunteers (288). Clinical development of this technique enabling rapid and absolute pO_2 data collection over various timepoints would enhance the clinical development of hypoxia-based therapies.

4. ^{19}F-magnetic resonance spectroscopy. ^{19}F-magnetic resonance spectroscopy (MRS) utilizes perfluorinated molecular probes to quantify tissue oxygen concentration with

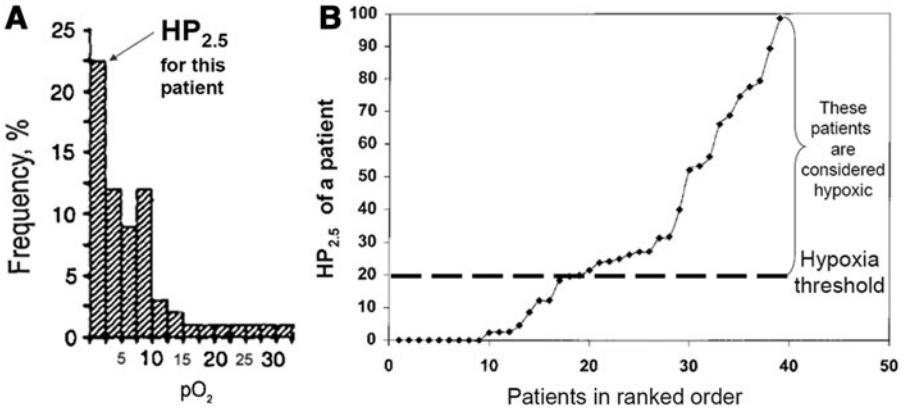

FIG. 5. pO_2 pressure data represented in histograph form. **(A)** The percent frequency of pO_2 pressures as measured in an individual head and neck cancer patient. Reprinted by permission from Lartigau *et al.* (158); **(B)** $HP_{2.5}$ distribution in the population. The hypoxic threshold is upper limit of the hypoxic range below which cellular, tissue, or organ function becomes progressively restricted (122). Reprinted by permission from Terris (262). $HP_{2.5}$, hypoxic fraction below 2.5 mmHg.

high specificity (147), which is made possible by the linear relationship between local oxygen tension and the spin-lattice relaxation rate of perfluorinated probes (49). This technique was validated preclinically against polarographic pO_2 measurements in rodents bearing human glioma xenograft tumors (mean $pO_2/_{relaxo}$ *vs.* median $pO_2/_{electrode}$, $R^2 = 0.95$). In a small group of rats bearing human prostrate carcinomas undergoing radiation treatments, the intratumoral oxygenation as assessed by electrodes and MRS revealed a significant correlation ($R^2 > 0.8$), suggesting that MRS is a sensitive modality for monitoring changes in oxygen tension as a function of radiation therapy (18). The preclinical results for assessing tumor hypoxia are encouraging, and the ability to translate this technology into the clinical setting requires further validation.

A recent report has disclosed the exploratory use of ^{19}F-MRS to detect hypoxic tissue in cancer patients using SR4554, a trifluorinated 2-nitroimidazole (164). The results indicated that MRS detected SR4554-related signals in various tumor types, including gastrointestinal (GI) stromal tumors, head and neck tumors, and melanomas at doses of 1400 mg/m^2, albeit with modest signal intensity. An increase in the number of fluorine atoms would theoretically boost the sensitivity of the method, but further confirmatory testing would be required.

5. Overhauser-enhanced MRI. Overhauser enhanced MRI (OMRI) is a hypoxia imaging technique combining the advantages of MRI with quantitative pO_2 measurements, providing both hypoxia and microvascular permeability data noninvasively. By saturating the electron spin of OX63, a paramagnetic oxygen-sensitive triaryl methyl radical contrast agent, water protons in tissue become hyperpolarized *via* dynamic nuclear polarization. The resultant images reflect both the concentration of the contrast agent and local oxygen concentration. Similar to EPR, this technique provides absolute pO_2 data in tissue. Using OMRI, simultaneous vascular and oxygen tension levels were successfully detected in mice bearing implanted hypoxic squamous cell carcinomas (36% HP_{10} [tumor] *vs.* 8% HP_{10} [muscle]) (188). These hypoxic regions displayed increased vessel permeability independent of blood perfusion, suggesting the presence of leaky vasculature and impaired oxygen delivery. Reduced pericyte density in the hyper-perfused regions matched areas of impaired and leaky vasculature caused by hypoxic conditioning. Noninvasive hypoxia imaging with OMRI is a powerful technique which simultaneously provides multiple blood and oxygen parameters that are critical for deducing tissue hypoxia and for enabling the therapeutic discovery of new hypoxia-targeted therapies.

B. Endogenous markers of hypoxia

1. Hypoxia-inducible factor-1α. HIF-1α is an oxygen-regulated transcriptional activator. It potentiates a variety of biochemical processes that are aimed at alleviating the effects of hypoxia (*vide supra*). It is constantly expressed and degraded *via* oxygen-dependent oxidation; therefore, its degradation is slowed at low oxygen pressure (103) with elevated protein levels found in many hypoxic tumors (245). HIF-1α is a critical molecule for translating tumor hypoxia into the expression of multiple hypoxia-related targets.

Activating HIF-1α expression in human cancer has ties to both hypoxic and normoxic signaling pathways (Fig. 1) (244). Activation of the phosphoinositide 3 kinase (PI3K)/Akt/mammalian target of rapamycin apoptosis pathway leads to increased gene expression of HIF-1α (127). In addition, mutated variants of phosphatase and tensin homolog (PTEN), VHL, succinate dehydrogenase, or fumarate hydratase are also known to increase HIF-1α transcription (296). Various growth factors such as insulin-like growth factor and epidermal growth factor stabilize the protein at normoxic conditions (167). Lastly, the formation of mitochondrial ROS can stimulate the accumulation of HIF-1α. Mechanistically, ROS may oxidize iron in the active site of PHD, blocking its ability to hydroxylate HIF-1α (246). Analysis of several human H&NC cell lines have suggested that HIF-1α expression is cell-line specific (12). Nevertheless, HIF-1α expression has been linked to reduced disease-specific survival (DSS) in colorectal cancer patients (6) with similar findings reported for gynecological cancer (242). In H&NC patients, researchers have reported that elevated levels of HIF-1α were associated with improved 5 year DFS in surgically treated patients (12).

2. Carbonic anhydrase IX. CA-IX is an enzyme that catalyzes the reversible transformation between bicarbonate anion and carbon dioxide, and its expression is elevated at oxygen tensions below 20 mmHg (178, 293). Consistent with its function as a modulator of tissue pH, CA-IX plays an integral role in tumor acidity, especially under hypoxic conditions, which can impede the effectiveness of ionizable drugs. For example, CA-IX expression was found to

significantly correlate with poor progression-free survival (PFS) ($P = 0.014$) and OS ($P = 0.01$) in breast cancer patients undergoing doxorubicin therapy (16). However, CA-IX expression does not significantly correlate with either pO_2 measurements or pimonidazole (PIMO) staining (136) in patients with H&NC (137, 161), suggesting that its expression is linked to other causative factors besides pO_2 levels. High CA-IX protein levels are moderately correlated with hypoxia in cervix tumors (178) but not with hypoxia in colorectal adenocarcinomas (104). CA-IX is a negative prognostic factor for survival in nonsmall-cell lung cancer (NSCLC) (24, 129, 142, 143), breast cancer (43), and cervical cancer (178) and its prognostic significance in H&NC has also been reported (136, 256). CA-IX expression has been linked to outcomes for H&NC patients undergoing accelerated radiotherapy with carbogen and nicotinamide (ARCON, *vide infra*) therapy (134). When using a dichotomized cut-off value for low *versus* high CA-IX expression in biopsy samples, high CA-IX expression was linked to increased LRC ($P = 0.04$) and freedom from distant metastases ($P = 0.02$). This unexpected result highlights the complex role of CA-IX expression in malignant tumors.

3. Glucose transporter 1. GLUT-1 is a membrane protein facilitating the translocation of glucose across cell membranes. Due to the intensification of glycolysis under hypoxic conditions, this transporter is up-regulated to satisfy the elevated glucose consumption of hypoxic cells. Multiple types of tumors display high levels of this protein (191), and its over-expression is associated with hypoxia in tumors of the head and neck (223) and cervix (3). Poor treatment outcomes are related to the expression of this protein in H&NC (154) and bladder cancer (126).

4. Osteopontin. Osteopontin (OPN) is a member of the small integrin binding ligand N-linked glycoprotein family. It is a secreted phosphorylated acidic glycoprotein and binds to several integrins through its arginine-glycine-aspartic acid (RGD) integrin binding motif. OPN is expressed in several different cells, including endothelial cells, macrophages, and smooth muscle cells for modulating cell adhesion, vascular remodeling, and immune functionality. The expression of OPN is up-regulated under hypoxic conditions through Akt activation and stimulation of the ras-activated enhancer (RAE) in the OPN promoter (298). In addition, plasma OPN was found to correlate inversely with pO_2 levels in patients with head and neck tumors (202). Tumor OPN expression in Stage IV head and neck patients linearly correlated with median pO_2 levels (9). The binding of OPN to cell surface receptors on tumor cells activates integrins and MMP signaling pathways, increasing the propensity for tumor cell invasion, adhesion, and increased tumor cell migration (42). In patients with locoregional nasopharyngeal carcinoma receiving curative radiotherapy, above median OPN plasma levels were a significant predictor of poor response to radiotherapy (128). Similar results were obtained in another study of H&NC patients. Patients with high plasma OPN levels exhibited a 28% chance of LRC 5 years after treatment, as opposed to 60%–64% for patients with both low and intermediate OPN levels ($P < 0.01$) (202). OPN has been found to be prognostic for other malignant diseases (8, 54, 183).

5. A combined IHC panel of protein markers for hypoxia. It was shown to have a higher predictive power for OS than any single marker alone (161, 286). Biopsy samples stained and scored individually for LOX, ephrin A1, galectin-1, and CA-IX resulted in an assignment of an aggregate ''hypoxic score.'' The combined ''hypoxic score'' was prognostic for cancer-specific survival ($\chi^2 = 14.03$, $P = 0.015$) and OS ($\chi^2 = 10.71$, $P = 0.057$) over 10 years.

6. Comet assay. The comet assay is widely accepted as a standard method for assessing DNA damage in individual cells (190). Since radiation produces approximately thrice more DNA damage in well-oxygenated cells as compared with hypoxic cells (*vide supra*), this assay attempts to measure the proportion of purported hypoxic cells present in a tumor sample, but not *via* direct oxygen concentrations measurements. This approach has been used to measure tumor hypoxia in radiotherapy patients with head and neck tumors (162), breast (210), and a range of metastatic tumors (4, 209). The correlation between comet assay data and pO_2 measurements was not always in agreement (4, 162, 209). Concerns about circulating blood cells contaminating the biopsy samples (209) in addition to a small sampling size could explain the observed correlative results.

C. Physiologic methods

1. Near-infrared spectroscopy/tomography–widely used for pulse oximetry. Near-infrared spectroscopy (700 to 900 nm) relies on the different absorption spectra of hemoglobin (Hb) and oxy-hemoglobin (HbO_2) to quantify a ratio of Hb/HbO_2. This method does not measure oxygen concentration directly, but the Hb/HbO_2 ratio is converted into oxygen partial pressure through well-studied hemoglobin saturation curves. One variation of this method is widely used in clinical practice for express analysis of blood oxygenation (pulse oximetry) (33). Other approaches based on spectroscopic differences of Hb and HbO_2 have been proposed as well (19). Notably, diffuse optical tomography (45) was used to reconstruct 3D oxygen distribution in breast cancer patients (150). The method has limited tissue penetration and is confined in body parts with a relatively low light attenuation (291).

2. Photoacoustic tomography. Photoacoustic tomography (PAT) is an imaging technology that is used for the noninvasive detection of tissue hypoxia, providing simultaneous functional and anatomical data. PAT is an ultrasound-based imaging modality that detects sound waves generated from absorbed light. The absorbed light generates heat, causing thermal elastic expansion within tissue. This expansion initiates a pressure change that propagates through tissue as ultrasonic waves. Transducers detect and pinpoint the ultrasonic source resulting in 3D tomographic images. To assess oxygen concentrations, PAT relies on the spectroscopic absorption differences between endogenous HbO_2 and Hb. Based on their differential feedback, oxygen saturation (SO_2) curves provide an estimate of oxygen concentration in blood. Since PAT is fundamentally an ultrasound technique, it has a high spatial resolution ($\sim 60\ \mu m$) and a tissue penetration depth of approximately 30 cm. One noted limitation is the restricted imaging window that is constrained by the laser

aperture. The combination of high structural resolution and optical contrast with excellent depth penetration makes this imaging modality a promising technique for hypoxia assessment.

Preclinical PAT hypoxia imaging readily detects hypoxic tissue and areas of impaired vascularity in various tumors. PAT imaging of mice bearing SKOV3× (ovarian cancer) tumors detected changes in SO_2 levels between feeding and nonfeeding blood vessels, a basic model for hypoxia (252). Intercranially innoculated ENU1564 tumor cells (rat mammary adenocarcinoma) formed distorted vascular networks with depressed SO_2 levels compared with unaffected areas of brain tissue, suggesting the presence of hypoxia (180). Several tumor samples stained positively for hypoxia-related proteins HIF-1α, VEGF receptor (VEGFR), and VEGF-A, indicating prevalent tumor hypoxia. A related study used PAT to detect regions of hypoxia in mice xenografts bearing U87 (glioblastoma) brain tumors (171) that were characterized as having higher relative total Hb but lower SO_2 caused by chaotic and leaky tumor vasculature.

While PAT hypoxia imaging relies on measureable differences in Hb and HbO_2, using an oxygen-sensitive reporter can also provide relevant hypoxia information. Photoacoustic lifetime imaging (PALI) measures the lifetime of an oxygen-sensitive dye, which is proportional to local oxygen concentration. This technique has been recently used to detect hypoxia in tumors and correlated against pO_2 electrode measurements measurements (249). After a local tumor injection of methylene blue in xenograft mice bearing LNCaP (prostate cancer) tumors, electrode pO_2 measurements and PALI imaging data detected lower oxygen concentrations in the tumor tissue (20 mmHg), confirming the presence of tumor hypoxia. The correlation of oxygen levels between the modalities was significant ($P<0.05$), supporting the ability of PALI to provide relevant tissue hypoxia data. Since PAT and PALI detect changes in oxygen levels in combination with relevant vascular information noninvasively, these imaging modalities offer a unique approach for identifying high-risk malignancies that are susceptible to treatment failure.

3. Contrast-enhanced color duplex sonography. Contrast-enhanced color duplex sonography (CDS) is a two-dimensional ultrasound-based imaging modality that visualizes blood movement (*i.e.,* blood flow) in tissue, typically using a contrast enhancer, to identify differential tissue perfusion to deduce areas of hypoxia. CDS can image vessels of very small diameter (0.1–0.2 mm), which is relevant to tumor flow as 10% of the tumor mass comprises such vessels (65). The correlation of CDS with tissue hypoxia using oxygen-sensitive polarographic electrodes was evaluated in H&NC patients from three different reports (65, 94, 95, 241). An inverse correlation was observed between tissue perfusion and hypoxic nodal volume when oxygen tensions were below 10 mmHg [$r=-0.551$; $P=0.021$ (241); $r=-0.71$, $P<0.0001$ (65); $r=-0.788$ (95); $r=-0.730$ (94)]. These studies confirm the link between poor tumoral perfusion and depressed tumor oxygen levels, but this technique does not measure oxygen directly, which may limit its widespread use as a hypoxia assessment tool.

4. MRI-based measurements. Tissue oxygenation has been deduced from perfusion data obtained with dynamic contrast-enhanced MRI (DCE-MRI) and a contrast agent comprised gadolinium (Gd)-based molecular probes, such as Gd-diethylenetriaminepentaacetic acid (Gd-DTPA) (48). Physiologically, since Gd-DTPA is a hydrophilic small molecule, it diffuses past blood vessel walls and distributes into a tumor's extracellular space as a function of blood perfusion, vascular density, tissue permeability, and extracellular volume fraction, a parameter closely related to cell density (182). Gd-DTPA decreases the proton spin lattice relaxation time (T_1), providing signal enhancement in T_1-weighted MR images. Since hypoxic tumors often exhibit poor perfusion characteristics and chaotic vasculature, Gd-DTPA is believed to provide insights into the extent of hypoxia present in tumors.

Three studies have investigated the link between DCE-MRI and oxygen tension using polarographic electrodes in patients with cervix carcinomas. The reported signal increase over baseline (SI-I) correlated well with HP_5 and median pO_2 values ($r=-0.49$, $P=0.002$ and $r=0.59$ $P<0.001$); however, the slope of the time intensity curve (SI-I/s) only weakly correlated with oxygen tension (53). A second study reported similar findings, observing a correlation between median pO_2 and SI-I ($r=0.44$, $P=0.008$) (177). The authors postulated that the steady-state enhancement parameter SI-I better reflects perfusion, which is linked to hypoxia, while tumor flow as described by SI-I/s is indicative of vascular density whose relationship to hypoxia is not well understood (53). In a third report, maximal relative signal intensity (RSI) between the pre- and postcontrast images was significantly correlated with several pO_2 descriptors (median $P<0.001$; $HP_{2.5}$ $P<0.001$, $HP_{5.0}$ $P<0.0001$), HP_{10} $P<0.001$) (182). As a general trend, tumors with high maximal RSI values were better oxygenated than tumors with low RSI, which was confirmed by pO_2 measurements.

MRI-DCE perfusion imaging was shown to positively correlate with PIMO staining in H&NC patients, indicating that hypoxia influences the perfusion signal. A significant correlation between the leakiness of vessels (K_{trans}) and PIMO staining was reported ($r=0.516$, $P=0.041$) for several tumors, while perfusion computed tomography (CT) did not reveal any significant correlations with PIMO (200). In a second study, a correlation was reported between both perfusion (Fb) and blood volume (PS) against PIMO staining ($r=-0.79$, $P=0.033$ for Fb and $r=-0.75$, $P=0.049$ for PS against PIMO), suggesting that factors which impact tumor perfusion also influence PIMO uptake (73). MRI perfusion has also been linked with ^{18}F-fluoromisonidazole (^{18}F-FMISO) PET imaging, another marker of hypoxia. From comparative imaging data gathered from patients with metastatic lymph nodes, the hypoxic nodes were poorly perfused compared with normoxic nodes, leading to an inverse correlation between k_{ep} (rate constant) and ^{18}F-FMISO standard uptake value (SUV) ($\rho=-0.58$, $P=0.042$). While MRI-DCE imaging and tissue pO_2 levels are not directly related, MRI-DCE may be useful in locating tumors with suspect perfusion that are at risk for treatment resistance and monitoring changes in perfusion during treatment, indicating critical changes in tumor hypoxia.

5. Blood oxygen level-dependent MRI. A technique estimating temporal changes of blood oxygenation has been recently investigated for the measurement of oxygenation in

human tumors (172, 259). The imaging signal from this technique is derived from endogenous paramagnetic deoxyhemoglobin, which is related to tissue oxygenation. The relaxivity of deoxyhemoglobin creates signal enhancement by accelerating spin–spin relaxation time (T_2) and T^*_2-weighted signal relaxation. From the T^*_2 signal, the transverse relaxation rate of water in blood and surrounding tissue ($R^*_2 = 1/T^*_2$) is calculated. Highly perfused tissues exhibiting an elevated R^*_2 value compared with tissue in a nearby region implies the presence of tissue hypoxia. The parameter R^*_2 is sensitive to changes in tissue oxygenation, but it is not a direct measure pO_2 and tends to be qualitative in nature (11). However, two independent studies have linked blood oxygen level-dependent (BOLD) MRI images with tissues oxygenation as assessed by polarographic electrodes and PIMO staining. A comparison between pO_2 and BOLD-MRI images was reported from measurements taken from prostate cancer patients (47). A positive correlation was observed between R^*_2 and HP_5 ($r = 0.76$ and $P = 0.02$) and a trend toward a negative correlation between R^*_2 and pO_2 ($r = -0.66$, $P = 0.07$), suggesting that hypoxic tumors trended toward exhibiting elevated R^*_2 values. From another published report, a high correlation between PIMO staining and elevated R^*_2 signals was also observed in prostate cancer patients (125). The sensitivity of R^*_2 to depict tumor hypoxia was 88%, but the low specificity (36%) impacted the PPV (76%) and the NPV (56%) of the technique. Across a cohort of patients of different tumor types undergoing carbogen respiration to improve tumor oxygenation, BOLD-MRI signal intensity changes were observed in 20 out of 36 patients (259), suggesting that BOLD-MRI imaging can detect changes in tumor hypoxia over time. Since BOLD-MRI is dependent on the concentration of deoxyhemoglobin rather than pO_2 directly, other independent variables not related to tissue oxygenation can influence R^*_2 values. However, BOLD-MRI may provide complementary information related to tissue oxygenation that aids in defining optimal treatment strategies for patients with hypoxic tumors.

6. Pimonidazole. PIMO is a lipophilic exogenous hypoxia marker [partition coefficient = 8.5 (2)], containing the hypoxia-targeting 2-nitroimidazole chemotype whose mechanism of localization is identical to other 2-nitromidazole hypoxia tracers (*vide infra*). PIMO was originally developed as a radiosensitizer to be more effective than misonidazole (MISO) (72), but it failed to demonstrate efficiency in follow-up clinical trials (71). PIMO is now used as an exogenous marker for hypoxia. PIMO administration occurs either intravenously or orally several hours before tumor biopsy. The detection of hypoxia in tissue samples relies on a PIMO metabolite staining kit using commercially available antibodies. The relationship between PIMO accumulation and oxygen tension was studied in phantoms (5, 40) and in animal tumor models (220), which have demonstrated a strong linear correlation ($r^2 = 0.81$) (226). However, a correlation was not observed between PIMO positivity in needle biopsies and pO_2 measurements in patients with uterine cervix cancer (203). However, the ability to extract composite hypoxia information from needle biopsies is not possible and may be considered a contributing factor in the apparent lack of correlation between the two assessment methods. Localization of PIMO was found to be a prognostic factor for both 2 year LRC and DFS in head and neck patients (136).

7. EF5 (pentafluorinated etanidazole). It is a 2-nitroimidazole-derived exogenous hypoxia biomarker which is characterized by a neutral lipophilic profile (partition coefficient = 5.7) that rapidly and uniformly distributes throughout all tissues *in vivo* (146). Despite its lipophilic profile and relatively long plasma half life ($t_{1/2} = 12$ h), none of the expected toxicities associated with exposure to 2-nitroimidazoles, including peripheral or central neuropathies, have been observed in patients (145). EF5 is administered to patients (21 mg/kg) generally 24–48 h before tumor biopsy or surgical resection (91).

EF5 binding in tissue is detected by either flow cytometry or IHC techniques using fluorescently labeled antibodies that specifically target the perfluorinated side chain of EF5 (292). Quantification of oxygen levels in EF5-stained tissues is accomplished by normalizing the EF5 binding against the maximal tracer uptake under hypoxic conditions (''cube reference binding'') and referencing a calibrated pO_2 scale that generates estimated pO_2 values ranging from 75 mmHg (normoxic) to 0.75 mmHg (severe hypoxia) (86, 88, 91).

The correlation between EF5 uptake in tumors with pO_2 levels derived from oxygen-sensitive electrodes is not significant for many tumor types (88, 89, 91, 132, 138). However, EF5 binding in FSa xenografts was significantly correlated with pO_2 levels as measured by EPR (0–30 mmHg, $r^2 = 0.54$, $P < 0.01$), confirming that EF5 binding occurs at oxygen levels ≤ 10 mmHg, which is consistent with earlier *in vitro* validation studies (144, 184). EF5 uptake in hypoxic tumors co-localizes with the expression of several hypoxia-derived genes and proteins, including CA-IX, HIF-1α, and VEGF, providing further evidence that EF5 targets hypoxic tumors (37, 186, 239, 300).

EF5 is prognostic for outcomes in patients with H&NC having severe hypoxia ($< 0.1\%$ oxygen, $p = 0.032$) (86) and can identify sarcomas having an increased metastatic potential ($P = 0.05$) (87). In patients with glial tumors, tumor regions having enhanced EF5 binding and proliferating cell populations characterized an aggressive tumor phenotype that was prognostic for both survival ($P = 0.0196$) and recurrence ($P = 0.074$) (90, 91). Recently, EF5 has also been shown to be a predictive biomarker for identifying hypoxic tumors that are sensitive toward treatment with the hypoxia pro-drug CEN-209 (284). Since both EF5 and CEN-209 are substrates for shared intracellular oxidoreductases, EF5-based tumor stratification could provide a means for identifying and treating patients who are responsive to CEN-209 therapy.

8. Hypoxia PET imaging—physiologic hypoxia measurement providing tomographic information. PET imaging of hypoxia is a noninvasive technique that uses radiolabeled reporters to detect tumor hypoxia. These tracers are administered intravenously, and their uptake in tissues is measured using a PET camera. Mechanistically, these small molecules freely diffuse into normoxic cells undergoing a reversible reduction by either intracellular cytochrome or nitroreductase enzymes (depending on the tracer type) followed by intracellular re-oxygenation under normoxic conditions.

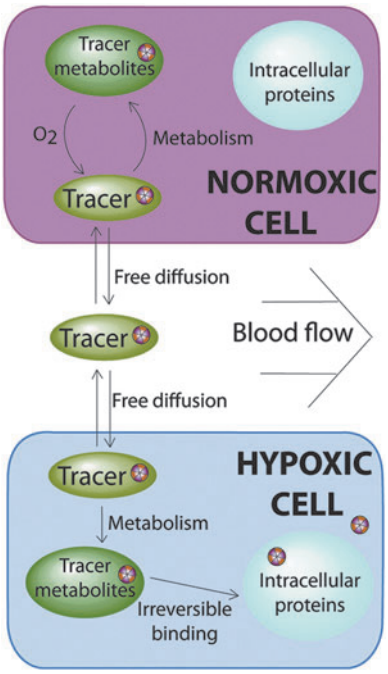

FIG. 6. Schematic of the selective PET tracer uptake of hypoxia imaging agents in hypoxic cells. Under hypoxic conditions, accumulated 2-nitroimidazole metabolites bind to intracellular thiol-rich proteins, while reduced copper species lose their chelator and become trapped intracellularly.

However, under hypoxic conditions, the lack of oxygen participation leads to the enrichment of a chemically reduced species, which localize intracellularly either through dechelation or covalent attachment to thiol-rich proteins (Fig. 6) (20). Since active enzymes (*e.g.,* cytochromes or nitroreductase) should be present in living cells and participate in the accumulation of radiolabeled metabolites, these tracers localize in viable, but not necrotic cells. The oxygen concentration relevant for identifying radioresistant hypoxic cells (1% oxygen volume or ~7 mmHg of partial oxygen pressure) (5, 40, 111) is sufficient to drive the uptake of 2-nitroimidazoles and Cu-chelated complexes into hypoxic tissues, making them relevant markers for assessing hypoxia. The differential uptake and washout between hypoxic and normoxic cells provides a selective demarcation of hypoxic cells *in vivo* (56). PET-based biomarker provides composite oxygenation information on tumors, and repeated measurements are possible. PET imaging with these tracers enables the visualization of the hypoxic status of the entire tumor and associated lesions in metastatic or locally advanced cancer situations, providing a 3D image of hypoxia, which is not possible using electrode- or biopsy-based methods. However, very low temporal resolution (*i.e.,* days between scans) prohibits real-time monitoring of tissue oxygenation. In addition, the relatively short half life of ^{18}F-fluorine ($t_{1/2}$ = 110 min) demands that the tracer is manufactured and imaged within several hours.

a. ^{18}F-Fluoromisonidazole. The development of 2-nitroimidazoles bearing radioactive ^{18}F-fluorine atoms for PET imaging of hypoxia was inspired by radiosensitizers of the same chemotype (see Fig. 7). ^{18}F-FMISO is a radiolabeled analog of the radiosensitizer MISO. ^{18}F-FMISO is the predominant PET tracer of this group that has been extensively investigated for noninvasively detecting hypoxia *in vivo* using PET imaging (227). ^{18}F-FMISO is a relatively lipophilic molecule (partition coefficient = 0.40, log P = −0.40), which, ultimately, influences its *in vivo* biodistribution profile. The mean total excretion of ^{18}F-FMISO in human urine is as low as 3% of the total injected dose (28, 107). ^{18}F-FMISO is stable in human plasma (92%–96% intact at 90 min postinjection), and metabolites are typically excreted into the urine (83% intact at 95 min postinjection).

Due to its lipophilic character, ^{18}F-FMISO accumulation in hypoxic tumors increases over a period of approximately 4 h, while the wash out from normoxic tissues starts at 30 min postinjection. The suggested static imaging times range from 2 h (168) to 4 h postinjection (264). In human H&NC, tumor to muscle (T:M) ratios usually range from 1.1 to 3.8, approximately 4 h postinjection (84). Subsequently, in humans, the ^{18}F-FMISO PET regions of interest with tumor-to-background (T:B) ratios of 1.3 and above are often demarcated as hypoxic, which is in agreement with preclinical imaging data (148). Other metrics for defining hypoxia were proposed as well for different tumor types (SUV > 2.0 for NSCLC, SUV > 1.6 for H&NC) (83).

Preclinical *in vivo* studies revealed that ^{18}F-FMISO uptake and pO_2 values have an inverse linear relationship between the PET image intensity and oxygen levels (Pearson product coefficient $R = -0.60$ to -0.83) (36). In addition, autoradiographic comparisons between ^{18}F-FMISO and ^{64}Cu-ATSM in rodent models showed a strong correlation in the update of the two tracers 24 h after ^{64}Cu-ATSM injection ($R^2 = 0.86$) (62). The uptake of ^{18}F-FMISO linearly corresponds to pO_2 levels H&NC patients ($HP_{2.5}$, $r = 0.75$–0.78; $HP_{5.0}$, $r = 0.76$–0.79) (96, 302), making it a relevant tracer for imaging tumor hypoxia (Fig. 8). Interestingly, no significant correlation exists between electrode measurements and ^{18}F-FMISO T:M ratios in patients with either STS (3 benign, 11 malignant) or benign tumors ($n = 4$) (14, 195).

Pretherapy ^{18}F-FMISO uptake is an independent prognostic factor in H&NC. In a multivariate analysis performed on 73 patients, $T:B_{max}$ was highly predictive for OS over a 9 year period ($P = 0.006$) (225). In a population of 25 H&NC patients, the pretreatment ^{18}F-FMISO T:B ratio above 1.6 predicted 11 out of 13 recurrences of H&NC 1 year after radiotherapy (84). A second report also observed that DFS rate for H&NC patients was negatively correlated with both baseline ^{18}F-FMISO scanning ($P = 0.04$) and scans performed during radiotherapy ($P = 0.02$) over a 5 year period (70). When used in combination with intensity-modulated radiation therapy (IMRT *vide infra*) and platinum-based chemotherapy, ^{18}F-FMISO PET imaging could detect a reduction of uptake in 16 out of 18 oropharyngeal cancer patients (168). No patients experienced local failure, and the 3-year PFS rate was 100%. Although this study was a single-arm study, it suggests that reductions in hypoxia during treatment provide a strong indication that patients will likely have improved outcomes. A recent prognostic clinical study suggests that early ^{18}F-FMISO imaging provides critical prognostic information related to tumor reoxygenation (303). While the baseline ^{18}F-FMISO imaging data were moderately prognostic for PFS ($P = 0.139$), ^{18}F-FMISO hypoxia PET imaging data obtained 2 weeks after the initiation of

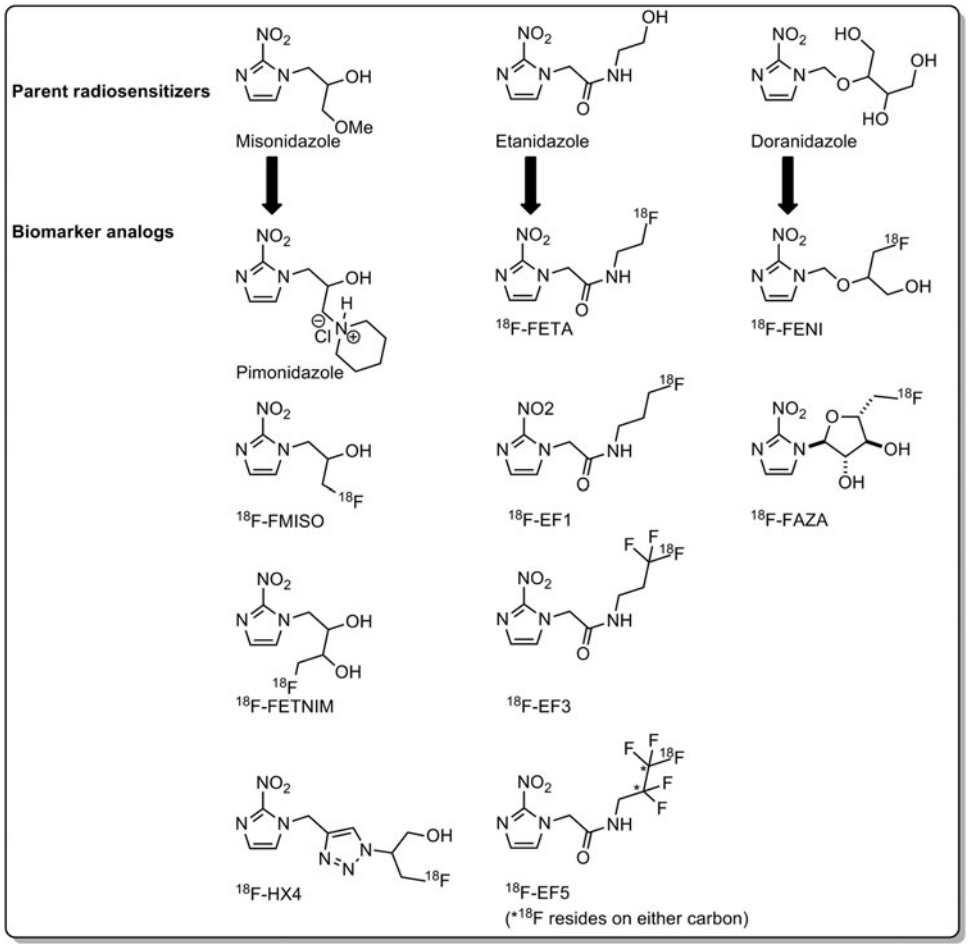

FIG. 7. ^{18}F-Tracers for PET hypoxia imaging grouped by parent radiosensitizers. ^{18}F-EF1, monofluorinated etanidazole; ^{18}F-EF3, trifluorinated etanidazole; ^{18}F-EF5, pentafluorinated etanidazole; ^{18}F-FAZA, ^{18}F-fluoroazomycinarabinofuranoside; ^{18}F-FENI, 1-(2-[^{18}F]fluoro-1-[hydroxymethyl]ethoxy)methyl-2-nitroimidazole; ^{18}F-FETA; ^{18}F-fluoroetanidazole; ^{18}F-FETNIM, ^{18}F-fluoroerythronidazole; ^{18}F-HX4, ^{18}F-flortanidazole.

chemoradiation therapy were a better predictor for local PFS ($P = 0.001$). The researchers explained that the stronger relationship observed between early imaging time points and PFS can conceivably arise from an improvement of tracer kinetics resulting from treatment-related changes in tumor perfusion. These results support a possible patient selection strategy that identifies patients in need of an adaptive therapy planning.

However, there are limitations associated with ^{18}F-FIMSO PET imaging. First, due to its relatively lipophilic nature and slow tissue washout, a suitable contrast between hypoxic and normal tissues is achieved no earlier than 2 h postinjection, and often requires approximately 4 h. This long wait time can be inconvenient to the patient. In addition, the relatively short half life of ^{18}F-fluorine restricts the length of prescanning uptake times as the radioactive signal continuously weakens. Second, a preliminary study of the reproducibility of ^{18}F-FMISO PET imaging revealed a considerable variability in scans performed 3 days apart in the same patient (199). This variable uptake would complicate radiation dose planning based on hypoxic areas within the tumor (*i.e.,* IMRT and ''dose painting'' strategies, vide infra). However, a recently published report disclosed that reproducible imaging of ^{18}F-FMISO is feasible (208) when using next-generation PET imaging technology with increased sensitivity.

Given the known imaging characteristics of ^{18}F-FMISO, several other molecules utilizing the 2-nitroimidazole scaffold have been developed in an effort to optimize the *in vivo* imaging properties *en route* to developing new PET hypoxia imaging tracers.

b. ^{18}F-fluoroazomycinarabinofuranoside. ^{18}F-fluoroazomycinarabinofuranoside (^{18}F-FAZA) is a hydrophilic (partition coefficient = 1.1) (153), ribose-containing PET hypoxia imaging agent with improved clearance and hypoxia targeting properties. ^{18}F-FAZA diffuses into cells faster than ^{18}F-FMISO (153) and clears from bodily organs more rapidly than ^{18}F-FMISO in preclinical models (219). In humans, the tracer eliminates predominantly *via* hepatic metabolism and biliary excretion as well as urinary excretion. As a result, liver, gallbladder, colon, and kidneys typically exhibit moderate to high tracer uptake. Uptake of ^{18}F-FAZA in the lungs, bone, fat tissue, and brain was reported to be relatively low (250). The accumulation of ^{18}F-FAZA correlates well with PIMO uptake in murine models ($r = 0.41$–0.73 (multiple tumor types); $P < 0.001$) and tumor pO_2 data (30, 194, 269).

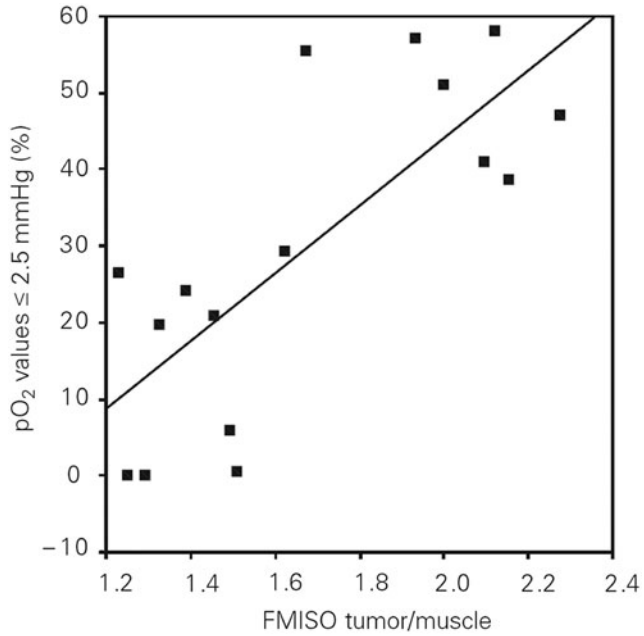

FIG. 8. Correlation between ^{18}F-FMISO tumor-to-muscle ratio and electrode measurements. Reprinted by permission from Gagel *et al.* (96).

^{18}F-FAZA is reported to produce images of adequate quality with T:B ratios ranging from 1.05 to 15.6 among a mixed population of cancer patients (117, 222), comparing favorably against ^{18}F-FMISO (228). ^{18}F-FAZA PET imaging is feasible in H&NC patients (174), showing promise for selecting candidates for TPZ-augmented chemoradiation (228) and IMRT therapy planning (113). However, a recent report found that neither ^{18}F-FAZA nor CA-IX IHC staining was suitable for detecting resectable, high-grade primary prostate tumors (99).

In a recently published report, H&NC patients enrolled into the Danish Head and Neck Cancer Group's (DAHANCA) 24 protocol were imaged with ^{18}F-FAZA before and after treatment, which consisted of primary radiotherapy, nimorzaole, and concomitant cisplatin (196). Using a T:M cut-off of 1.4, 63% of the patients were identified as having hypoxic tumors, with the location of hypoxia remaining generally localized during treatment. ^{18}F-FAZA was associated with poor LRC (93% *vs.* 66%, $p = 0.07$) and DFS (93% *vs.* 60%, $P = 0.04$), and all treatment failures were found in patients with hypoxic tumors. There was a positive correlation between the tracer's uptake in the primary tumor and the lymph node, although some discordance in uptake was reported. Although it is not possible to determine the extent at which nimorazole ameliorated the effects of tumor hypoxia, the results indicate how ^{18}F-FAZA can enable the selection of patients at risk for treatment failure.

c. ^{18}F-EF5 (pentafluorinated etanidazole). It is an ^{18}F-radiolabeled analog of the exogenous hypoxia marker EF-5, and it is the third iteration of the fluorinated ''EF'' etanidazole derivatives. It is characterized by a markedly high lipophilic character (partition coefficient = 5.7) and multiple fluorine atoms (146). Unlike other hypoxia tracers that are designed to possess low lipophilic characteristics, ^{18}F-EF5's high lipophilicity affects a rapid and homogenous distribution throughout all bodily organs, including the brain as confirmed from biodistribution studies in both rodents and humans (176, 299). The increased lipophilicity of ^{18}F-EF5 extends the blood half life to a range of 7.5 to 10 h (176), which is longer than the blood half life of ^{18}F-EF3. From a human patient radiation dosimetry study, ^{18}F-EF5 was reported to be safe for PET imaging (176). The urinary bladder received the highest radiation-absorbed dose (0.12 ± 0.034 mSv/MBq) with an average fractional urinary excretion of 25% over an average of 320 min postinjection (176). The tracer was found to be very stable with the intact tracer being virtually the only radioactive species present in the blood, with polar metabolites being excreted into the urine (146). In rodent tumor models, uptake of ^{18}F-EF5 was low in 9L (oxic) tumors and elevated in large Q7 (hypoxic) tumors, suggesting that the tracer's side chain does not impede the localizing properties of the 2-nitroimidazole pharmacophore (299). ^{18}F-EF5 has recently undergone clinical evaluations in humans showing significant accumulation on head and neck tumors (149) as well as brain malignancies (146). In brain gliomas, areas of increased ^{18}F-EF5 uptake by PET imaging matched areas of increased EF5 binding by IHC staining (88).

d. ^{18}F-flortanidazole. A recently developed tracer of 2-nitroimidazole family was designed to achieve better water solubility and faster background clearance, resulting in improved pharmacokinetic and clearance properties as compared with ^{18}F-FMISO. ^{18}F-flortanidazole (^{18}F-HX4) is a hydrophilic molecule (partition coefficient = 0.21, log P = −0.69) incorporating a polar 1,2,3-triazole moiety within its molecular scaffold. Accordingly, the dosimetry profile of ^{18}F-HX4 is comparable to both ^{18}F-fluorodeoxyglucose (^{18}F-FDG) and ^{18}F-FETNIM; its bio-distribution is characterized not only by reduced brain and heart uptake as compared with ^{18}F-FMISO (74, 148) but also by diminished GI uptake, enabling imaging in the abdominal region. The clearance of ^{18}F-HX4 from normoxic tissues is more rapid than ^{18}F-FMISO, suggesting that PET imaging can be performed at an earlier time point. Its metabolic stability is comparable to ^{18}F-FMISO, with 82% of the tracer intact in human plasma at 135 min postinjection. The *in vivo* uptake of ^{18}F-HX4 has been correlated with hypoxic IHC staining using PIMO in rodents, and its tumor uptake is dependent on tissue oxygenation (75). In patients with lung, thymus, and colon tumors, the observed (T:M) ratios ranged between 0.63 and 1.98 two hours postinjection (272). The uptake of ^{18}F-HX4 among various tumors is highly reproducible, with tumor-to-blood ratios taken from different days correlating well with each other ($r = 0.945$, $P < 0.001$, 90% CI 0.904–0.967). In H&NC patients, ^{18}F-HX4 uptake correlated well with ^{18}F-FMISO uptake, suggesting that both tracers target the same biology (41). In addition, ^{18}F-HX4 demonstrated a better sensitivity and specificity for hypoxia than ^{18}F-FMISO based on CA-IX IHC staining of resected tumors (41).

e. Copper (II) (diacetyl-bis (N4-methylthiosemicarbazone)). Copper (II) (diacetyl-bis (N4-methylthiosemicarbazone)) (Cu-ATSM) is a hypoxia tracer utilizing an oxidation/reduction of chelated copper ion for the selective accumulation into hypoxic tissue (20). Various positron-emitting isotopes of copper can be used: ^{60}Cu ($t_{1/2} = 0.39$ h), ^{61}Cu ($t_{1/2} = 3.33$ h), ^{62}Cu ($t_{1/2} = 0.16$ h), and ^{64}Cu ($t_{1/2} = 12.70$ h). The tracer

has been validated *in vivo* (170) and is currently under clinical investigation. The two major advantages of using Cu-ATSM over 2-nitroimidazole derivatives are the shorter imaging times (as low as 30 min after administration (123)) and a higherT:B ratio despite its relatively lipophilic character [log P = 2.2 (10)]. The tracer tends to accumulate in the liver with moderate accumulation observed in both the kidneys and spleens in humans (156). For the discrimination of hypoxic tumor tissue, CuATSM T:B ratios from 2.0 (38), 3.0 (61), and approximately 4 (123) have been used as hypoxia demarcation thresholds. ^{60}Cu-ATSM has been shown to identify NSCLC patient responders from nonresponders undergoing radiation with or without chemotherapy ($P = 0.002$) (61). The tracer uptake is inversely related to 3 year PFS and OS rates in cervical cancer patients (59, 60).

f. ^{18}F-FDG imaging of hypoxia. As previously mentioned, malignant and hypoxic tumors have increased levels of glucose transporters and hexokinase overexpression, suggesting a link between hypoxia and glucose metabolism. However, ^{18}F-FDG PET imaging, a measure of glucose metabolism, does not distinguish between hypoxic and normoxic tumors when compared against several hypoxia assessment modalities. According to three separate publications, the uptake of ^{18}F-FDG (SUV_{max} or SUV_{mean}) in a combined total of 47 H&NC patients was not correlative against common pO_2 descriptors, including $HP_{2.5}$ and HP_5 as measured by oxygen-sensitive polarographic electrodes (95, 96, 302). While there was a reported trend of increasing ^{18}F-FDG SUVmax values among hypoxic tumors, this relationship was observed only among a small number of patients. A similar discordance between ^{18}F-FDG uptake and ^{18}F-FMISO hypoxia imaging data has also been reported. PET imaging data collected from head and neck, sarcoma, breast cancer, and brain tumors revealed no clear correlation between ^{18}F-FMISO uptake and ^{18}F-FDG uptake (^{18}F-FDG SUV_{mean} in hypoxic tumors [6.2 ± 3.0] *versus* normoxic tumors [6.9 ± 3.2, $P = 0.478$]) (95, 96, 302). While both ^{18}F-FDG and ^{18}F-FMISO are known to identify aggressive tumors, their mechanisms of tumor localization are not clearly linked. Further reports have cited a lack of correlation between ^{18}F-FDG uptake and ^{60}Cu-ATSM uptake in both rectal tumors ($r = 0.4$; $P = 0.9$) (68) and oropharynx carcinomas ($R = 0.50$) (207). The observed lack of correlative uptake between ^{18}F-FDG and $^{60/61}$Cu-ATSM mirrors the reported discordance in uptake between ^{18}F-FMISO and ^{18}F-FDG, despite mechanistic differences between the uptake of $^{60/61}$Cu-ATSM and ^{18}F-FMISO in hypoxic tissue. While ^{18}F-FDG does not appear to be a specific means for assessing tumor hypoxia, its intrinsic value may reside in an ability to help define specific tumor phenotypes that are overtly aggressive, providing mutually complementary information which can be used in conjunction with PET hypoxia data (Fig. 9) (95, 224).

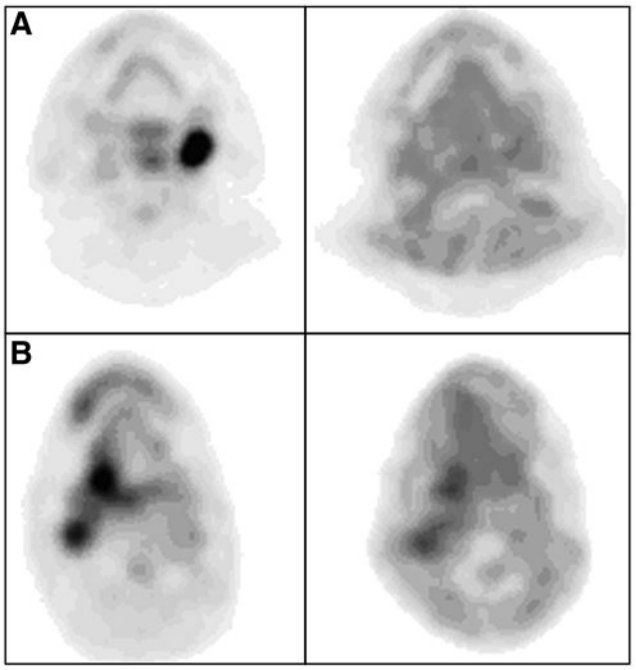

FIG. 9. From left to right: transaxial ^{18}F-FDG PET; transaxial ^{18}F-FMISO PET of head and neck tumors. (A) normoxic ($HP_{2.5} = 13.0\%$; ^{18}F-$FDG_{SUVmean} = 14.80$; ^{18}F-$FMISO_{T/M} = 1.31$). **(B)** hypoxic ($HP_{2.5} = 37.7\%$; ^{18}F-$FDG_{SUVmean} = 8.00$; ^{18}F-$FMISO_{T/M} = 1.60$). Reprinted by permission from Gagel *et al.* (95). ^{18}F-FDG, ^{18}F-fluorodeoxyglucose; $HP_{2.5}$, hypoxic fraction below 2.5 mmHg; SUV, standard uptake value; T/M, tumor to muscle ratio.

IV. Modifying Hypoxia to Improve Therapeutic Outcomes

The poor prognosis associated with tumor hypoxia, especially in head and neck tumors, has led to the development of distinct hypoxia-targeted therapies for the improvement of treatment outcomes. While data from more than 30 distinct clinical trials demonstrates that hypoxic modification improves LRC and disease-free survival for H&NC patients, the reported improvements are generally modest in magnitude (Table 5, Studies I and J) (213, 214). However, despite the overall heterogeneous distribution of tumor hypoxia and the lack of hypoxia assessment in these studies, the improvement in patient outcomes supports the concept that hypoxia remains a relevant therapeutic target.

In retrospect, the lack of hypoxia assessment in these trials (15) has made it difficult to extract the maximal benefit of hypoxia modification therapies for patients, consequently hindering the development of hypoxia modification therapies. The apparent lack of efficacy has also diminished the urgency for future work in this area and stalled efforts to improve outcomes in radiation therapy by overcoming the effects of hypoxia. The development of hypoxia amelioration strategies for patients with radioresistant tumors is an unmet medical need, especially considering the high percentage of cancer patients who undergo radiotherapy as a part of their treatment (211). In recognizing the potential increase in cure rates and OS by coupling radiation therapy with radiosensitizers, the NCI-RTOG recently published strategic guidelines for the early-stage development of radiosensitizers to accelerate drug development with radiation (159).

Recognizing the critical need for hypoxia assessment, recent clinical hypoxia-modification trials have begun to identify patient subgroups according to their hypoxia status. Such hypoxia stratification data now identify patients with hypoxic tumors at risk for treatment failure and reveal how hypoxia-modification therapy benefits patients with hypoxic tumors as evidenced by an overall increase in LRC, DSS, and

local failure free rates. In addition, hypoxia stratification identifies patients with normoxic tumors who, as nonresponders to modification therapy, would forego unnecessary treatment and avoid the negative treatment side effects.

The clinical value in assessing tumor hypoxia now becomes compelling as researchers successfully identify high-risk ''hypoxic'' patient subgroups as candidates for alternate therapy management strategies, which may include hypoxia-modification therapy. The use of biomarkers and functional imaging to identify sensitive or resistive tumor types that link the biological target with a targeted therapy is consistent with a personalized medicine approach. Biomarkers may also aid in the monitoring of therapy to assess the response to therapy. The incorporation of hypoxia assessment for patient stratification can be valuable to radiation oncologists, surgeons, and biotechnology and pharmaceutical companies who are developing tumor hypoxia therapies or other new treatment strategies for treating hypoxic tumors (13, 17, 26, 130, 192, 211, 214, 230).

A. Use of hypoxia information in radiation therapy planning

IMRT is a recently developed radiotherapy technique that incorporates tomographic imaging data to deliver nonuniform radiation intensities to regions of interest within a tumor (38, 169, 221). The imaging information supplied for IMRT planning comes from anatomical tomographic imaging modalities such as MRI and CT, or functional imaging (*i.e.,* metabolic), such as ^{18}F-FDG-PET (46, 112). However, the reported failure mode of IMRT is locoregional recurrence within the clinical tumor volume (57) ascribable to the presence of undetectable radio-resistant hypoxic cells (39, 243). The incorporation of PET hypoxia imaging is uniquely suited for IMRT because of the full utilization of the spatial tomographic PET data for therapy planning. While there is currently no validated hypoxia imaging technique used for IMRT planning, several studies described next used PET hypoxia imaging data to model how dose escalation to hypoxic (radioresistant) regions within a tumor increased tumor control. The use of ^{18}F-FMISO-PET imaging for IMRT planning was first explored by Lee and co-workers in H&NC patients (168). The hypoxic regions delineated by ^{18}F-FMISO-PET received a 20% dose escalation (84 Gy), while nontarget tissue doses were maintained below normal tissue tolerances, making this a feasible strategy for IMRT therapy planning. In a separate study in 10 H&NC patients, IMRT planning and dose escalations using ^{18}F-FMISO PET imaging data was shown to increase tumor control probability by an average of 17% as a result of the modeled dose increases (119). Dose painting by numbers (DPBN), which escalates radiation doses based on the intensity of the ^{18}F-FMISO PET imaging data, enabled additional precision in therapy planning over uniform dose estimates (uniDE) derived from ^{18}F-FDG (265, 266). In this model, the average increase in tumor-control probability (TCP) in 13 patients was $\sim$15% for ^{18}F-FMISO DPBN, which was higher than the 2% increase in tumor control probability for the ^{18}F-FDG uniDE protocol based on modeled dose increases to the hypoxic regions of the tumor. A recent biological modeling study comparing hypoxia dose-painted plans against both standard and uniform dose escalation plans confirms the increases in tumor control probability. A cohort of eight H&NC patients underwent ^{18}F-FMISO PET imaging to define the regions of tumor hypoxia. From the biological modeling analyses, the hypoxia dose plan had higher TCP (93% [hypoxia plan] *vs.* 73% [standard plan]), equivalent normal tissue complication probability, and higher uncomplicated tumor control probability relative to the standard plan (66% [hypoxia plan] *vs.* 48% [standard plan]). Compared with the uniDE plan, the hypoxia plan was equivalent in TCP, but higher in the UTCP (66% [hypoxia plan] *vs.* 37% [uniDE plan]). Consequently, the researchers concluded that the hypoxia plan may have a beneficial impact on the therapeutic ratio. These techniques are still under clinical evaluation and are in need of a validated means for assessing hypoxia to further their development. Fortunately, these techniques are feasible, and demonstrations of increased tumor control probability are a necessary step toward the development and incorporation of these methods into clinical practice.

B. Use of hypoxia assessment for selection of patients responsive to nimorazole

Hypoxic cell sensitizers modify a hypoxic tissue's response to radiation by mimicking oxygen's ability to induce the formation and stabilization of toxic DNA radicals (235). The most common hypoxic sensitizers are based on the 2-nitroimidazole scaffold that can localize into hypoxic regions of tumors and tissues, especially at pO_2 levels below 10 mmHg (111). A meta-analysis of more than 7000 patients treated with nitroimidazole-based radiosensitizers across various tumor types of unknown tumor hypoxia status demonstrated an overall improvement in patient outcomes, including both LRC and OS, with greatest treatment benefit occurring in head and neck tumors (Study I) (213). Subsequent clinical trials of various 2-nitroimidazole analogs performed among an undefined hypoxic population in H&NC has not demonstrated improvements in treatment outcomes, citing both minimal therapeutic efficacy and competing toxic side effects (165, 166, 285).

A notable exception is the DAHANCA study (Fig. 10), which incorporated a less toxic 2-nitroimidazole analog, called nimorazole, as a part of their clinical research radiation treatment protocol (Study K, Table 5). Radiotherapy augmented with nimorazole has been subsequently introduced into clinical practice for treating patients with head and neck tumors in Denmark (217).The incorporation of the nimorazole-based treatment for patients with head and neck tumors may not be beneficial to all H&NC patients, so the question of how nimorazole directly impacts the outcomes of patients with hypoxic tumors remains unanswered. Accordingly, three important retrospective studies using patient data from the nimorazole DAHANCA study have examined whether hypoxia assessment could identify patients with radioresistant tumors who would respond positively to nimorazole-augmented radiotherapy (Table 5, Study K). The first report disclosed by Overgaard and coworkers used plasma OPN levels, an endogenous marker linked to hypoxia, as a means for identifying patients with hypoxic tumors (Fig. 11) (215). Overall, patients with high OPN levels in the placebo group were associated with significantly poorer 5-year outcomes, increased locoregional failure (LRF), and higher disease-specific mortality than the moderate-to-low OPN groups (Fig. 11, column 3). Conversely, patients with high OPN levels receiving nimorazole augmentation had both a lower LRF and disease-specific mortality as compared

Table 5. Hypoxia Modification Trials, Including Trials with Hypoxia Stratification

Study ID (cancer type)	N	*Hypoxia stratification*	*Tx*	*Findings*	P-*value or relative risk*
(I) Nitroimidazole-sensitizer meta analysis(213) (bladder, cervix, head and neck, lung, esophagus, CNS)	7000	None	RT ± Hypoxic sensitizer	LRC OR: 1.17 OS OR: 1.13	0.005 0.02
(J) Hypoxia modification therapy meta-analysis (214) (head and neck)	4805	None	RT ± hypoxia modifier: Normobaric O_2 Hyperbaric O_2 Hypoxic sensitizer	LRF OR: 0.71 DSD OR: 0.73 OD OR: 0.87 DM OR: 0.87	< 0.001 < 0.001 < 0.001 ND
(K) DAHANCA (82, 215, 216, 268) (head and neck)	422	None	RT ± Nimorazole	5 year LRC: 33% (PL) *vs.* 49% (NM) 10 year OS: 16% (PL) *vs.* 26% (NM)	0.002 0.32
	320	OPN: high (> 167 g/L) moderate (69–166 g/L) low (< 68 g/L)		High OPN 5 year LRTF: 79% (PL) *vs.* 42% (NM) 5 year DSM: 79% (PL) *vs.* 49% (NM)	 0.19 RR (95% CI 0.08–0.44) 0.25 RR (95% CI 0.11–0.59)
	386	CA-IX: CA-IX < 1% CA-IX 1%–10% CA-IX 10%–30% CA-IX > 30%		5 year LRC CA-IX < 1%: 35% (PL) *vs.* 47% (NM) CA-IX 1%–10%: 36% (PL) *vs.* 54% (NM) CA-IX 10%–30%: 31% (PL) *vs.* 47% (NM) CA-IX > 30%: 40% (PL) *vs.* 43% (NM)	 0.2 0.4 0.2 0.2
	414	Genetic profiling ''more hypoxic'' (35% of the patients) ''less hypoxic'' (65% of the patients)		''More hypoxic'' group 5 year LRC: 18% (PL) *vs.* 49% (NM) 5 year DSS: 30% (PL) *vs.* 40% (NM) More hypoxic group, HPV^+: 5 year LRC: 47% (PL) *vs.* 62% (NM) More hypoxic group, HPV^- 5 year LRC: 9% (PL) *vs.* 43% (NM)	 0.001 0.04 0.55 0.002

(*continued*)

TABLE 5. (CONTINUED)

Study ID (cancer type)	N	*Hypoxia stratification*	*Tx*	*Findings*	P-*value or relative risk*
(L) Trans-Tasman TROG 98.02 Phase II (229, 230)	122	None	Arm 1: Cisplatin and radiotherapy plus 5-fluorouracil	3 year FFS: 44% (R+C) *vs.* 55% (TPZ)	0.16
				3 year LRF 66% (R+C) *vs.* 84% (TPZ)	0.069
	45	^{18}F-FMISO: signal scored 0 through 4 based on focal uptake relative to background	Arm 2: TPZ with chemoradiotherapy (cisplatin)	Hypoxic patients	
				Increased LRF for R+C (HR=7.1)	0.038
				Increased LRF: R+C *vs.* TPZ (HR=15)	0.001
				Shorter FFS for R+C (HR=3.2)	0.095
				Increased risk of failure/death: R+C *vs.* TPZ (HR=4.7)	0.004
				Shorter OS: R+C *vs.* TPZ (HR=2.45)	0.11
(M) TROG 02.02 HeadSTART Phase III (175, 232)	861	None	Arm 1: Cisplatin and radiotherapy plus 5-fluorouracil	2 year OS: 65.7% (R+C) *vs.* 66.2% (TPZ)	0.53
				2 year FFS: 57% (R+C) *vs.* 56% (TPZ)	0.96
				2 year LRFF: 74% (R+C) *vs.* 75% (TPZ).	0.44
	578	OPN: high (>711 ng/ml), middle (407–710 ng/ml) and low (<407 ng/ml)	Arm 2: TPZ with chemoradiotherapy (cisplatin)	Highest OPN tertile:	
				2 year OS: 66% (R+C) *vs.* 67% (TPZ)	0.67
				LRFF HR: R+C *vs.* TPZ=0.84	0.57
(N) ARCON Phase III (131)	345	None	Accelerated radiotherapy (AR)±ARCON	2 year LRC: 80% (AR) *vs.* 83% (ARCON)	0.80
				5 year LRC: 78% (AR) *vs.* 79% (ARCON)	0.80
				2 year RC: 88% (AR) *vs.* 95% (ARCON)	0.04
				5 year RC: 86% (AR) *vs.* 93% (ARCON)	0.04
				DFS (HR: 0.75, 95% CI, 0.50–1.13)	0.16
				OS (HR: 1.03, 95% CI, 0.73–1.46)	0.86
	79	Pimonidazole: 2.6% cut-off for hypoxia		RC (hypoxic tumors):	
				55% (AR) *vs.* 100% (ARCON)	0.01
				RC (normoxic tumors):	
				92% (AR) *vs.* 96% (ARCON)	0.7
				5 year DFS (hypoxic tumors):	
				40% (AR) *vs.* 86% (ARCON)	0.08

ARCON, accelerated radiotherapy with carbogen and nicotinamide; OR, odds ratio; LRF, locoregional failure; DSD, disease-specific death; DSS, disease-specific survival; OD, overall death; DM, distant metastasis; LRTF, locoregional tumor failure; DSM, disease-specific mortality; HPV, human papillomavirus; ^{18}F-FMISO, ^{18}F-fluoromisonidazole; FFS, failure-free survival; LRFF, locoregional failure free; RC, regional control; RR, relative risk; PL, placebo; AR, accelerated radiotherapy; R, radiation; R+C, radiation plus chemotherapy; NM, nimorazole; RT, radiotherapy; TPZ, tirapazamine; OPN, osteopontin; CA-IX, carbonic anhydrase IX.

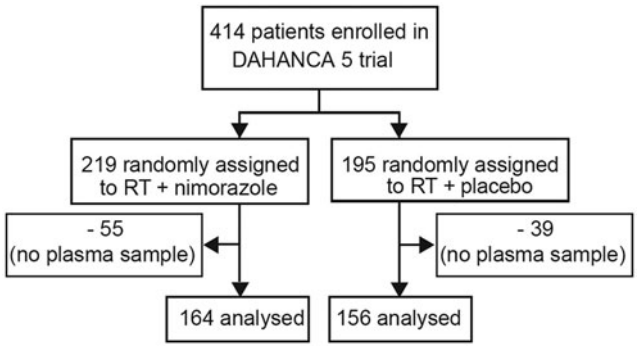

FIG. 10. Danish head and neck cancer group's (DAHNCA) protocol 5 study design. Reprinted by permission from Overgaard *et al.* (215).

with the high OPN placebo group. Based on the stratification information, nimorazole-augmentation offers a clinical means for modifying hypoxia-mediated radioresistance in head and neck tumors, but does not significantly improve treatment outcomes in patients with low to moderate OPN levels. The results from this study clearly indicate a potential therapy decision: H&NC patients with high plasma OPN levels are candidates for nimorazole-supplemented therapy.

In a second analysis, CA-IX expression levels were evaluated in head and neck tumor tissues in an attempt to identify differences in treatment results between the control and nimorazole treated groups, consistent with the purported link between CA-IX expression and tissue hypoxia (82). No significant trend was observed when comparing either treatment group against the various expression levels of CA-IX, and neither a prognostic value nor a predictive value for patients receiving nimorazole was observed. This suggests that tissue CA-IX is not an optimal prognostic marker for H&NC, possibly because it has been found to not correlate well with the hypoxia status as determined by pO_2 measurements (202).

In a third study analysis, patient samples from the DAHANCA study were stratified by using a panel of 15 hypoxia-related genes to determine whether radioresistant tumors could be identified and their hypoxic status could be altered using nimorazole (268). Patients classified as ''more hypoxic'' receiving nimorazole had a significant benefit in both 5 year LRC (Fig. 12, column 1) and 5 year DSS. The effects of nimorazole on the ''less hypoxic'' groups for 5 year LRC and 5 year DSS were not significant. The stratification of patients by their human papillomavirus (HPV) status revealed further outcome information: The effect of nimorazole treatment on the ''more hypoxic'' HPV-negative group showed a large difference in 5 year LRC, indicating that these patients are at high risk for treatment failures (Fig. 13). The remaining groups ''less hypoxic'' HPV-negative/positive and the ''more hypoxic'' HPV-positive did not achieve a statistical difference between the treatment arms. The authors noted that the distribution of tumors being ''more'' or ''less'' hypoxic occurred essentially equally between the HPV-positive and HPV-negative groups, which was consistent with earlier reports noting no statistical relationship between HPV status and

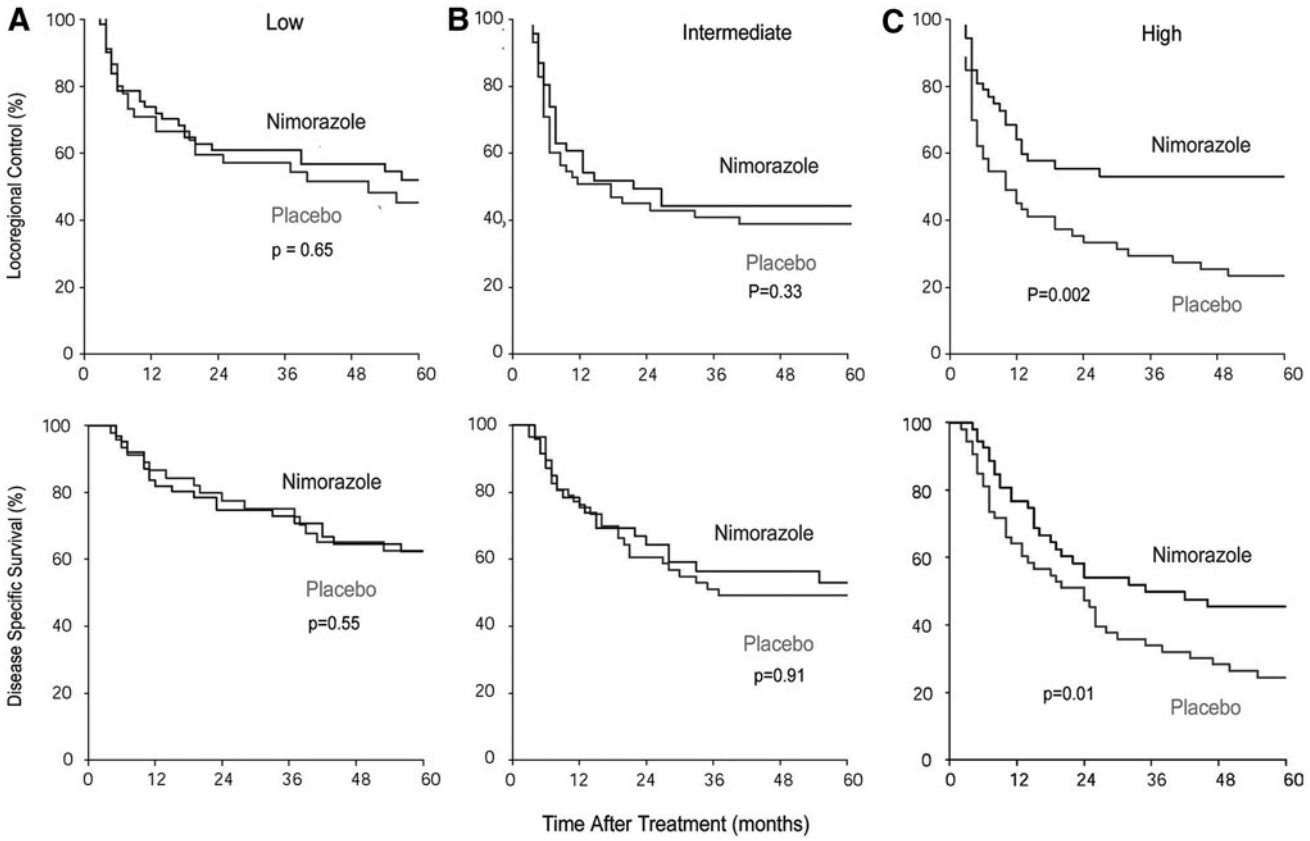

FIG. 11. Primary outcomes by treatment group and concentration of osteopontin. Low **(A)**; Intermediate **(B);** and High osteopontin **(C)**. Reprinted by permission from Overgaard *et al.* (215).

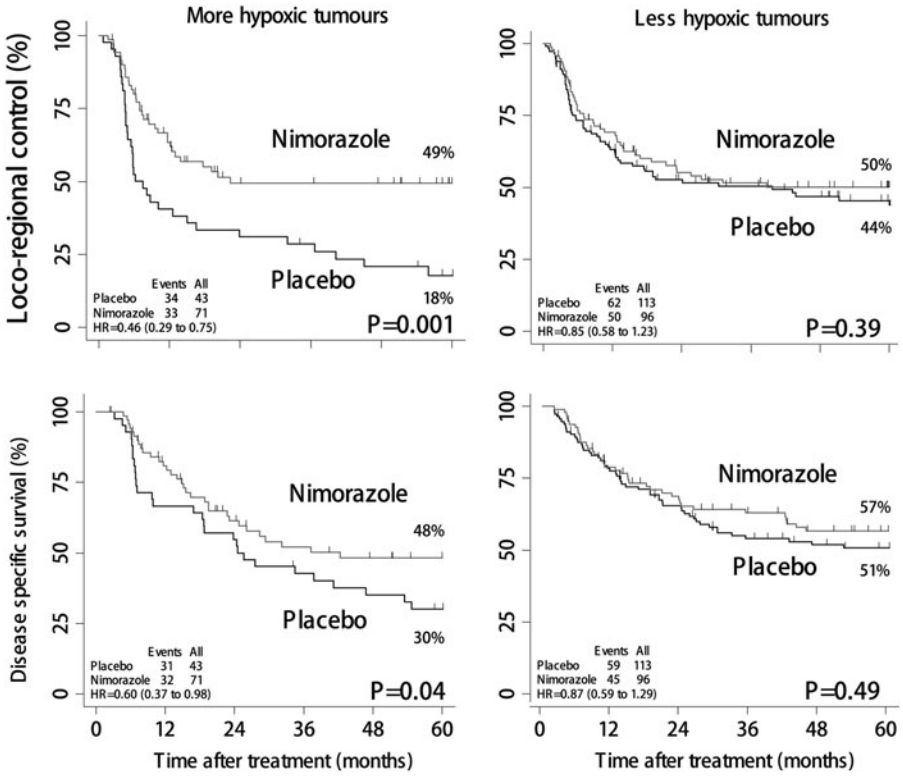

FIG. 12. DAHANCA patients stratified by hypoxia status as determined by a panel of markers. Reprinted by permission from Toustrup *et al.* (268).

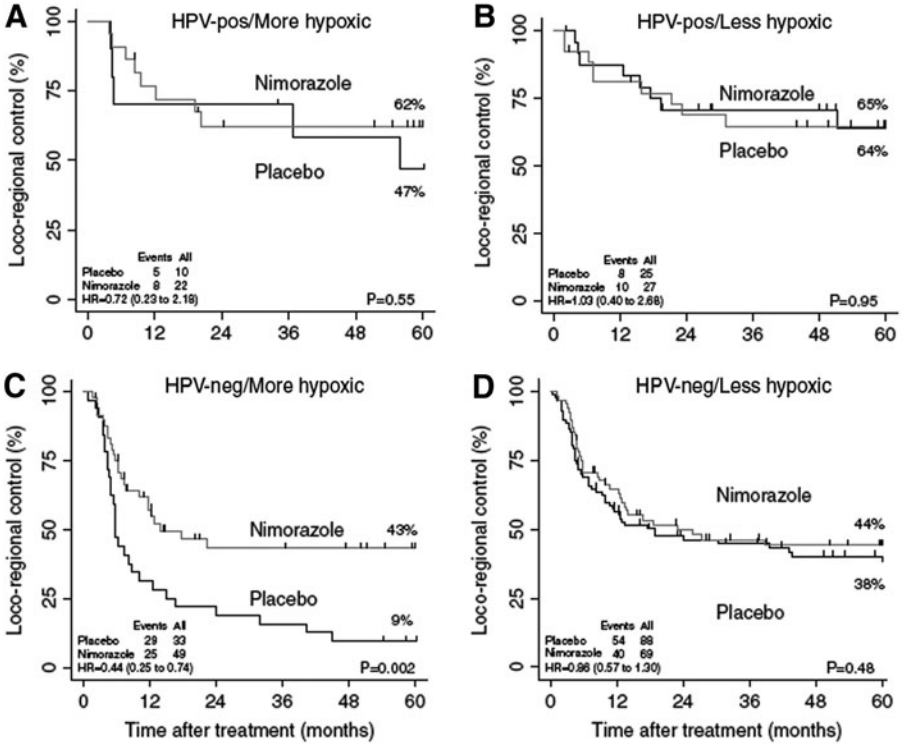

FIG. 13. Correlation between hypoxia [more hypoxic (A, C) *vs.* less hypoxic (B, D)] and HPV [HPV-pos (A, B) *vs.* HPV-neg (C, D)] status in head and neck tumors. Reprinted by permission from Toustrup *et al.* (268). HPV, human papillomavirus.

intratumoral pO_2 levels (151). This analysis supports the hypothesis that HPV-negative patients identified with hypoxic tumors are at high risk for treatment failure and, therefore, candidates for nimorazole supplementation; whereas the other treatment groups are unlikely to receive any additional benefit from nimorazole-supplemented therapy.

C. Use of hypoxia assessment for selection of patients responsive to tirapazamine

Another hypoxic modifier is tirapazamine (TPZ), a cytotoxin that synergistically enhances the cytotoxic effect of cisplatin in hypoxic cells by 1.2 × to 3 × over cisplatin alone (25). As opposed to nimorazole, TPZ does not enhance the effects of radiation, but confers its own toxic effects in hypoxic environments by inducing double-strand DNA breaks. Early phase clinical trials have reported mixed results on the effectiveness of tirapazamine-supplemented chemotherapy in cancer patients (163, 231, 282). Additional clinical studies have focused on using hypoxia detection strategies in an effort to identify patients responsive to tirapazamine-supplemented therapy.

Rischin and co-workers revealed how the detection of intratumoral hypoxia using ^{18}F-FMISO PET imaging illuminated the relationship between tumor hypoxia treatment and local failure for patients treated with chemoradiation therapy with or without TPZ (Table 5, Study L) (229) (Fig. 14). As a sub-study of the promising Phase II TROG 98.02 study (230), ^{18}F-FMISO imaging identified patients with high-risk hypoxic tumors who ultimately performed poorly in the absence of TPZ augmentation. Those patients with hypoxic tumors in the control group (*i.e.,* chemoboost only, no TPZ radiosensitizer) had the lowest complete response rate and were at risk for increased LRF and shorter OS over 6 years (232). Conversely, the complete response rate for hypoxic tumors treated with TPZ was nearly as high as the complete response rate for the normoxic group receiving chemoboost only. Interestingly, patients with baseline hypoxic tumors were more likely to experience distant metastases (8 out of 32) compared with patients with normoxic tumors (1 out of 13) as the cause of first failure. This is consistent with the finding that hypoxia is linked to increased metastatic potential (255). Analysis of this data clearly indicates another potential therapy decision: H&NC patients with hypoxic tumors are candidates for TPZ-supplemented therapy, while normoxic patients would not benefit from such therapy.

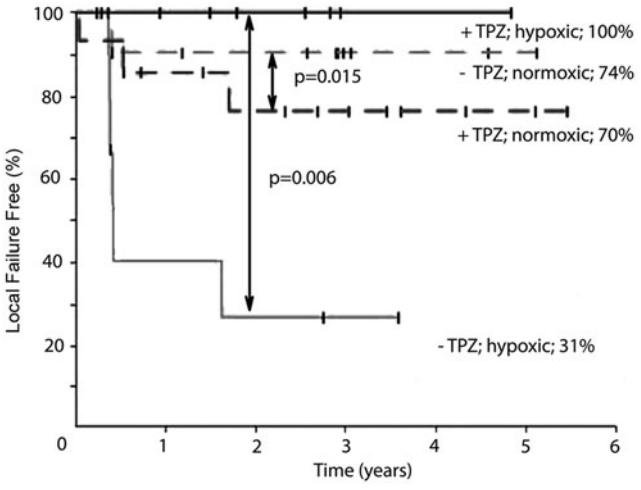

FIG. 14. TPZ treated and untreated patients stratified by the hypoxia status as imaged by ^{18}F-FMISO. Reprinted by permission from Rischin *et al.* (229). TPZ, tirapazamine.

The TROG 02.02 HeadSTART Phase 3 trial (Trans-Tasman Radiation Oncology Group) was designed to examined TPZ augmenting with cisplatin and radiation treatment H&NC patients of unknown hypoxia tumor status (Table 5, Study M). Despite the promising effects of TPZ reported in earlier trials, no evidence of patient benefit of TPZ augmentation was observed for patients in this trial as reported by the 2 year OS, failure-free survival or locoregional failure-free (LRFF) rates (232). The authors noted that it was not possible to determine the maximal effect of TPZ-augmentation on patients without a hypoxia-based diagnostic tool and suggested a PET-based hypoxia imaging approach (225, 229). The authors also suggested that future hypoxia-based treatment trials in H&NC would be worthwhile only if patients were identified as being at high risk for LRF as determined by their hypoxic status (218).

In an attempt to identify high-risk patients with hypoxic tumors, Rischin and co-workers examined the predictive potential of plasma OPN using samples from the previously mentioned TROG 02.02 Phase 3 study (175). Unlike the results from the DAHANCA study, there were no associated differences between the treatment groups (cisplatin *vs.* TPZ) as determined by the 2-year OS or LRFF rates. The discrepancy in these results as compared with the DAHANCA results (vide supra) were rationalized on the basis of the different treatment protocols, that is, chemoradiotherapy in the HeadSTART trial as opposed to radiation therapy alone used in the DAHANCA study. In addition, the authors cited the lack of a standardized procedure for assigning high, middle and low OPN thresholds for separating patients into the various hypoxia groups. The discordant results of this study highlight the complicated nature of defining hypoxia, especially when using endogenous biomarkers (168).

D. Use of hypoxia assessment for selection of patients responsive to oxygen delivery therapies

Oxygen delivery therapies are designed to increase local oxygen concentration in hypoxic tumors (116). One method for improving intra-tumor oxygenation is through the normalization of tumor vasculature, which transiently improves oxygenation and creates a therapeutic window of increased treatment sensitization (32). Historically, several therapeutics were developed to inactivate VEGF by halting angiogenesis and isolating the tumor from a recurring blood supply. Unfortunately, prolonged inhibition of vessel growth using such therapies triggered an adaptation response to treatment, causing poor treatment efficacy. However, there is an initial transient normalization of tumor vessels during anti-angiogenic therapy that is characterized by improved blood flow, increased local oxygenation concentration, and enhanced tumor treatment sensitivity. In addition, by repairing leaky vasculature, both tumor cell intravasation and extravasation are considerably reduced, lowering the propensity for metastatic formation. Selective targeting of critical proteins, including VEGF, VEGF receptor 2 (VEGFR2) (290), regulator of G-protein signaling 5 (RGS5) (115), angiopoietin-2 (ANG2) (35), placenta growth factor (PlGF) (234), and prolyl hydroxylase domain protein 2 (PHD2)

(189), is known to lead to transient improvements in vascular function, including the stabilization or amelioration of tumor hypoxia. Up-regulation of proteins involved with endothelial cell function, including angiopoietin-1 (ANG1) (267), semaphorin 3A (Sema3A) (185), and PTEN (114), also lead to tumor vessel stabilization and decreased tumor hypoxia. Since the reduction of hypoxia is transient, it becomes critical to identify opportune states of oxygenation for maximizing treatment efficacy. Vessel normalization, rather than destruction, is a new therapeutic strategy for treating cancer (32), and its combination with hypoxia modification therapies may usher in a new paradigm for treating hypoxic tumors.

Several preclinical studies have investigated the transient improvement of tumor vessel normalization and comparing treatment regimens based on changes in vessel normalization and hypoxia in an effort to improve outcomes. Across several different human tumor cell lines, including gliomas, mammary ovary, and melanoma carcinomas, VEGF-targeting therapies, including antibodies (*e.g.,* DC-101, bevacizumab) and kinase inhibitors (*e.g.,* sunitinib and semaxanib), create a transient vessel normalization window, leading to improvements in vessel function and a concomitant decrease in hypoxia as assessed by PIMO, PET imaging, or pO_2 electrode measurements (69, 78, 271, 290). In addition, supplemental radiation therapy administered during this normalization window decreases in tumor growth compared with radiation administered outside the normalization window ($P < 0.05$), ascribable to a transient decrease of hypoxia. The treatment of hypoxic squamous cell carcinoma xenografts with the EGFR inhibitor erlotinib resulted in decreased tumor hypoxia with a concomitant increase in tumor vascular normalization and blood flow, which enhanced the effect of adjuvant treatment using either cisplatin or radiation therapy (34). Paclitaxel has also been reported to also induce vessel normalization in hypoxic liver tumors, leading to a decrease in hypoxia assessed by EPR (55). Mice treated with combined paclitaxel and radiation therapy outperformed mice receiving monotherapy ($P < 0.01$), suggesting a synergistic treatment effect made possible through vessel normalization and tumor oxygenation.

Given the unique molecular signaling that affects vessel normalization and tumor oxygen, unique molecular targets may identify new therapeutic strategies that improve treatment outcomes. A recent report describes inducing tumor vessel normalization and reversing tumor hypoxia during treatment by activating endothelial PTEN, an enzyme that inhibits PI3K and leads to tumor vessel normalization (141). The administration of inositoltrispryrophosphate (ITPP) in combination with paclitaxel and cisplatine decreased tumor size (0.5 g [treated] *vs.* 2.5 g [un-treated]) with no visible signs of metastatic invasion in nearby organs. Tumor pO_2 measurements, PIMO staining, and ^{18}F-FMISO PET imaging confirmed an increase in pO_2 levels after the administration of ITPP, suggesting a normalization of tumor function and creation of a normalization window for treatment. MRI imaging revealed vessel reorganization, and CD31 staining was better delineated in treated tumors compared with nontreated tumors, which was consistent with the effects of vessel normalization. PCR analysis showed a strong down-regulation of hypoxia-related mRNAs for HIF-1 and HIF-2 along with a reduction of PHD-2 protein. There was also an enhancement of CD31, VEGFR1, and VEGFR2 mRNAs, which was consistent with the notion of vessel maturation. Although still in preclinical development, emerging treatment strategies that improve vessel growth, reduce tumor hypoxia, and improve the effectiveness of chemo- and radiotherapy may lead to new treatment paradigms for improving outcomes in patients with hypoxic tumors. Identifying the normalization window in cancer patients using perfusion and hypoxia assessment

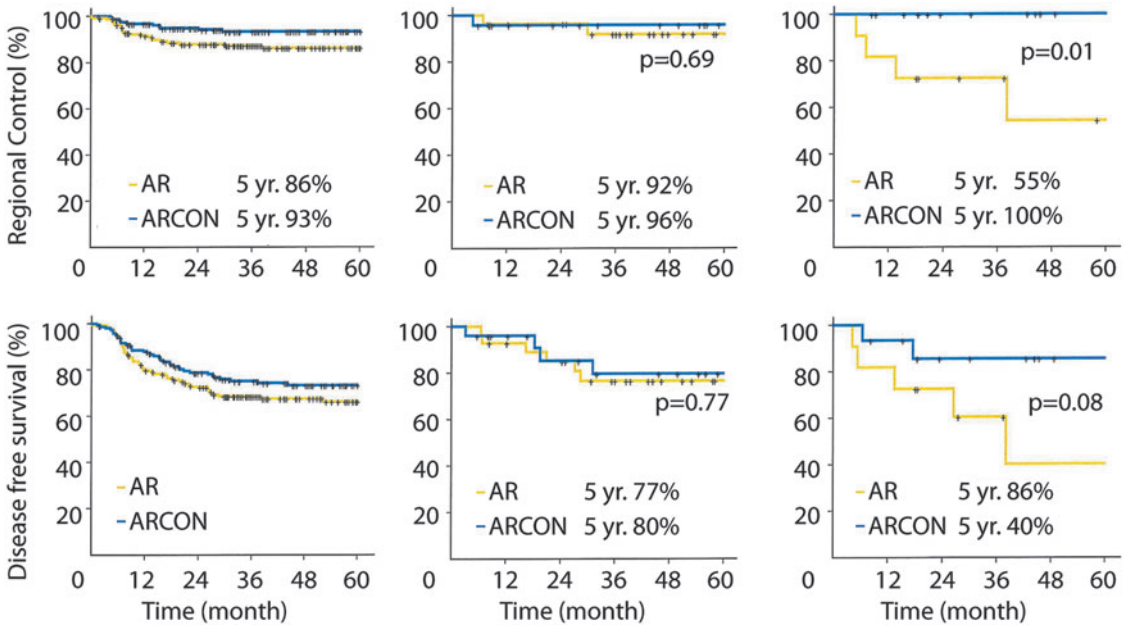

FIG. 15. Kaplan–Meier curves for mixed population, normoxic patients, and hypoxic patients only. [1]Hypoxia information was not used in these analyses. [2]Patients were assigned their hypoxia status based on PIMO staining from tumor biopsy samples. Reprinted by permission from Janssens *et al.* (131). AR, accelerated radiotherapy; ARCON, accelerated radiotherapy with carbogen and nicotinamide.

techniques will aid in the transition of this therapeutic strategy into clinical practice.

Another method for improving intra-tumor oxygenation is through vasodilatation that is achievable by combining carbogen inhalation with the administration of nicotinamide. ARCON couples carbogen and nicotinamide treatments with accelerated radiotherapy (AR). ARCON therapy was studied in H&NC patients in a Phase 2 clinical trial in which high local and regional control rates ($>80\%$) were achieved in patients with advanced stage squamous cell carcinomas of unknown hypoxic status in the larynx and oropharynx; however, other tumor types such as oral cavity (37%) were still poorly controlled (135).

Due to the high LRC rates (80%) observed for patients with larynx carcinomas receiving ARCON treatment, researchers proceeded with a multi-center Phase 3 trial comparing AR against ARCON (Table 5, Study N). Given the importance of hypoxia information in understanding the effects of hypoxia-modification therapy, a sub-study of this trial gathered tumor hypoxia data from tumor biopsies using PIMO staining. For the entire patient population (lacking hypoxia assessment), there were no significant differences for patients with regard to the 2- and 5-year LCRs or in the DFS or OS rates, suggesting that ARCON treatment did not provide a significant patient benefit relative to AR (Fig. 15, column 1) (131).

However, when the sub-group data were analyzed using tumor hypoxia information, an obvious difference in the response rates emerged between the AR and ARCON treatment arms. There was a significant improvement in regional control in the high hypoxia group treated with ARCON Figure 15, column 3). A similar trend was observed for the hypoxia group treated with ARCON, resulting in improved 5 year DFS as compared with the AR group. In addition, the patient group with hypoxic tumors was at high risk for treatment failures as evidenced by their depressed regional control and DFS percentages. ARCON treatment had little effect on patients with normoxic tumors, as there was no statistical difference in regional control or DFS in either treatment regimen (cf. Fig. 15, column 2). The authors noted that selecting patients based on the treatment mechanism is critical, as the hypoxia status determination revealed those patients more likely to experience improved outcomes when receiving ARCON treatment. In summary, the analysis of the ARCON data supports the application of hypoxia assessment for both patient selection and therapy decisions: Patients assessed early for hypoxic head and neck tumors are candidates for ARCON therapy, while normoxic patients would not experience a benefit from this therapy.

V. Concluding Remarks

Tumor hypoxia is a well-established biological phenomenon that is often present in malignant solid tumors, including tumors of head and neck, cervix, breast, prostate, and lung. Tumor hypoxia disperses heterogeneously, and is independent of tumor size, stage, grade, or histology. Hypoxic tumors employ several different survival mechanisms, which may result in a loss of apoptotic potential, increased proliferative potential, and formation of new blood vessels that encourages the evolutionary selection for a more malignant phenotype. As such, hypoxia affects the curability of solid tumors, regardless of treatment modality.

Given the compelling link between tumor hypoxia and negative treatment outcomes, clinical research has turned to studying the effectiveness of hypoxia-targeted therapies. However, several trials lacked an appropriate method for accurately identifying and selecting patient subgroups with hypoxic tumors. As a result, the indiscriminate use of hypoxia-modification therapy, as evidenced by several meta-analyses, showed marginal benefits of such therapy when given to a patient population having both normoxic and hypoxic tumors. Due to the invasive nature of the ''gold standard'' method for measuring tumor oxygenation (pO_2 electrode measurements), hypoxia-based patient stratification has not been readily adopted into clinical practice. Sponsors currently face the choice of either enrolling both tumor types in their clinical trials, which will dilute their efficacy results and threaten the success of the trial, or utilizing an unapproved diagnostic tool (*e.g.,* hypoxia PET imaging) for selecting patients with hypoxic tumors. This situation impedes the clinical development of hypoxia-based therapies. Several studies, including recent secondary analyses from larger trials, suggest that hypoxia assessment is predictive for outcomes and can identify high-risk patients in need of treatment modification.

Given the negative treatment and outcome problems associated with tumor hypoxia, a major goal for clinicians has been to identify hypoxic tumors through a number of different diagnostic approaches. The polarographic electrode has emerged as the ''gold standard'' for detecting and characterizing hypoxia, which enabled clinical studies to establish the significance of tumor hypoxia in patients. The presence of tumor hypoxia is prognostic for LRC and OS in cervix, breast, lung, prostate, and H&NC supported by data from more than 2000 patients. However, despite its ability to generate prognostic data, the use of polarographic electrodes is not viable for the widespread clinical assessment of tumor hypoxia given the technical limitations of this instrument. Several different methods for assessing tumor hypoxia have evolved and replaced polarographic pO_2 measurements. These modalities, either individually or in combination with other modalities, provide functional and physiological information on tumor hypoxia that has prognostic and predictive value.

There is an acute need for an approved diagnostic technology for determining the hypoxia status of cancer lesions, as it would enable the clinical development of personalized, hypoxia-based therapies, which will, ultimately, improve outcomes. The assessment of tumor hypoxia will be valuable to radiation oncologists, surgeons, and biotechnology and pharmaceutical companies who are engaged in developing hypoxia-based therapies or treatment strategies.

Acknowledgments

The authors would like to thank Helen Su and Katrin Szardenings for both helpful discussions and proofreading this article.

Author Disclosure Statement

Joseph C. Walsh is an employee of Siemens MI, a company that developed PET biomarkers for imaging hypoxia. Artem Lebedev and Hartmuth C. Kolb are former employees of Siemens MI. Kathleen Madsen is a consultant statistician to Siemens Molecular Imaging, with compensation based on fair market value and not tied to outcomes. Edward Aten is

acting as Interim Medical Director to Siemens Molecular Imaging, with compensation based on fair market value and not tied to outcomes. Liane Marciano is a consultant to Siemens Molecular Imaging, with compensation based on fair market value and not tied to outcomes.

References

1. Adam MF, Gabalski EC, Bloch DA, Oehlert JW, Brown JM, Elsaid AA, Pinto HA, and Terris DJ. Tissue oxygen distribution in head and neck cancer patients. *Head Neck* 21: 146–153, 1999.
2. Adams GE, Ahmed I, Sheldon PW, and Stratford IJ. Radiation sensitization and chemopotentiation: RSU 1069, a compound more efficient than misonidazole *in vitro* and *in vivo*. *Br J Cancer* 49: 571–577, 1984.
3. Airley RE, Loncaster J, Raleigh JA, Harris AL, Davidson SE, Hunter RD, West CM, and Stratford IJ. GLUT-1 and CAIX as intrinsic markers of hypoxia in carcinoma of the cervix: relationship to pimonidazole binding. *Int J Cancer* 104: 85–91, 2003.
4. Aquino-Parsons C, Luo C, Vikse CM, and Olive PL. Comparison between the comet assay and the oxygen microelectrode for measurement of tumor hypoxia. *Radiother Oncol* 51: 179–185, 1999.
5. Arteel GE, Thurman RG, Yates JM, and Raleigh JA. Evidence that hypoxia markers detect oxygen gradients in liver: pimonidazole and retrograde perfusion of rat liver. *Br J Cancer* 72: 889–895, 1995.
6. Baba Y, Nosho K, Shima K, Irahara N, Chan AT, Meyerhardt JA, Chung DC, Giovannucci EL, Fuchs CS, and Ogino S. HIF1A overexpression is associated with poor prognosis in a cohort of 731 colorectal cancers. *Am J Pathol* 176: 2292–2301, 2010.
7. Bache M, Kappler M, Said HM, Staab A, and Vordermark D. Detection and specific targeting of hypoxic regions within solid tumors: current preclinical and clinical strategies. *Curr Med Chem* 15: 322–338, 2008.
8. Bache M, Kappler M, Wichmann H, Rot S, Hahnel A, Greither T, Said HM, Kotzsch M, Wurl P, Taubert H, and Vordermark D. Elevated tumor and serum levels of the hypoxia-associated protein osteopontin are associated with prognosis for soft tissue sarcoma patients. *BMC Cancer* 10: 132, 2010.
9. Bache M, Reddemann R, Said HM, Holzhausen HJ, Taubert H, Becker A, Kuhnt T, Hansgen G, Dunst J, and Vordermark D. Immunohistochemical detection of osteopontin in advanced head-and-neck cancer: prognostic role and correlation with oxygen electrode measurements, hypoxia-inducible-factor-1alpha-related markers, and hemoglobin levels. *Int J Radiat Oncol Biol Phys* 66: 1481–1487, 2006.
10. Basken NE and Green MA. Cu(II) bis(thiosemicarbazone) radiopharmaceutical binding to serum albumin: further definition of species dependence and associated substituent effects. *Nucl Med Biol* 36: 495–504, 2009.
11. Baudelet C and Gallez B. How does blood oxygen level-dependent (BOLD) contrast correlate with oxygen partial pressure (pO2) inside tumors? *Magn Reson Med* 48: 980–986, 2002.
12. Beasley NJ, Leek R, Alam M, Turley H, Cox GJ, Gatter K, Millard P, Fuggle S, and Harris AL. Hypoxia-inducible factors HIF-1alpha and HIF-2alpha in head and neck cancer: relationship to tumor biology and treatment outcome in surgically resected patients. *Cancer Res* 62: 2493–2497, 2002.
13. Bennewith KL and Dedhar S. Targeting hypoxic tumour cells to overcome metastasis. *BMC Cancer* 11: 504, 2011.
14. Bentzen L, Keiding S, Nordsmark M, Falborg L, Hansen SB, Keller J, Nielsen OS, and Overgaard J. Tumour oxygenation assessed by 18F-fluoromisonidazole PET and polarographic needle electrodes in human soft tissue tumours. *Radiother Oncol* 67: 339–344, 2003.
15. Betensky RA, Louis DN, and Cairncross JG. Influence of unrecognized molecular heterogeneity on randomized clinical trials. *J Clin Oncol* 20: 2495–2499, 2002.
16. Betof AS, Rabbani ZN, Hardee ME, Kim SJ, Broadwater G, Bentley RC, Snyder SA, Vujaskovic Z, Oosterwijk E, Harris LN, Horton JK, Dewhirst MW, and Blackwell KL. Carbonic anhydrase IX is a predictive marker of doxorubicin resistance in early-stage breast cancer independent of HER2 and TOP2A amplification. *Br J Cancer* 106: 916–922, 2012.
17. Bollineni VR, Wiegman EM, Pruim J, Groen HJ, and Langendijk JA. Hypoxia imaging using positron emission tomography in non-small cell lung cancer: implications for radiotherapy. *Cancer Treat Rev* 38: 1027–1032, 2012.
18. Bourke VA, Zhao D, Gilio J, Chang CH, Jiang L, Hahn EW, and Mason RP. Correlation of radiation response with tumor oxygenation in the Dunning prostate R3327-AT1 tumor. *Int J Radiat Oncol Biol Phys* 67: 1179–1186, 2007.
19. Boushel R, Langberg H, Olesen J, Gonzales-Alonzo J, Bulow J, and Kjaer M. Monitoring tissue oxygen availability with near infrared spectroscopy (NIRS) in health and disease. *Scand J Med Sci Sports* 11: 213–222, 2001.
20. Bowen SR, van der Kogel AJ, Nordsmark M, Bentzen SM, and Jeraj R. Characterization of positron emission tomography hypoxia tracer uptake and tissue oxygenation via electrochemical modeling. *Nucl Med Biol* 38: 771–780, 2011.
21. Brizel DM, Dodge RK, Clough RW, and Dewhirst MW. Oxygenation of head and neck cancer: changes during radiotherapy and impact on treatment outcome. *Radiother Oncol* 53: 113–117, 1999.
22. Brizel DM, Prosnitz RG, Hunter S, Fisher SR, Clough RL, Downey MA, and Scher RL. Necessity for adjuvant neck dissection in setting of concurrent chemoradiation for advanced head-and-neck cancer. *Int J Radiat Oncol Biol Phys* 58: 1418–1423, 2004.
23. Brizel DM, Scully SP, Harrelson JM, Layfield LJ, Bean JM, Prosnitz LR, and Dewhirst MW. Tumor oxygenation predicts for the likelihood of distant metastases in human soft tissue sarcoma. *Cancer Res* 56: 941–943, 1996.
24. Brockton N, Dort J, Lau H, Hao D, Brar S, Klimowicz A, Petrillo S, Diaz R, Doll C, and Magliocco A. High stromal carbonic anhydrase IX expression is associated with decreased survival in P16-negative head-and-neck tumors. *Int J Radiat Oncol Biol Phys* 80: 249–257, 2011.
25. Brown JM. The hypoxic cell: a target for selective cancer therapy—eighteenth and Bruce F. Cain Memorial Award lecture. *Cancer Res* 59: 5863–5870, 1999.
26. Brown JM, Diehn M, and Loo BW, Jr. Stereotactic ablative radiotherapy should be combined with a hypoxic cell radiosensitizer. *Int J Radiat Oncol Biol Phys* 78: 323–327, 2010.
27. Brown JM and Wilson WR. Exploiting tumour hypoxia in cancer treatment. *Nat Rev Cancer* 4: 437–447, 2004.

28. Bruehlmeier M, Roelcke U, Schubiger PA, and Ametamey SM. Assessment of hypoxia and perfusion in human brain tumors using PET with 18F-fluoromisonidazole and 15O-H2O. *J Nucl Med* 45: 1851–1859, 2004.
29. Burgman P, Odonoghue JA, Humm JL, and Ling CC. Hypoxia-Induced increase in FDG uptake in MCF7 cells. *J Nucl Med* 42: 170–175, 2001.
30. Busk M, Horsman MR, Jakobsen S, Keiding S, van der Kogel AJ, Bussink J, and Overgaard J. Imaging hypoxia in xenografted and murine tumors with 18F-fluoroazomycin arabinoside: a comparative study involving microPET, autoradiography, PO2-polarography, and fluorescence microscopy. *Int J Radiat Oncol Biol Phys* 70: 1202–1212, 2008.
31. Canning MT, Postovit LM, Clarke SH, and Graham CH. Oxygen-mediated regulation of gelatinase and tissue inhibitor of metalloproteinases-1 expression by invasive cells. *Exp Cell Res* 267: 88–94, 2001.
32. Carmeliet P and Jain RK. Principles and mechanisms of vessel normalization for cancer and other angiogenic diseases. *Nat Rev Drug Discov* 10: 417–427, 2011.
33. Casey G. Oxygen transport and the use of pulse oximetry. *Nurs Stand* 15: 46–53, 2001.
34. Cerniglia GJ, Pore N, Tsai JH, Schultz S, Mick R, Choe R, Xing X, Durduran T, Yodh AG, Evans SM, Koch CJ, Hahn SM, Quon H, Sehgal CM, Lee WM, and Maity A. Epidermal growth factor receptor inhibition modulates the microenvironment by vascular normalization to improve chemotherapy and radiotherapy efficacy. *PLoS One* 4: e6539, 2009.
35. Chae SS, Kamoun WS, Farrar CT, Kirkpatrick ND, Niemeyer E, de Graaf AM, Sorensen AG, Munn LL, Jain RK, and Fukumura D. Angiopoietin-2 interferes with anti-VEGFR2-induced vessel normalization and survival benefit in mice bearing gliomas. *Clin Cancer Res* 16: 3618–3627, 2010.
36. Chang J, Wen B, Kazanzides P, Zanzonico P, Finn RD, Fichtinger G, and Ling CC. A robotic system for 18F-FMISO PET-guided intratumoral pO2 measurements. *Med Phys* 36: 5301–5309, 2009.
37. Chang Q, Jurisica I, Do T, and Hedley DW. Hypoxia predicts aggressive growth and spontaneous metastasis formation from orthotopically grown primary xenografts of human pancreatic cancer. *Cancer Res* 71: 3110–3120, 2011.
38. Chao KS, Bosch WR, Mutic S, Lewis JS, Dehdashti F, Mintun MA, Dempsey JF, Perez CA, Purdy JA, and Welch MJ. A novel approach to overcome hypoxic tumor resistance: Cu-ATSM-guided intensity-modulated radiation therapy. *Int J Radiat Oncol Biol Phys* 49: 1171–1182, 2001.
39. Chao KS, Ozyigit G, Tran BN, Cengiz M, Dempsey JF, and Low DA. Patterns of failure in patients receiving definitive and postoperative IMRT for head-and-neck cancer. *Int J Radiat Oncol Biol Phys* 55: 312–321, 2003.
40. Chapman JD, Franko AJ, and Sharplin J. A marker for hypoxic cells in tumours with potential clinical applicability. *Br J Cancer* 43: 546–550, 1981.
41. Chen L, Zhang Z, Kolb HC, Walsh JC, Zhang J, and Guan Y. 18F-HX4 hypoxia imaging with PET/CT in head and neck cancer: a comparison with (18)F-FMISO. *Nucl Med Commun* 33: 1096–1102, 2012.
42. Chen YJ, Wei YY, Chen HT, Fong YC, Hsu CJ, Tsai CH, Hsu HC, Liu SH, and Tang CH. Osteopontin increases migration and MMP-9 up-regulation via alphavbeta3 integrin, FAK, ERK, and NF-kappaB-dependent pathway in human chondrosarcoma cells. *J Cell Physiol* 221: 98–108, 2009.
43. Chia SK, Wykoff CC, Watson PH, Han C, Leek RD, Pastorek J, Gatter KC, Ratcliffe P, and Harris AL. Prognostic significance of a novel hypoxia-regulated marker, carbonic anhydrase IX, in invasive breast carcinoma. *J Clin Oncol* 19: 3660–3668, 2001.
44. Chiche J, Brahimi-Horn MC, and Pouyssegur J. Tumour hypoxia induces a metabolic shift causing acidosis: a common feature in cancer. *J Cell Mol Med* 14: 771–794, 2010.
45. Choe R and Yodh AG. *Diffuse Optical Tomography of the Breast.* Valencia, CA: American Scientific Publishers, 2006, p. 600.
46. Chong LM and Hunt MA. *IMRT for Head and Neck Cancer.* Madison, WI: Medical Physics Publishing, 2003.
47. Chopra S, Foltz WD, Milosevic MF, Toi A, Bristow RG, Menard C, and Haider MA. Comparing oxygen-sensitive MRI (BOLD R2*) with oxygen electrode measurements: a pilot study in men with prostate cancer. *Int J Radiat Biol* 85: 805–813, 2009.
48. Choyke PL, Dwyer AJ, and Knopp MV. Functional tumor imaging with dynamic contrast-enhanced magnetic resonance imaging. *J Magn Reson Imaging* 17: 509–520, 2003.
49. Clark LC, Jr., Ackerman JL, Thomas SR, Millard RW, Hoffman RE, Pratt RG, Ragle-Cole H, Kinsey RA, and Janakiraman R. Perfluorinated organic liquids and emulsions as biocompatible NMR imaging agents for 19F and dissolved oxygen. *Adv Exp Med Biol* 180: 835–845, 1984.
50. Collet G, Skrzypek K, Grillon C, Matejuk A, Hafni-Rhabi BE, Lamerant N, and Kieda C. Hypoxia control to normalize pathologic angiogenesis: potential role for endothelial precursor cells and miRNAs regulation. *Vascul Pharmacol* 56: 252–261, 2012.
51. Collingridge DR, Piepmeier JM, Rockwell S, and Knisely JP. Polarographic measurements of oxygen tension in human glioma and surrounding peritumoural brain tissue. *Radiother Oncol* 53: 127–131, 1999.
52. Conley SJ, Gheordunescu E, Kakarala P, Newman B, Korkaya H, Heath AN, Clouthier SG, and Wicha MS. Antiangiogenic agents increase breast cancer stem cells via the generation of tumor hypoxia. *Proc Natl Acad Sci U S A* 109: 2784–2789.
53. Cooper RA, Carrington BM, Loncaster JA, Todd SM, Davidson SE, Logue JP, Luthra AD, Jones AP, Stratford I, Hunter RD, and West CM. Tumour oxygenation levels correlate with dynamic contrast-enhanced magnetic resonance imaging parameters in carcinoma of the cervix. *Radiother Oncol* 57: 53–59, 2000.
54. Dai N, Bao Q, Lu A, and Li J. Protein expression of osteopontin in tumor tissues is an independent prognostic indicator in gastric cancer. *Oncology* 72: 89–96, 2007.
55. Danhier F, Danhier P, Magotteaux N, De Preter G, Ucakar B, Karroum O, Jordan B, Gallez B, and Preat V. Electron paramagnetic resonance highlights that the oxygen effect contributes to the radiosensitizing effect of paclitaxel. *PLoS One* 7: e40772, 2012.
56. Davda S and Bezabeh T. Advances in methods for assessing tumor hypoxia *in vivo*: implications for treatment planning. *Cancer Metastasis Rev* 25: 469–480, 2006.
57. Dawson LA, Anzai Y, Marsh L, Martel MK, Paulino A, Ship JA, and Eisbruch A. Patterns of local-regional recurrence following parotid-sparing conformal and segmental intensity-modulated radiotherapy for head and neck cancer. *Int J Radiat Oncol Biol Phys* 46: 1117–1126, 2000.

58. Dean M, Fojo T, and Bates S. Tumour stem cells and drug resistance. *Nat Rev Cancer* 5: 275–284, 2005.
59. Dehdashti F, Grigsby PW, Lewis JS, Laforest R, Siegel BA, and Welch MJ. Assessing tumor hypoxia in cervical cancer by PET with 60Cu-labeled diacetyl-bis(N4-methylthiosemicarbazone). *J Nucl Med* 49: 201–205, 2008.
60. Dehdashti F, Grigsby PW, Mintun MA, Lewis JS, Siegel BA, and Welch MJ. Assessing tumor hypoxia in cervical cancer by positron emission tomography with 60Cu-ATSM: relationship to therapeutic response-a preliminary report. *Int J Radiat Oncol Biol Phys* 55: 1233–1238, 2003.
61. Dehdashti F, Mintun MA, Lewis JS, Bradley J, Govindan R, Laforest R, Welch MJ, and Siegel BA. *In vivo* assessment of tumor hypoxia in lung cancer with 60Cu-ATSM. *Eur J Nucl Med Mol Imaging* 30: 844–850, 2003.
62. Dence CS, Ponde DE, Welch MJ, and Lewis JS. Autoradiographic and small-animal PET comparisons between (18)F-FMISO, (18)F-FDG, (18)F-FLT and the hypoxic selective (64)Cu-ATSM in a rodent model of cancer. *Nucl Med Biol* 35: 713–720, 2008.
63. Dengler J, Frenzel C, Vajkoczy P, Wolf S, and Horn P. Cerebral tissue oxygenation measured by two different probes: challenges and interpretation. *Intensive Care Med* 37: 1809–1815, 2011.
64. Dent JG and Netter KJ. Errors in oxygen tension measurements caused by halothane. *Br J Anaesth* 48: 195–197, 1976.
65. Di Martino EF, Gagel B, Schramm O, Maneschi P, and Westhofen M. Evaluation of tumor oxygenation by color duplex sonography: a new approach. *Otolaryngol Head Neck Surg* 132: 765–769, 2005.
66. Diehn M, Cho RW, Lobo NA, Kalisky T, Dorie MJ, Kulp AN, Qian D, Lam JS, Ailles LE, Wong M, Joshua B, Kaplan MJ, Wapnir I, Dirbas FM, Somlo G, Garberoglio C, Paz B, Shen J, Lau SK, Quake SR, Brown JM, Weissman IL, and Clarke MF. Association of reactive oxygen species levels and radioresistance in cancer stem cells. *Nature* 458: 780–783, 2009.
67. Dietz A, Vanselow B, Rudat V, Conradt C, Weidauer H, Kallinowski F, and Dollner R. Prognostic impact of reoxygenation in advanced cancer of the head and neck during the initial course of chemoradiation or radiotherapy alone. *Head Neck* 25: 50–58, 2003.
68. Dietz DW, Dehdashti F, Grigsby PW, Malyapa RS, Myerson RJ, Picus J, Ritter J, Lewis JS, Welch MJ, and Siegel BA. Tumor hypoxia detected by positron emission tomography with 60Cu-ATSM as a predictor of response and survival in patients undergoing Neoadjuvant chemoradiotherapy for rectal carcinoma: a pilot study. *Dis Colon Rectum* 51: 1641–1648, 2008.
69. Dings RP, Loren M, Heun H, McNiel E, Griffioen AW, Mayo KH, and Griffin RJ. Scheduling of radiation with angiogenesis inhibitors anginex and Avastin improves therapeutic outcome via vessel normalization. *Clin Cancer Res* 13: 3395–3402, 2007.
70. Dirix P, Vandecaveye V, De Keyzer F, Stroobants S, Hermans R, and Nuyts S. Dose painting in radiotherapy for head and neck squamous cell carcinoma: value of repeated functional imaging with (18)F-FDG PET, (18)F-fluoromisonidazole PET, diffusion-weighted MRI, and dynamic contrast-enhanced MRI. *J Nucl Med* 50: 1020–1027, 2009.
71. Dische S, Machin D, and Chassagne D. A trial of Ro 03–8799 (pimonidazole) in carcinoma of the uterine cervix: an interim report from the Medical Research Council Working Party on advanced carcinoma of the cervix. *Radiother Oncol* 26: 93–103, 1993.
72. Dische S, Saunders MI, Bennett MH, Dunphy EP, Des Rochers C, Stratford MR, Minchinton AI, and Wardman P. A comparison of the tumour concentrations obtainable with misonidazole and Ro 03–8799. *Br J Radiol* 59: 911–917, 1986.
73. Donaldson SB, Betts G, Bonington SC, Homer JJ, Slevin NJ, Kershaw LE, Valentine H, West CM, and Buckley DL. Perfusion estimated with rapid dynamic contrast-enhanced magnetic resonance imaging correlates inversely with vascular endothelial growth factor expression and pimonidazole staining in head-and-neck cancer: a pilot study. *Int J Radiat Oncol Biol Phys* 81: 1176–1183, 2011.
74. Doss M, Zhang JJ, Belanger MJ, Stubbs JB, Hostetler ED, Alpaugh K, Kolb HC, and Yu JQ. Biodistribution and radiation dosimetry of the hypoxia marker 18F-HX4 in monkeys and humans determined by using whole-body PET/CT. *Nucl Med Commun* 31: 1016–1024, 2010.
75. Dubois LJ, Lieuwes NG, Janssen MH, Peeters WJ, Windhorst AD, Walsh JC, Kolb HC, Ollers MC, Bussink J, van Dongen GA, van der Kogel A, and Lambin P. Preclinical evaluation and validation of [18F]HX4, a promising hypoxia marker for PET imaging. *Proc Natl Acad Sci U S A* 108: 14620–14625, 2011.
76. Dunphy I, Vinogradov SA, and Wilson DF. Oxyphor R2 and G2: phosphors for measuring oxygen by oxygen-dependent quenching of phosphorescence. *Anal Biochem* 310: 191–198, 2002.
77. Dunst J, Stadler P, Becker A, Lautenschlager C, Pelz T, Hansgen G, Molls M, and Kuhnt T. Tumor volume and tumor hypoxia in head and neck cancers. The amount of the hypoxic volume is important. *Strahlenther Onkol* 179: 521–526, 2003.
78. Eichhorn ME, Strieth S, Luedemann S, Kleespies A, Noth U, Passon A, Brix G, Jauch KW, Bruns CJ, and Dellian M. Contrast enhanced MRI and intravital fluorescence microscopy indicate improved tumor microcirculation in highly vascularized melanomas upon short-term anti-VEGFR treatment. *Cancer Biol Ther* 7: 1006–1013, 2008.
79. Elas M, Ahn KH, Parasca A, Barth ED, Lee D, Haney C, and Halpern HJ. Electron paramagnetic resonance oxygen images correlate spatially and quantitatively with Oxylite oxygen measurements. *Clin Cancer Res* 12: 4209–4217, 2006.
80. Elas M, Bell R, Hleihel D, Barth ED, McFaul C, Haney CR, Bielanska J, Pustelny K, Ahn KH, Pelizzari CA, Kocherginsky M, and Halpern HJ. Electron paramagnetic resonance oxygen image hypoxic fraction plus radiation dose strongly correlates with tumor cure in FSa fibrosarcomas. *Int J Radiat Oncol Biol Phys* 71: 542–549, 2008.
81. Elas M, Magwood JM, Butler B, Li C, Wardak R, Barth ED, Epel B, Rubinstein S, Pelizzari CA, Weichselbaum RR, and Halpern HJ. EPR Oxygen Images Predict Tumor Control by a 50% Tumor Control Radiation Dose. *Cancer Res* 73: 5328–5335, 2013.
82. Eriksen JG and Overgaard J. Lack of prognostic and predictive value of CA IX in radiotherapy of squamous cell carcinoma of the head and neck with known modifiable hypoxia: an evaluation of the DAHANCA 5 study. *Radiother Oncol* 83: 383–388, 2007.
83. Eschmann SM, Paulsen F, Bedeshem C, Machulla HJ, Hehr T, Bamberg M, and Bares R. Hypoxia-imaging with (18)F-Misonidazole and PET: changes of kinetics during

radiotherapy of head-and-neck cancer. *Radiother Oncol* 83: 406–410, 2007.
84. Eschmann SM, Paulsen F, Reimold M, Dittmann H, Welz S, Reischl G, Machulla HJ, and Bares R. Prognostic impact of hypoxia imaging with 18F-misonidazole PET in non-small cell lung cancer and head and neck cancer before radiotherapy. *J Nucl Med* 46: 253–260, 2005.
85. Esipova TV, Karagodov A, Miller J, Wilson DF, Busch TM, and Vinogradov SA. Two new ''protected'' oxyphors for biological oximetry: properties and application in tumor imaging. *Anal Chem* 83: 8756–8765, 2011.
86. Evans SM, Du KL, Chalian AA, Mick R, Zhang PJ, Hahn SM, Quon H, Lustig R, Weinstein GS, and Koch CJ. Patterns and levels of hypoxia in head and neck squamous cell carcinomas and their relationship to patient outcome. *Int J Radiat Oncol Biol Phys* 69: 1024–1031, 2007.
87. Evans SM, Fraker D, Hahn SM, Gleason K, Jenkins WT, Jenkins K, Hwang WT, Zhang P, Mick R, and Koch CJ. EF5 binding and clinical outcome in human soft tissue sarcomas. *Int J Radiat Oncol Biol Phys* 64: 922–927, 2006.
88. Evans SM, Hahn S, Pook DR, Jenkins WT, Chalian AA, Zhang P, Stevens C, Weber R, Weinstein G, Benjamin I, Mirza N, Morgan M, Rubin S, McKenna WG, Lord EM, and Koch CJ. Detection of hypoxia in human squamous cell carcinoma by EF5 binding. *Cancer Res* 60: 2018–2024, 2000.
89. Evans SM, Hahn SM, Magarelli DP, Zhang PJ, Jenkins WT, Fraker DL, Hsi RA, McKenna WG, and Koch CJ. Hypoxia in human intraperitoneal and extremity sarcomas. *Int J Radiat Oncol Biol Phys* 49: 587–596, 2001.
90. Evans SM, Jenkins KW, Chen HI, Jenkins WT, Judy KD, Hwang WT, Lustig RA, Judkins AR, Grady MS, Hahn SM, and Koch CJ. The relationship among hypoxia, proliferation, and outcome in patients with de novo glioblastoma: a pilot study. *Transl Oncol* 3: 160–169, 2010.
91. Evans SM, Judy KD, Dunphy I, Jenkins WT, Nelson PT, Collins R, Wileyto EP, Jenkins K, Hahn SM, Stevens CW, Judkins AR, Phillips P, Geoerger B, and Koch CJ. Comparative measurements of hypoxia in human brain tumors using needle electrodes and EF5 binding. *Cancer Res* 64: 1886–1892, 2004.
92. Frederiksen LJ, Siemens DR, Heaton JP, Maxwell LR, Adams MA, and Graham CH. Hypoxia induced resistance to doxorubicin in prostate cancer cells is inhibited by low concentrations of glyceryl trinitrate. *J Urol* 170: 1003–1007, 2003.
93. Gaertner FC, Souvatzoglou M, Brix G, and Beer AJ. Imaging of hypoxia using PET and MRI. *Curr Pharm Biotechnol* 13: 552–570, 2012.
94. Gagel B, DiMartino E, Schramm O, Pinkawa M, Piroth M, Demirel C, Maneschi P, Stanzel S, Asadpour B, Westhofen M, and Eble MJ. Contrast-enhanced color duplex sonography (CDS): an alternative for the evaluation of therapy-relevant tumor oxygenation? *Strahlenther Onkol* 182: 604–609, 2006.
95. Gagel B, Piroth M, Pinkawa M, Reinartz P, Zimny M, Kaiser HJ, Stanzel S, Asadpour B, Demirel C, Hamacher K, Coenen HH, Scholbach T, Maneschi P, DiMartino E, and Eble MJ. pO polarography, contrast enhanced color duplex sonography (CDS), [18F] fluoromisonidazole and [18F] fluorodeoxyglucose positron emission tomography: validated methods for the evaluation of therapy-relevant tumor oxygenation or only bricks in the puzzle of tumor hypoxia? *BMC Cancer* 7: 113, 2007.
96. Gagel B, Reinartz P, Dimartino E, Zimny M, Pinkawa M, Maneschi P, Stanzel S, Hamacher K, Coenen HH, Westhofen M, Bull U, and Eble MJ. pO2 Polarography versus positron emission tomography ([(18)F] fluoromisonidazole, [(18)F]-2-fluoro-2′-deoxyglucose). An appraisal of radiotherapeutically relevant hypoxia. *Strahlenther Onkol* 180: 616–622, 2004.
97. Gallez B, Baudelet C, and Jordan BF. Assessment of tumor oxygenation by electron paramagnetic resonance: principles and applications. *NMR Biomed* 17: 240–262, 2004.
98. Gammon L, Biddle A, Heywood HK, Johannessen AC, and Mackenzie IC. Sub-sets of cancer stem cells differ intrinsically in their patterns of oxygen metabolism. *PLoS One* 8: e62493.
99. Garcia-Parra R, Wood D, Shah RB, Siddiqui J, Hussain H, Park H, Desmond T, Meyer C, and Piert M. Investigation on tumor hypoxia in resectable primary prostate cancer as demonstrated by 18F-FAZA PET/CT utilizing multimodality fusion techniques. *Eur J Nucl Med Mol Imaging* 38: 1816–1823, 2011.
100. Gatenby RA, Kessler HB, Rosenblum JS, Coia LR, Moldofsky PJ, Hartz WH, and Broder GJ. Oxygen distribution in squamous cell carcinoma metastases and its relationship to outcome of radiation therapy. *Int J Radiat Oncol Biol Phys* 14: 831–838, 1988.
101. Gaustad JV, Simonsen TG, Leinaas MN, and Rofstad EK. Sunitinib treatment does not improve blood supply but induces hypoxia in human melanoma xenografts. *BMC Cancer* 12: 388, 2012.
102. Giaccia AJ. Hypoxic stress proteins: survival of the fittest. *Semin Radiat Oncol* 6: 46–58, 1996.
103. Giatromanolaki A and Harris AL. Tumour hypoxia, hypoxia signaling pathways and hypoxia inducible factor expression in human cancer. *Anticancer Res* 21: 4317–4324, 2001.
104. Goethals L, Debucquoy A, Perneel C, Geboes K, Ectors N, De Schutter H, Penninckx F, McBride WH, Begg AC, and Haustermans KM. Hypoxia in human colorectal adenocarcinoma: comparison between extrinsic and potential intrinsic hypoxia markers. *Int J Radiat Oncol Biol Phys* 65: 246–254, 2006.
105. Graeber TG, Osmanian C, Jacks T, Housman DE, Koch CJ, Lowe SW, and Giaccia AJ. Hypoxia-mediated selection of cells with diminished apoptotic potential in solid tumours. *Nature* 379: 88–91, 1996.
106. Graham CH, Forsdike J, Fitzgerald CJ, and Macdonald-Goodfellow S. Hypoxia-mediated stimulation of carcinoma cell invasiveness via upregulation of urokinase receptor expression. *Int J Cancer* 80: 617–623, 1999.
107. Graham MM, Peterson LM, Link JM, Evans ML, Rasey JS, Koh WJ, Caldwell JH, and Krohn KA. Fluorine-18-fluoromisonidazole radiation dosimetry in imaging studies. *J Nucl Med* 38: 1631–1636, 1997.
108. Graves EE, Vilalta M, Cecic IK, Erler JT, Tran PT, Felsher D, Sayles L, Sweet-Cordero A, Le QT, and Giaccia AJ. Hypoxia in models of lung cancer: implications for targeted therapeutics. *Clin Cancer Res* 16: 4843–4852, 2010.
109. Gray LH, Conger AD, Ebert M, Hornsey S, and Scott OC. The concentration of oxygen dissolved in tissues at the time of irradiation as a factor in radiotherapy. *Br J Radiol* 26: 638–648, 1953.
110. Griffiths JR and Robinson SP. The OxyLite: a fibre-optic oxygen sensor. *Br J Radiol* 72: 627–630, 1999.

111. Gross MW, Karbach U, Groebe K, Franko AJ, and Mueller-Klieser W. Calibration of misonidazole labeling by simultaneous measurement of oxygen tension and labeling density in multicellular spheroids. *Int J Cancer* 61: 567–573, 1995.
112. Grosu AL, Piert M, Weber WA, Jeremic B, Picchio M, Schratzenstaller U, Zimmermann FB, Schwaiger M, and Molls M. Positron emission tomography for radiation treatment planning. *Strahlenther Onkol* 181: 483–499, 2005.
113. Grosu AL, Souvatzoglou M, Roper B, Dobritz M, Wiedenmann N, Jacob V, Wester HJ, Reischl G, Machulla HJ, Schwaiger M, Molls M, and Piert M. Hypoxia imaging with FAZA-PET and theoretical considerations with regard to dose painting for individualization of radiotherapy in patients with head and neck cancer. *Int J Radiat Oncol Biol Phys* 69: 541–551, 2007.
114. Hamada K, Sasaki T, Koni PA, Natsui M, Kishimoto H, Sasaki J, Yajima N, Horie Y, Hasegawa G, Naito M, Miyazaki J, Suda T, Itoh H, Nakao K, Mak TW, Nakano T, and Suzuki A. The PTEN/PI3K pathway governs normal vascular development and tumor angiogenesis. *Genes Dev* 19: 2054–2065, 2005.
115. Hamzah J, Jugold M, Kiessling F, Rigby P, Manzur M, Marti HH, Rabie T, Kaden S, Grone HJ, Hammerling GJ, Arnold B, and Ganss R. Vascular normalization in Rgs5-deficient tumours promotes immune destruction. *Nature* 453: 410–414, 2008.
116. Harrison LB, Chadha M, Hill RJ, Hu K, and Shasha D. Impact of tumor hypoxia and anemia on radiation therapy outcomes. *Oncologist* 7: 492–508, 2002.
117. Havelund BM, Holdgaard PC, Rafaelsen SR, Mortensen LS, Theil J, Bender D, Ploen J, Spindler KL, and Jakobsen A. Tumour hypoxia imaging with 18F-fluoroazomycinarabinofuranoside PET/CT in patients with locally advanced rectal cancer. *Nucl Med Commun* 34: 155–161, 2013.
118. Helczynska K, Kronblad A, Jogi A, Nilsson E, Beckman S, Landberg G, and Pahlman S. Hypoxia promotes a dedifferentiated phenotype in ductal breast carcinoma *in situ*. *Cancer Res* 63: 1441–1444, 2003.
119. Hendrickson K, Phillips M, Smith W, Peterson L, Krohn K, and Rajendran J. Hypoxia imaging with [F-18] FMISO-PET in head and neck cancer: potential for guiding intensity modulated radiation therapy in overcoming hypoxia-induced treatment resistance. *Radiother Oncol* 101: 369–375, 2011.
120. Hockel M, Knoop C, Schlenger K, Vorndran B, Baussmann E, Mitze M, Knapstein PG, and Vaupel P. Intratumoral pO2 predicts survival in advanced cancer of the uterine cervix. *Radiother Oncol* 26: 45–50, 1993.
121. Hockel M, Schlenger K, Aral B, Mitze M, Schaffer U, and Vaupel P. Association between tumor hypoxia and malignant progression in advanced cancer of the uterine cervix. *Cancer Res* 56: 4509–4515, 1996.
122. Hockel M and Vaupel P. Tumor hypoxia: definitions and current clinical, biologic, and molecular aspects. *J Natl Cancer Inst* 93: 266–276, 2001.
123. Holland JP, Lewis JS, and Dehdashti F. Assessing tumor hypoxia by positron emission tomography with Cu-ATSM. *Q J Nucl Med Mol Imaging* 53: 193–200, 2009.
124. Hoogsteen IJ, Marres HA, Bussink J, van der Kogel AJ, and Kaanders JH. Tumor microenvironment in head and neck squamous cell carcinomas: predictive value and clinical relevance of hypoxic markers. A review. *Head Neck* 29: 591–604, 2007.
125. Hoskin PJ, Carnell DM, Taylor NJ, Smith RE, Stirling JJ, Daley FM, Saunders MI, Bentzen SM, Collins DJ, d'Arcy JA, and Padhani AP. Hypoxia in prostate cancer: correlation of BOLD-MRI with pimonidazole immunohistochemistry-initial observations. *Int J Radiat Oncol Biol Phys* 68: 1065–1071, 2007.
126. Hoskin PJ, Sibtain A, Daley FM, and Wilson GD. GLUT1 and CAIX as intrinsic markers of hypoxia in bladder cancer: relationship with vascularity and proliferation as predictors of outcome of ARCON. *Br J Cancer* 89: 1290–1297, 2003.
127. Hudson CC, Liu M, Chiang GG, Otterness DM, Loomis DC, Kaper F, Giaccia AJ, and Abraham RT. Regulation of hypoxia-inducible factor 1alpha expression and function by the mammalian target of rapamycin. *Mol Cell Biol* 22: 7004–7014, 2002.
128. Hui EP, Sung FL, Yu BK, Wong CS, Ma BB, Lin X, Chan A, Wong WL, and Chan AT. Plasma osteopontin, hypoxia, and response to radiotherapy in nasopharyngeal cancer. *Clin Cancer Res* 14: 7080–7087, 2008.
129. Ilie M, Mazure NM, Hofman V, Ammadi RE, Ortholan C, Bonnetaud C, Havet K, Venissac N, Mograbi B, Mouroux J, Pouyssegur J, and Hofman P. High levels of carbonic anhydrase IX in tumour tissue and plasma are biomarkers of poor prognostic in patients with non-small cell lung cancer. *Br J Cancer* 102: 1627–1635, 2010.
130. Isa AY, Ward TH, West CM, Slevin NJ, and Homer JJ. Hypoxia in head and neck cancer. *Br J Radiol* 79: 791–798, 2006.
131. Janssens GO, Rademakers SE, Terhaard CH, Doornaert PA, Bijl HP, van den Ende P, Chin A, Marres HA, de Bree R, van der Kogel AJ, Hoogsteen IJ, Bussink J, Span PN, and Kaanders JH. Accelerated radiotherapy with carbogen and nicotinamide for laryngeal cancer: results of a phase III randomized trial. *J Clin Oncol* 30: 1777–1783, 2012.
132. Jenkins WT, Evans SM, and Koch CJ. Hypoxia and necrosis in rat 9L glioma and Morris 7777 hepatoma tumors: comparative measurements using EF5 binding and the Eppendorf needle electrode. *Int J Radiat Oncol Biol Phys* 46: 1005–1017, 2000.
133. Jin F, Brockmeier U, Otterbach F, and Metzen E. New insight into the SDF-1/CXCR4 axis in a breast carcinoma model: hypoxia-induced endothelial SDF-1 and tumor cell CXCR4 are required for tumor cell intravasation. *Mol Cancer Res* 10: 1021–1031, 2012.
134. Jonathan RA, Wijffels KI, Peeters W, de Wilde PC, Marres HA, Merkx MA, Oosterwijk E, van der Kogel AJ, and Kaanders JH. The prognostic value of endogenous hypoxia-related markers for head and neck squamous cell carcinomas treated with ARCON. *Radiother Oncol* 79: 288–297, 2006.
135. Kaanders JH, Pop LA, Marres HA, Bruaset I, van den Hoogen FJ, Merkx MA, and van der Kogel AJ. ARCON: experience in 215 patients with advanced head-and-neck cancer. *Int J Radiat Oncol Biol Phys* 52: 769–778, 2002.
136. Kaanders JH, Wijffels KI, Marres HA, Ljungkvist AS, Pop LA, van den Hoogen FJ, de Wilde PC, Bussink J, Raleigh JA, and van der Kogel AJ. Pimonidazole binding and tumor vascularity predict for treatment outcome in head and neck cancer. *Cancer Res* 62: 7066–7074, 2002.
137. Kappler M, Taubert H, Holzhausen HJ, Reddemann R, Rot S, Becker A, Kuhnt T, Dellas K, Dunst J, Vordermark D, Hansgen G, and Bache M. Immunohistochemical detection of HIF-1alpha and CAIX in advanced head-and-neck

cancer. Prognostic role and correlation with tumor markers and tumor oxygenation parameters. *Strahlenther Onkol* 184: 393–399, 2008.
138. Kavanagh MC, Tsang V, Chow S, Koch C, Hedley D, Minkin S, and Hill RP. A comparison in individual murine tumors of techniques for measuring oxygen levels. *Int J Radiat Oncol Biol Phys* 44: 1137–1146, 1999.
139. Kayama T, Yoshimoto T, Fujimoto S, and Sakurai Y. Intratumoral oxygen pressure in malignant brain tumor. *J Neurosurg* 74: 55–59, 1991.
140. Khan N, Mupparaju S, Hou H, Williams BB, and Swartz H. Repeated assessment of orthotopic glioma pO(2) by multi-site EPR oximetry: a technique with the potential to guide therapeutic optimization by repeated measurements of oxygen. *J Neurosci Methods* 204: 111–117, 2012.
141. Kieda C, El Hafny-Rahbi B, Collet G, Lamerant-Fayel N, Grillon C, Guichard A, Dulak J, Jozkowicz A, Kotlinowski J, Fylaktakidou KC, Vidal A, Auzeloux P, Miot-Noirault E, Beloeil JC, Lehn JM, and Nicolau C. Stable tumor vessel normalization with pO(2) increase and endothelial PTEN activation by inositol trispyrophosphate brings novel tumor treatment. *J Mol Med (Berl)* 91: 883–899, 2013.
142. Kim SJ, Rabbani ZN, Dewhirst MW, Vujaskovic Z, Vollmer RT, Schreiber EG, Oosterwijk E, and Kelley MJ. Expression of HIF-1alpha, CA IX, VEGF, and MMP-9 in surgically resected non-small cell lung cancer. *Lung Cancer* 49: 325–335, 2005.
143. Kim SJ, Rabbani ZN, Vollmer RT, Schreiber EG, Oosterwijk E, Dewhirst MW, Vujaskovic Z, and Kelley MJ. Carbonic anhydrase IX in early-stage non-small cell lung cancer. *Clin Cancer Res* 10: 7925–7933, 2004.
144. Koch CJ, Evans SM, and Lord EM. Oxygen dependence of cellular uptake of EF5 [2-(2-nitro-1H-imidazol-1-yl)-N-(2,2,3,3,3-pentafluoropropyl)a cet amide]: analysis of drug adducts by fluorescent antibodies vs bound radioactivity. *Br J Cancer* 72: 869–874, 1995.
145. Koch CJ, Hahn SM, Rockwell K, Jr., Covey JM, McKenna WG, and Evans SM. Pharmacokinetics of EF5 [2-(2-nitro-1-H-imidazol-1-yl)-N-(2,2,3,3,3-pentafluoropropyl) acetamide] in human patients: implications for hypoxia measurements *in vivo* by 2-nitroimidazoles. *Cancer Chemother Pharmacol* 48: 177–187, 2001.
146. Koch CJ, Scheuermann JS, Divgi C, Judy KD, Kachur AV, Freifelder R, Reddin JS, Karp J, Stubbs JB, Hahn SM, Driesbaugh J, Smith D, Prendergast S, and Evans SM. Biodistribution and dosimetry of (18)F-EF5 in cancer patients with preliminary comparison of (18)F-EF5 uptake versus EF5 binding in human glioblastoma. *Eur J Nucl Med Mol Imaging* 37: 2048–2059, 2010.
147. Kodibagkar VD, Wang X, and Mason RP. Physical principles of quantitative nuclear magnetic resonance oximetry. *Front Biosci* 13: 1371–1384, 2008.
148. Koh WJ, Rasey JS, Evans ML, Grierson JR, Lewellen TK, Graham MM, Krohn KA, and Griffin TW. Imaging of hypoxia in human tumors with [F-18]fluoromisonidazole. *Int J Radiat Oncol Biol Phys* 22: 199–212, 1992.
149. Komar G, Seppanen M, Eskola O, Lindholm P, Gronroos TJ, Forsback S, Sipila H, Evans SM, Solin O, and Minn H. 18F-EF5: a new PET tracer for imaging hypoxia in head and neck cancer. *J Nucl Med* 49: 1944–1951, 2008.
150. Konecky SD, Choe R, Corlu A, Lee K, Wiener R, Srinivas SM, Saffer JR, Freifelder R, Karp JS, Hajjioui N, Azar F, and Yodh AG. Comparison of diffuse optical tomography of human breast with whole-body and breast-only positron emission tomography. *Med Phys* 35: 446–455, 2008.
151. Kong CS, Narasimhan B, Cao H, Kwok S, Erickson JP, Koong A, Pourmand N, and Le QT. The relationship between human papillomavirus status and other molecular prognostic markers in head and neck squamous cell carcinomas. *Int J Radiat Oncol Biol Phys* 74: 553–561, 2009.
152. Koong AC, Mehta VK, Le QT, Fisher GA, Terris DJ, Brown JM, Bastidas AJ, and Vierra M. Pancreatic tumors show high levels of hypoxia. *Int J Radiat Oncol Biol Phys* 48: 919–922, 2000.
153. Kumar P, Stypinski D, Xia H, McEwan AJB, Machulla H-J, and Wiebe LI. Fluoroazomycin arabinoside (FAZA): synthesis, 2H and 3H-labelling and preliminary biological evaluation of a novel 2-nitroimidazole marker of tissue hypoxia. *J Label Compd Radiopharm* 42: 3–16, 1999.
154. Kunkel M, Reichert TE, Benz P, Lehr HA, Jeong JH, Wieand S, Bartenstein P, Wagner W, and Whiteside TL. Overexpression of Glut-1 and increased glucose metabolism in tumors are associated with a poor prognosis in patients with oral squamous cell carcinoma. *Cancer* 97: 1015–1024, 2003.
155. Kunz M and Ibrahim SM. Molecular responses to hypoxia in tumor cells. *Mol Cancer* 2: 23, 2003.
156. Laforest R, Dehdashti F, Lewis JS, and Schwarz SW. Dosimetry of 60/61/62/64Cu-ATSM: a hypoxia imaging agent for PET. *Eur J Nucl Med Mol Imaging* 32: 764–770, 2005.
157. Lally BE, Rockwell S, Fischer DB, Collingridge DR, Piepmeier JM, and Knisely JP. The interactions of polarographic measurements of oxygen tension and histological grade in human glioma. *Cancer J* 12: 461–466, 2006.
158. Lartigau E, Le Ridant AM, Lambin P, Weeger P, Martin L, Sigal R, Lusinchi A, Luboinski B, Eschwege F, and Guichard M. Oxygenation of head and neck tumors. *Cancer* 71: 2319–2325, 1993.
159. Lawrence YR, Vikram B, Dignam JJ, Chakravarti A, Machtay M, Freidlin B, Takebe N, Curran WJ, Jr., Bentzen SM, Okunieff P, Coleman CN, and Dicker AP. NCI-RTOG translational program strategic guidelines for the early-stage development of radiosensitizers. *J Natl Cancer Inst* 105: 11–24, 2012.
160. Le QT, Chen E, Salim A, Cao H, Kong CS, Whyte R, Donington J, Cannon W, Wakelee H, Tibshirani R, Mitchell JD, Richardson D, O'Byrne KJ, Koong AC, and Giaccia AJ. An evaluation of tumor oxygenation and gene expression in patients with early stage non-small cell lung cancers. *Clin Cancer Res* 12: 1507–1514, 2006.
161. Le QT, Kong C, Lavori PW, O'Byrne K, Erler JT, Huang X, Chen Y, Cao H, Tibshirani R, Denko N, Giaccia AJ, and Koong AC. Expression and prognostic significance of a panel of tissue hypoxia markers in head-and-neck squamous cell carcinomas. *Int J Radiat Oncol Biol Phys* 69: 167–175, 2007.
162. Le QT, Kovacs MS, Dorie MJ, Koong A, Terris DJ, Pinto HA, Goffinet DR, Nowels K, Bloch D, and Brown JM. Comparison of the comet assay and the oxygen microelectrode for measuring tumor oxygenation in head-and-neck cancer patients. *Int J Radiat Oncol Biol Phys* 56: 375–383, 2003.
163. Le QT, Taira A, Budenz S, Jo Dorie M, Goffinet DR, Fee WE, Goode R, Bloch D, Koong A, Martin Brown J, and Pinto HA. Mature results from a randomized Phase II trial

of cisplatin plus 5-fluorouracil and radiotherapy with or without tirapazamine in patients with resectable Stage IV head and neck squamous cell carcinomas. *Cancer* 106: 1940–1949, 2006.
164. Lee CP, Payne GS, Oregioni A, Ruddle R, Tan S, Raynaud FI, Eaton D, Campbell MJ, Cross K, Halbert G, Tracy M, McNamara J, Seddon B, Leach MO, Workman P, and Judson I. A phase I study of the nitroimidazole hypoxia marker SR4554 using 19F magnetic resonance spectroscopy. *Br J Cancer* 101: 1860–1868, 2009.
165. Lee DJ, Cosmatos D, Marcial VA, Fu KK, Rotman M, Cooper JS, Ortiz HG, Beitler JJ, Abrams RA, Curran WJ, *et al.* Results of an RTOG phase III trial (RTOG 85–27) comparing radiotherapy plus etanidazole with radiotherapy alone for locally advanced head and neck carcinomas. *Int J Radiat Oncol Biol Phys* 32: 567–576, 1995.
166. Lee DJ, Pajak TF, Stetz J, Order SE, Weissberg JB, and Fischer JJ. A phase I/II study of the hypoxic cell sensitizer misonidazole as an adjunct to high fractional dose radiotherapy in patients with unresectable squamous cell carcinoma of the head and neck: a RTOG randomized study (#79–04). *Int J Radiat Oncol Biol Phys* 16: 465–470, 1989.
167. Lee JW, Bae SH, Jeong JW, Kim SH, and Kim KW. Hypoxia-inducible factor (HIF-1)alpha: its protein stability and biological functions. *Exp Mol Med* 36: 1–12, 2004.
168. Lee NY, Mechalakos JG, Nehmeh S, Lin Z, Squire OD, Cai S, Chan K, Zanzonico PB, Greco C, Ling CC, Humm JL, and Schoder H. Fluorine-18-labeled fluoromisonidazole positron emission and computed tomography-guided intensity-modulated radiotherapy for head and neck cancer: a feasibility study. *Int J Radiat Oncol Biol Phys* 70: 2–13, 2008.
169. Lee SW, Back GM, Yi BY, Choi EK, Ahn SD, Shin SS, Kim JH, Kim SY, Lee BJ, Nam SY, Choi SH, Kim SB, Park JH, Lee KK, Park SH, and Kim JH. Preliminary results of a phase I/II study of simultaneous modulated accelerated radiotherapy for nondisseminated nasopharyngeal carcinoma. *Int J Radiat Oncol Biol Phys* 65: 152–160, 2006.
170. Lewis JS, Sharp TL, Laforest R, Fujibayashi Y, and Welch MJ. Tumor uptake of copper-diacetyl-bis(N(4)-methylthiosemicarbazone): effect of changes in tissue oxygenation. *J Nucl Med* 42: 655–661, 2001.
171. Li M-L, Oh J-T, XIe X, Ku G, Wang W, Li C, Lungu GF, Stoica G, and Wang LV. Simultaneous molecular and hypoxia imaging of brain tumors in vivo using spectroscopic photoacoustic tomography. *Proc IEEE* 96: 481–489, 2008.
172. Li SP, Padhani AR, and Makris A. Dynamic contrast-enhanced magnetic resonance imaging and blood oxygenation level-dependent magnetic resonance imaging for the assessment of changes in tumor biology with treatment. *J Natl Cancer Inst Monogr* 2011: 103–107, 2011.
173. Li Z, Bao S, Wu Q, Wang H, Eyler C, Sathornsumetee S, Shi Q, Cao Y, Lathia J, McLendon RE, Hjelmeland AB, and Rich JN. Hypoxia-inducible factors regulate tumorigenic capacity of glioma stem cells. *Cancer Cell* 15: 501–513, 2009.
174. Lim AM, Corry J, Collins M, Peters L, Hicks RJ, D'Costa I, Coleman A, Chua M, Solomon B, and Rischin D. A phase II study of induction carboplatin and gemcitabine followed by chemoradiotherapy for the treatment of locally advanced nasopharyngeal carcinoma. *Oral Oncol* 49: 468–474, 2013.
175. Lim AM, Rischin D, Fisher R, Cao H, Kwok K, Truong D, McArthur GA, Young RJ, Giaccia A, Peters L, and Le QT. Prognostic significance of plasma osteopontin in patients with locoregionally advanced head and neck squamous cell carcinoma treated on TROG 02.02 phase III trial. *Clin Cancer Res* 18: 301–307, 2012.
176. Lin LL, Silvoniemi A, Stubbs JB, Rengan R, Suilamo S, Solin O, Divgi C, Eskola O, Sorger JM, Stabin MG, Kachur A, Hahn SM, Gronroos TJ, Forsback S, Evans SM, Koch CJ, and Minn H. Radiation dosimetry and biodistribution of the hypoxia tracer (1)(8)F-EF5 in oncologic patients. *Cancer Biother Radiopharm* 27: 412–419, 2012.
177. Loncaster JA, Carrington BM, Sykes JR, Jones AP, Todd SM, Cooper R, Buckley DL, Davidson SE, Logue JP, Hunter RD, and West CM. Prediction of radiotherapy outcome using dynamic contrast enhanced MRI of carcinoma of the cervix. *Int J Radiat Oncol Biol Phys* 54: 759–767, 2002.
178. Loncaster JA, Harris AL, Davidson SE, Logue JP, Hunter RD, Wycoff CC, Pastorek J, Ratcliffe PJ, Stratford IJ, and West CM. Carbonic anhydrase (CA IX) expression, a potential new intrinsic marker of hypoxia: correlations with tumor oxygen measurements and prognosis in locally advanced carcinoma of the cervix. *Cancer Res* 61: 6394–6399, 2001.
179. Lu X and Kang Y. Hypoxia and hypoxia-inducible factors: master regulators of metastasis. *Clin Cancer Res* 16: 5928–5935, 2010.
180. Lungu GF, Li ML, Xie X, Wang LV, and Stoica G. *In vivo* imaging and characterization of hypoxia-induced neovascularization and tumor invasion. *Int J Oncol* 30: 45–54, 2007.
181. Lyng H, Sundfor K, Trope C, and Rofstad EK. Disease control of uterine cervical cancer: relationships to tumor oxygen tension, vascular density, cell density, and frequency of mitosis and apoptosis measured before treatment and during radiotherapy. *Clin Cancer Res* 6: 1104–1112, 2000.
182. Lyng H, Vorren AO, Sundfor K, Taksdal I, Lien HH, Kaalhus O, and Rofstad EK. Assessment of tumor oxygenation in human cervical carcinoma by use of dynamic Gd-DTPA-enhanced MR imaging. *J Magn Reson Imaging* 14: 750–756, 2001.
183. Mack PC, Redman MW, Chansky K, Williamson SK, Farneth NC, Lara PN, Jr., Franklin WA, Le QT, Crowley JJ, and Gandara DR. Lower osteopontin plasma levels are associated with superior outcomes in advanced non-small-cell lung cancer patients receiving platinum-based chemotherapy: SWOG Study S0003. *J Clin Oncol* 26: 4771–4776, 2008.
184. Mahy P, De Bast M, Gallez B, Gueulette J, Koch CJ, Scalliet P, and Gregoire V. *In vivo* colocalization of 2-nitroimidazole EF5 fluorescence intensity and electron paramagnetic resonance oximetry in mouse tumors. *Radiother Oncol* 67: 53–61, 2003.
185. Maione F, Molla F, Meda C, Latini R, Zentilin L, Giacca M, Seano G, Serini G, Bussolino F, and Giraudo E. Semaphorin 3A is an endogenous angiogenesis inhibitor that blocks tumor growth and normalizes tumor vasculature in transgenic mouse models. *J Clin Invest* 119: 3356–3372, 2009.
186. Marotta D, Karar J, Jenkins WT, Kumanova M, Jenkins KW, Tobias JW, Baldwin D, Hatzigeorgiou A, Alexiou P, Evans SM, Alarcon R, Maity A, Koch C, and Koumenis

C. *In vivo* profiling of hypoxic gene expression in gliomas using the hypoxia marker EF5 and laser-capture microdissection. *Cancer Res* 71: 779–789, 2011.
187. Matsumoto S, Hyodo F, Subramanian S, Devasahayam N, Munasinghe J, Hyodo E, Gadisetti C, Cook JA, Mitchell JB, and Krishna MC. Low-field paramagnetic resonance imaging of tumor oxygenation and glycolytic activity in mice. *J Clin Invest* 118: 1965–1973, 2008.
188. Matsumoto S, Yasui H, Batra S, Kinoshita Y, Bernardo M, Munasinghe JP, Utsumi H, Choudhuri R, Devasahayam N, Subramanian S, Mitchell JB, and Krishna MC. Simultaneous imaging of tumor oxygenation and microvascular permeability using Overhauser enhanced MRI. *Proc Natl Acad Sci U S A* 106: 17898–17903, 2009.
189. Mazzone M, Dettori D, Leite de Oliveira R, Loges S, Schmidt T, Jonckx B, Tian YM, Lanahan AA, Pollard P, Ruiz de Almodovar C, De Smet F, Vinckier S, Aragones J, Debackere K, Luttun A, Wyns S, Jordan B, Pisacane A, Gallez B, Lampugnani MG, Dejana E, Simons M, Ratcliffe P, Maxwell P, and Carmeliet P. Heterozygous deficiency of PHD2 restores tumor oxygenation and inhibits metastasis via endothelial normalization. *Cell* 136: 839–851, 2009.
190. McKenna DJ, McKeown SR, and McKelvey-Martin VJ. Potential use of the comet assay in the clinical management of cancer. *Mutagenesis* 23: 183–190, 2008.
191. Medina RA and Owen GI. Glucose transporters: expression, regulation and cancer. *Biol Res* 35: 9–26, 2002.
192. Meng X, Kong FM, and Yu J. Implementation of hypoxia measurement into lung cancer therapy. *Lung Cancer* 75: 146–150, 2012.
193. Moeller BJ, Cao Y, Li CY, and Dewhirst MW. Radiation activates HIF-1 to regulate vascular radiosensitivity in tumors: role of reoxygenation, free radicals, and stress granules. *Cancer Cell* 5: 429–441, 2004.
194. Mortensen LS, Busk M, Nordsmark M, Jakobsen S, Theil J, Overgaard J, and Horsman MR. Accessing radiation response using hypoxia PET imaging and oxygen sensitive electrodes: a preclinical study. *Radiother Oncol* 99: 418–423, 2011.
195. Mortensen LS, Buus S, Nordsmark M, Bentzen L, Munk OL, Keiding S, and Overgaard J. Identifying hypoxia in human tumors: a correlation study between 18F-FMISO PET and the Eppendorf oxygen-sensitive electrode. *Acta Oncol* 49: 934–940, 2010.
196. Mortensen LS, Johansen J, Kallehauge J, Primdahl H, Busk M, Lassen P, Alsner J, Sorensen BS, Toustrup K, Jakobsen S, Petersen J, Petersen H, Theil J, Nordsmark M, and Overgaard J. FAZA PET/CT hypoxia imaging in patients with squamous cell carcinoma of the head and neck treated with radiotherapy: results from the DAHANCA 24 trial. *Radiother Oncol* 105: 14–20, 2012.
197. Mottram JC. A factor of importance in the radio sensitivity of tumours. *Br J Radiol* 9: 606–614, 1936.
198. Movsas B, Chapman JD, Horwitz EM, Pinover WH, Greenberg RE, Hanlon AL, Iyer R, and Hanks GE. Hypoxic regions exist in human prostate carcinoma. *Urology* 53: 11–18, 1999.
199. Nehmeh SA, Lee NY, Schroder H, Squire O, Zanzonico PB, Erdi YE, Greco C, Mageras G, Pham HS, Larson SM, Ling CC, and Humm JL. Reproducibility of intratumor distribution of (18)F-fluoromisonidazole in head and neck cancer. *Int J Radiat Oncol Biol Phys* 70: 235–242, 2008.
200. Newbold K, Castellano I, Charles-Edwards E, Mears D, Sohaib A, Leach M, Rhys-Evans P, Clarke P, Fisher C, Harrington K, and Nutting C. An exploratory study into the role of dynamic contrast-enhanced magnetic resonance imaging or perfusion computed tomography for detection of intratumoral hypoxia in head-and-neck cancer. *Int J Radiat Oncol Biol Phys* 74: 29–37, 2009.
201. Nordsmark M, Bentzen SM, Rudat V, Brizel D, Lartigau E, Stadler P, Becker A, Adam M, Molls M, Dunst J, Terris DJ, and Overgaard J. Prognostic value of tumor oxygenation in 397 head and neck tumors after primary radiation therapy. An international multi-center study. *Radiother Oncol* 77: 18–24, 2005.
202. Nordsmark M, Eriksen JG, Gebski V, Alsner J, Horsman MR, and Overgaard J. Differential risk assessments from five hypoxia specific assays: the basis for biologically adapted individualized radiotherapy in advanced head and neck cancer patients. *Radiother Oncol* 83: 389–397, 2007.
203. Nordsmark M, Loncaster J, Aquino-Parsons C, Chou SC, Gebski V, West C, Lindegaard JC, Havsteen H, Davidson SE, Hunter R, Raleigh JA, and Overgaard J. The prognostic value of pimonidazole and tumour pO2 in human cervix carcinomas after radiation therapy: a prospective international multi-center study. *Radiother Oncol* 80: 123–131, 2006.
204. Nordsmark M and Overgaard J. A confirmatory prognostic study on oxygenation status and loco-regional control in advanced head and neck squamous cell carcinoma treated by radiation therapy. *Radiother Oncol* 57: 39–43, 2000.
205. Nordsmark M and Overgaard J. Tumor hypoxia is independent of hemoglobin and prognostic for loco-regional tumor control after primary radiotherapy in advanced head and neck cancer. *Acta Oncol* 43: 396–403, 2004.
206. Nordsmark M, Overgaard M, and Overgaard J. Pretreatment oxygenation predicts radiation response in advanced squamous cell carcinoma of the head and neck. *Radiother Oncol* 41: 31–39, 1996.
207. Nyflot MJ, Harari PM, Yip S, Perlman SB, and Jeraj R. Correlation of PET images of metabolism, proliferation and hypoxia to characterize tumor phenotype in patients with cancer of the oropharynx. *Radiother Oncol* 105: 36–40, 2012.
208. Okamoto S, Shiga T, Yasuda K, Ito YM, Magota K, Kasai K, Kuge Y, Shirato H, and Tamaki N. High reproducibility of tumor hypoxia evaluated by 18F-fluoromisonidazole PET for head and neck cancer. *J Nucl Med* 54: 201–207, 2013.
209. Olive PL, Durand RE, Jackson SM, Le Riche JC, Luo C, Ma R, McLaren DB, Aquino-Parsons C, Thomson TA, and Trotter T. The comet assay in clinical practice. *Acta Oncol* 38: 839–844, 1999.
210. Olive PL, Durand RE, Le Riche J, Olivotto IA, and Jackson SM. Gel electrophoresis of individual cells to quantify hypoxic fraction in human breast cancers. *Cancer Res* 53: 733–736, 1993.
211. Oronsky BT, Knox SJ, and Scicinski J. Six degrees of separation: the oxygen effect in the development of radiosensitizers. *Transl Oncol* 4: 189–198, 2011.
212. This reference has been deleted.
213. Overgaard J. Clinical evaluation of nitroimidazoles as modifiers of hypoxia in solid tumors. *Oncol Res* 6: 509–518, 1994.
214. Overgaard J. Hypoxic modification of radiotherapy in squamous cell carcinoma of the head and neck—a systematic review and meta-analysis. *Radiother Oncol* 100: 22–32, 2011.

215. Overgaard J, Eriksen JG, Nordsmark M, Alsner J, and Horsman MR. Plasma osteopontin, hypoxia, and response to the hypoxia sensitiser nimorazole in radiotherapy of head and neck cancer: results from the DAHANCA 5 randomised double-blind placebo-controlled trial. *Lancet Oncol* 6: 757–764, 2005.
216. Overgaard J, Hansen HS, Overgaard M, Bastholt L, Berthelsen A, Specht L, Lindelov B, and Jorgensen K. A randomized double-blind phase III study of nimorazole as a hypoxic radiosensitizer of primary radiotherapy in supraglottic larynx and pharynx carcinoma. Results of the Danish Head and Neck Cancer Study (DAHANCA) Protocol 5–85. *Radiother Oncol* 46: 135–146, 1998.
217. Overgaard J, Hansen HS, Specht L, Overgaard M, Grau C, Andersen E, Bentzen J, Bastholt L, Hansen O, Johansen J, Andersen L, and Evensen JF. Five compared with six fractions per week of conventional radiotherapy of squamous-cell carcinoma of head and neck: DAHANCA 6 and 7 randomised controlled trial. *Lancet* 362: 933–940, 2003.
218. Peters L and Rischin D. Elusive goal of targeting tumor hypoxia for therapeutic gain. *J Clin Oncol* 30: 1741–1743, 2012.
219. Piert M, Machulla HJ, Picchio M, Reischl G, Ziegler S, Kumar P, Wester HJ, Beck R, McEwan AJ, Wiebe LI, and Schwaiger M. Hypoxia-specific tumor imaging with 18F-fluoroazomycin arabinoside. *J Nucl Med* 46: 106–113, 2005.
220. Pogue BW, Paulsen KD, O'Hara JA, Wilmot CM, and Swartz HM. Estimation of oxygen distribution in RIF-1 tumors by diffusion model-based interpretation of pimonidazole hypoxia and eppendorf measurements. *Radiat Res* 155: 15–25, 2001.
221. Popple RA, Ove R, and Shen S. Tumor control probability for selective boosting of hypoxic subvolumes, including the effect of reoxygenation. *Int J Radiat Oncol Biol Phys* 54: 921–927, 2002.
222. Postema EJ, McEwan AJ, Riauka TA, Kumar P, Richmond DA, Abrams DN, and Wiebe LI. Initial results of hypoxia imaging using 1-alpha-D: -(5-deoxy-5-[18F]-fluoroarabinofuranosyl)-2-nitroimidazole (18F-FAZA). *Eur J Nucl Med Mol Imaging* 36: 1565–1573, 2009.
223. Rademakers SE, Lok J, van der Kogel AJ, Bussink J, and Kaanders JH. Metabolic markers in relation to hypoxia; staining patterns and colocalization of pimonidazole, HIF-1alpha, CAIX, LDH-5, GLUT-1, MCT1 and MCT4. *BMC Cancer* 11: 167, 2011.
224. Rajendran JG, Mankoff DA, O'Sullivan F, Peterson LM, Schwartz DL, Conrad EU, Spence AM, Muzi M, Farwell DG, and Krohn KA. Hypoxia and glucose metabolism in malignant tumors: evaluation by [18F]fluoromisonidazole and [18F]fluorodeoxyglucose positron emission tomography imaging. *Clin Cancer Res* 10: 2245–2252, 2004.
225. Rajendran JG, Schwartz DL, O'Sullivan J, Peterson LM, Ng P, Scharnhorst J, Grierson JR, and Krohn KA. Tumor hypoxia imaging with [F-18] fluoromisonidazole positron emission tomography in head and neck cancer. *Clin Cancer Res* 12: 5435–5441, 2006.
226. Raleigh JA, Chou SC, Arteel GE, and Horsman MR. Comparisons among pimonidazole binding, oxygen electrode measurements, and radiation response in C3H mouse tumors. *Radiat Res* 151: 580–589, 1999.
227. Rasey JS, Grunbaum Z, Magee S, Nelson NJ, Olive PL, Durand RE, and Krohn KA. Characterization of radiolabeled fluoromisonidazole as a probe for hypoxic cells. *Radiat Res* 111: 292–304, 1987.
228. Rischin D, Fisher R, Peters L, Corry J, and Hicks R. Hypoxia in head and neck cancer: studies with hypoxic positron emission tomography imaging and hypoxic cytotoxins. *Int J Radiat Oncol Biol Phys* 69: S61–S63, 2007.
229. Rischin D, Hicks RJ, Fisher R, Binns D, Corry J, Porceddu S, and Peters LJ. Prognostic significance of [18F]-misonidazole positron emission tomography-detected tumor hypoxia in patients with advanced head and neck cancer randomly assigned to chemoradiation with or without tirapazamine: a substudy of Trans-Tasman Radiation Oncology Group Study 98.02. *J Clin Oncol* 24: 2098–2104, 2006.
230. Rischin D, Peters L, Fisher R, Macann A, Denham J, Poulsen M, Jackson M, Kenny L, Penniment M, Corry J, Lamb D, and McClure B. Tirapazamine, Cisplatin, and Radiation versus Fluorouracil, Cisplatin, and Radiation in patients with locally advanced head and neck cancer: a randomized phase II trial of the Trans-Tasman Radiation Oncology Group (TROG 98.02). *J Clin Oncol* 23: 79–87, 2005.
231. Rischin D, Peters L, Hicks R, Hughes P, Fisher R, Hart R, Sexton M, D'Costa I, and von Roemeling R. Phase I trial of concurrent tirapazamine, cisplatin, and radiotherapy in patients with advanced head and neck cancer. *J Clin Oncol* 19: 535–542, 2001.
232. Rischin D, Peters LJ, O'Sullivan B, Giralt J, Fisher R, Yuen K, Trotti A, Bernier J, Bourhis J, Ringash J, Henke M, and Kenny L. Tirapazamine, cisplatin, and radiation versus cisplatin and radiation for advanced squamous cell carcinoma of the head and neck (TROG 02.02, HeadSTART): a phase III trial of the Trans-Tasman Radiation Oncology Group. *J Clin Oncol* 28: 2989–2995, 2010.
233. Roizin-Towle L and Hall EJ. The effect of bleomycin on aerated and hypoxic cells *in vitro*, in combination with irradiation. *Int J Radiat Oncol Biol Phys* 5: 1491–1494, 1979.
234. Rolny C, Mazzone M, Tugues S, Laoui D, Johansson I, Coulon C, Squadrito ML, Segura I, Li X, Knevels E, Costa S, Vinckier S, Dresselaer T, Akerud P, De Mol M, Salomaki H, Phillipson M, Wyns S, Larsson E, Buysschaert I, Botling J, Himmelreich U, Van Ginderachter JA, De Palma M, Dewerchin M, Claesson-Welsh L, and Carmeliet P. HRG inhibits tumor growth and metastasis by inducing macrophage polarization and vessel normalization through downregulation of PlGF. *Cancer Cell* 19: 31–44, 2011.
235. Rowinsky EK. Novel radiation sensitizers targeting tissue hypoxia. *Oncology (Williston Park)* 13: 61–70, 1999.
236. Rudat V, Stadler P, Becker A, Vanselow B, Dietz A, Wannenmacher M, Molls M, Dunst J, and Feldmann HJ. Predictive value of the tumor oxygenation by means of pO2 histography in patients with advanced head and neck cancer. *Strahlenther Onkol* 177: 462–468, 2001.
237. Rudat V, Vanselow B, Wollensack P, Bettscheider C, Osman-Ahmet S, Eble MJ, and Dietz A. Repeatability and prognostic impact of the pretreatment pO(2) histography in patients with advanced head and neck cancer. *Radiother Oncol* 57: 31–37, 2000.
238. Rumsey WL, Vanderkooi JM, and Wilson DF. Imaging of phosphorescence: a novel method for measuring oxygen distribution in perfused tissue. *Science* 241: 1649–1651, 1988.
239. Russell J, Carlin S, Burke SA, Wen B, Yang KM, and Ling CC. Immunohistochemical detection of changes in

tumor hypoxia. *Int J Radiat Oncol Biol Phys* 73: 1177–1186, 2009.
240. Samouilov A, Caia GL, Kesselring E, Petryakov S, Wasowicz T, and Zweier JL. Development of a hybrid EPR/NMR coimaging system. *Magn Reson Med* 58: 156–166, 2007.
241. Scholbach T, Scholbach J, Krombach GA, Gagel B, Maneschi P, and Di Martino E. New method of dynamic color doppler signal quantification in metastatic lymph nodes compared to direct polarographic measurements of tissue oxygenation. *Int J Cancer* 114: 957–962, 2005.
242. Seeber LM, Horree N, Vooijs MA, Heintz AP, van der Wall E, Verheijen RH, and van Diest PJ. The role of hypoxia inducible factor-1alpha in gynecological cancer. *Crit Rev Oncol Hematol* 78: 173–184, 2011.
243. Seiwert TY, Salama JK, and Vokes EE. The chemoradiation paradigm in head and neck cancer. *Nat Clin Pract Oncol* 4: 156–171, 2007.
244. Semenza GL. Involvement of hypoxia-inducible factor 1 in human cancer. *Intern Med* 41: 79–83, 2002.
245. Semenza GL. Targeting HIF-1 for cancer therapy. *Nat Rev Cancer* 3: 721–732, 2003.
246. Semenza GL. Hypoxia-inducible factor 1: regulator of mitochondrial metabolism and mediator of ischemic preconditioning. *Biochim Biophys Acta* 1813: 1263–1268, 2011.
247. Semenza GL. Oxygen sensing, homeostasis, and disease. *N Engl J Med* 365: 537–547, 2011.
248. Severinghaus JW, Weiskopf RB, Nishimura M, and Bradley AF. Oxygen electrode errors due to polarographic reduction of halothane. *J Appl Physiol* 31: 640–642, 1971.
249. Shao Q, Morgounova E, Jiang C, Choi J, Bischof J, and Ashkenazi S. *In vivo* photoacoustic lifetime imaging of tumor hypoxia in small animals. *J Biomed Opt* 18: 076019, 2013.
250. Souvatzoglou M, Grosu AL, Roper B, Krause BJ, Beck R, Reischl G, Picchio M, Machulla HJ, Wester HJ, and Piert M. Tumour hypoxia imaging with [18F]FAZA PET in head and neck cancer patients: a pilot study. *Eur J Nucl Med Mol Imaging* 34: 1566–1575, 2007.
251. Stadler P, Becker A, Feldmann HJ, Hansgen G, Dunst J, Wurschmidt F, and Molls M. Influence of the hypoxic subvolume on the survival of patients with head and neck cancer. *Int J Radiat Oncol Biol Phys* 44: 749–754, 1999.
252. Stanz K, Liu B, Minsong C, Reinecke D, Miller K, and Kruger R. Photoacoustic spectoscopic imaging of intratumor heterogeneity and molecular identification. *SPIE Proc* 6086: 605–608, 2006.
253. Stone HB, Brown JM, Phillips TL, and Sutherland RM. Oxygen in human tumors: correlations between methods of measurement and response to therapy. Summary of a workshop held November 19–20, 1992, at the National Cancer Institute, Bethesda, Maryland. *Radiat Res* 136: 422–434, 1993.
254. Subarsky P and Hill RP. The hypoxic tumour microenvironment and metastatic progression. *Clin Exp Metastasis* 20: 237–250, 2003.
255. Sullivan R and Graham CH. Hypoxia-driven selection of the metastatic phenotype. *Cancer Metastasis Rev* 26: 319–331, 2007.
256. Tanaka N, Kato H, Inose T, Kimura H, Faried A, Sohda M, Nakajima M, Fukai Y, Miyazaki T, Masuda N, Fukuchi M, and Kuwano H. Expression of carbonic anhydrase 9, a potential intrinsic marker of hypoxia, is associated with poor prognosis in oesophageal squamous cell carcinoma. *Br J Cancer* 99: 1468–1475, 2008.
257. Tannock IF. Conventional cancer therapy: promise broken or promise delayed? *Lancet* 351 Suppl 2: SII9–SII16, 1998.
258. Tatum JL, Kelloff GJ, Gillies RJ, Arbeit JM, Brown JM, Chao KS, Chapman JD, Eckelman WC, Fyles AW, Giaccia AJ, Hill RP, Koch CJ, Krishna MC, Krohn KA, Lewis JS, Mason RP, Melillo G, Padhani AR, Powis G, Rajendran JG, Reba R, Robinson SP, Semenza GL, Swartz HM, Vaupel P, Yang D, Croft B, Hoffman J, Liu G, Stone H, and Sullivan D. Hypoxia: importance in tumor biology, noninvasive measurement by imaging, and value of its measurement in the management of cancer therapy. *Int J Radiat Biol* 82: 699–757, 2006.
259. Taylor NJ, Baddeley H, Goodchild KA, Powell ME, Thoumine M, Culver LA, Stirling JJ, Saunders MI, Hoskin PJ, Phillips H, Padhani AR, and Griffiths JR. BOLD MRI of human tumor oxygenation during carbogen breathing. *J Magn Reson Imaging* 14: 156–163, 2001.
260. Teicher BA. Hypoxia and drug resistance. *Cancer Metastasis Rev* 13: 139–168, 1994.
261. Teicher BA, Holden SA, al-Achi A, and Herman TS. Classification of antineoplastic treatments by their differential toxicity toward putative oxygenated and hypoxic tumor subpopulations *in vivo* in the FSaIIC murine fibrosarcoma. *Cancer Res* 50: 3339–3344, 1990.
262. Terris DJ. Head and neck cancer: the importance of oxygen. *Laryngoscope* 110: 697–707, 2000.
263. Thomlinson RH and Gray LH. The histological structure of some human lung cancers and the possible implications for radiotherapy. *Br J Cancer* 9: 539–549, 1955.
264. Thorwarth D, Eschmann SM, Holzner F, Paulsen F, and Alber M. Combined uptake of [18F]FDG and [18F]FMISO correlates with radiation therapy outcome in head-and-neck cancer patients. *Radiother Oncol* 80: 151–156, 2006.
265. Thorwarth D, Eschmann SM, Paulsen F, and Alber M. Hypoxia dose painting by numbers: a planning study. *Int J Radiat Oncol Biol Phys* 68: 291–300, 2007.
266. Toma-Dasu I, Uhrdin J, Antonovic L, Dasu A, Nuyts S, Dirix P, Haustermans K, and Brahme A. Dose prescription and treatment planning based on FMISO-PET hypoxia. *Acta Oncol* 51: 222–230, 2012.
267. Tong RT, Boucher Y, Kozin SV, Winkler F, Hicklin DJ, and Jain RK. Vascular normalization by vascular endothelial growth factor receptor 2 blockade induces a pressure gradient across the vasculature and improves drug penetration in tumors. *Cancer Res* 64: 3731–3736, 2004.
268. Toustrup K, Sorensen BS, Lassen P, Wiuf C, Alsner J, and Overgaard J. Gene expression classifier predicts for hypoxic modification of radiotherapy with nimorazole in squamous cell carcinomas of the head and neck. *Radiother Oncol* 102: 122–129, 2012.
269. Tran LB, Bol A, Labar D, Jordan B, Magat J, Mignion L, Gregoire V, and Gallez B. Hypoxia imaging with the nitroimidazole 18F-FAZA PET tracer: a comparison with OxyLite, EPR oximetry and 19F-MRI relaxometry. *Radiother Oncol* 105: 29–35, 2012.
270. Turaka A, Buyyounouski MK, Hanlon AL, Horwitz EM, Greenberg RE, and Movsas B. Hypoxic prostate/muscle PO2 ratio predicts for outcome in patients with localized prostate cancer: long-term results. *Int J Radiat Oncol Biol Phys* 82: e433–e439, 2012.
271. Valable S, Petit E, Roussel S, Marteau L, Toutain J, Divoux D, Sobrio F, Delamare J, Barre L, and Bernaudin M. Complementary information from magnetic resonance

imaging and (18)F-fluoromisonidazole positron emission tomography in the assessment of the response to an anti-angiogenic treatment in a rat brain tumor model. *Nucl Med Biol* 38: 781–793, 2011.
272. van Loon J, Janssen MH, Ollers M, Aerts HJ, Dubois L, Hochstenbag M, Dingemans AM, Lalisang R, Brans B, Windhorst B, van Dongen GA, Kolb H, Zhang J, De Ruysscher D, and Lambin P. PET imaging of hypoxia using [18F]HX4: a phase I trial. *Eur J Nucl Med Mol Imaging* 37: 1663–1668, 2010.
273. Vanderkooi JM and Wilson DF. A new method for measuring oxygen concentration in biological systems. *Adv Exp Med Biol* 200: 189–193, 1986.
274. Vaupel P. The role of hypoxia-induced factors in tumor progression. *Oncologist* 9 Suppl 5: 10–17, 2004.
275. Vaupel P. *Pathophysiology of Solid Tumors.* Berlin, Heidelberg: Springer-Verlag, 2009.
276. Vaupel P and Harrison L. Tumor hypoxia: causative factors, compensatory mechanisms, and cellular response. *Oncologist* 9 Suppl 5: 4–9, 2004.
277. Vaupel P, Hockel M, and Mayer A. Detection and characterization of tumor hypoxia using pO2 histography. *Antioxid Redox Signal* 9: 1221–1235, 2007.
278. Vaupel P, Mayer A, Briest S, and Hockel M. Oxygenation gain factor: a novel parameter characterizing the association between hemoglobin level and the oxygenation status of breast cancers. *Cancer Res* 63: 7634–7637, 2003.
279. Vaupel P, Schlenger K, Knoop C, and Hockel M. Oxygenation of human tumors: evaluation of tissue oxygen distribution in breast cancers by computerized O2 tension measurements. *Cancer Res* 51: 3316–3322, 1991.
280. Vaupel P, Thews O, and Hoeckel M. Treatment resistance of solid tumors: role of hypoxia and anemia. *Med Oncol* 18: 243–259, 2001.
281. Vergis R, Corbishley CM, Norman AR, Bartlett J, Jhavar S, Borre M, Heeboll S, Horwich A, Huddart R, Khoo V, Eeles R, Cooper C, Sydes M, Dearnaley D, and Parker C. Intrinsic markers of tumour hypoxia and angiogenesis in localised prostate cancer and outcome of radical treatment: a retrospective analysis of two randomised radiotherapy trials and one surgical cohort study. *Lancet Oncol* 9: 342–351, 2008.
282. von Pawel J, von Roemeling R, Gatzemeier U, Boyer M, Elisson LO, Clark P, Talbot D, Rey A, Butler TW, Hirsh V, Olver I, Bergman B, Ayoub J, Richardson G, Dunlop D, Arcenas A, Vescio R, Viallet J, and Treat J. Tirapazamine plus cisplatin versus cisplatin in advanced non-small-cell lung cancer: a report of the international CATAPULT I study group. Cisplatin and Tirapazamine in Subjects with Advanced Previously Untreated Non-Small-Cell Lung Tumors. *J Clin Oncol* 18: 1351–1359, 2000.
283. Vordermark D and Brown JM. Endogenous markers of tumor hypoxia predictors of clinical radiation resistance? *Strahlenther Onkol* 179: 801–811, 2003.
284. Wang J, Foehrenbacher A, Su J, Patel R, Hay MP, Hicks KO, and Wilson WR. The 2-nitroimidazole EF5 is a biomarker for oxidoreductases that activate the bioreductive prodrug CEN-209 under hypoxia. *Clin Cancer Res* 18: 1684–1695, 2012.
285. Wasserman TH, Lee DJ, Cosmatos D, Coleman N, Phillips T, Davis L, Marcial V, and Stetz J. Clinical trials with etanidazole (SR-2508) by the Radiation Therapy Oncology Group (RTOG). *Radiother Oncol* 20 Suppl 1: 129–135, 1991.
286. Weber GF. The cancer biomarker osteopontin: combination with other markers. *Cancer Genomics Proteomics* 8: 263–288, 2011.
287. Wiedenmann N, Hentschel M, Bucher S, Mix M, Adebahr S, Offermann C, Nestle U, Weber W, and Grosu AL. Dynamics of tumor hypoxia in patients undergoing radiochemotherapy for head and neck cancer evaluated with serial 18F-fluoromisonidazole PET. *Int J Radiat Oncol* 78: S703, 2010.
288. Williams BB, Khan N, Zaki B, Hartford A, Ernstoff MS, and Swartz HM. Clinical electron paramagnetic resonance (EPR) oximetry using India ink. *Adv Exp Med Biol* 662: 149–156, 2010.
289. Wilson DF, Lee WM, Makonnen S, Apreleva S, and Vinogradov SA. Oxygen pressures in the interstitial space of skeletal muscle and tumors *in vivo*. *Adv Exp Med Biol* 614: 53–62, 2008.
290. Winkler F, Kozin SV, Tong RT, Chae SS, Booth MF, Garkavtsev I, Xu L, Hicklin DJ, Fukumura D, di Tomaso E, Munn LL, and Jain RK. Kinetics of vascular normalization by VEGFR2 blockade governs brain tumor response to radiation: role of oxygenation, angiopoietin-1, and matrix metalloproteinases. *Cancer Cell* 6: 553–563, 2004.
291. Wolf M, Ferrari M, and Quaresima V. Progress of near-infrared spectroscopy and topography for brain and muscle clinical applications. *J Biomed Opt* 12: 062104, 2007.
292. Woods ML, Koch CJ, and Lord EM. Detection of individual hypoxic cells in multicellular spheroids by flow cytometry using the 2-nitroimidazole, EF5, and monoclonal antibodies. *Int J Radiat Oncol Biol Phys* 34: 93–101, 1996.
293. Wykoff CC, Beasley NJ, Watson PH, Turner KJ, Pastorek J, Sibtain A, Wilson GD, Turley H, Talks KL, Maxwell PH, Pugh CW, Ratcliffe PJ, and Harris AL. Hypoxia-inducible expression of tumor-associated carbonic anhydrases. *Cancer Res* 60: 7075–7083, 2000.
294. Xia Y, Choi HK, and Lee K. Recent advances in hypoxia-inducible factor (HIF)-1 inhibitors. *Eur J Med Chem* 49: 24–40, 2012.
295. Yasui H, Matsumoto S, Devasahayam N, Munasinghe JP, Choudhuri R, Saito K, Subramanian S, Mitchell JB, and Krishna MC. Low-field magnetic resonance imaging to visualize chronic and cycling hypoxia in tumor-bearing mice. *Cancer Res* 70: 6427–6436, 2010.
296. Zhong H, Chiles K, Feldser D, Laughner E, Hanrahan C, Georgescu MM, Simons JW, and Semenza GL. Modulation of hypoxia-inducible factor 1alpha expression by the epidermal growth factor/phosphatidylinositol 3-kinase/PTEN/AKT/FRAP pathway in human prostate cancer cells: implications for tumor angiogenesis and therapeutics. *Cancer Res* 60: 1541–1545, 2000.
297. Zhong H, De Marzo AM, Laughner E, Lim M, Hilton DA, Zagzag D, Buechler P, Isaacs WB, Semenza GL, and Simons JW. Overexpression of hypoxia-inducible factor 1alpha in common human cancers and their metastases. *Cancer Res* 59: 5830–5835, 1999.
298. Zhu Y, Denhardt DT, Cao H, Sutphin PD, Koong AC, Giaccia AJ, and Le QT. Hypoxia upregulates osteopontin expression in NIH-3T3 cells via a Ras-activated enhancer. *Oncogene* 24: 6555–6563, 2005.
299. Ziemer LS, Evans SM, Kachur AV, Shuman AL, Cardi CA, Jenkins WT, Karp JS, Alavi A, Dolbier WR, Jr., and Koch CJ. Noninvasive imaging of tumor hypoxia in rats

using the 2-nitroimidazole 18F-EF5. *Eur J Nucl Med Mol Imaging* 30: 259–266, 2003.
300. Ziemer LS, Koch CJ, Maity A, Magarelli DP, Horan AM, and Evans SM. Hypoxia and VEGF mRNA expression in human tumors. *Neoplasia* 3: 500–508, 2001.
301. Ziemer LS, Lee WM, Vinogradov SA, Sehgal C, and Wilson DF. Oxygen distribution in murine tumors: characterization using oxygen-dependent quenching of phosphorescence. *J Appl Physiol* 98: 1503–1510, 2005.
302. Zimny M, Gagel B, DiMartino E, Hamacher K, Coenen HH, Westhofen M, Eble M, Buell U, and Reinartz P. FDG—a marker of tumour hypoxia? A comparison with [18F]fluoromisonidazole and pO2-polarography in metastatic head and neck cancer. *Eur J Nucl Med Mol Imaging* 33: 1426–1431, 2006.
303. Zips D, Zophel K, Abolmaali N, Perrin R, Abramyuk A, Haase R, Appold S, Steinbach J, Kotzerke J, and Baumann M. Exploratory prospective trial of hypoxia-specific PET imaging during radiochemotherapy in patients with locally advanced head-and-neck cancer. *Radiother Oncol* 105: 21–28, 2012.

Address correspondence to:
Dr. Hartmuth C. Kolb
Siemens Molecular Imaging, Inc.
6140 Bristol Parkway
Culver City, CA 90230

E-mail: hckolb@me.com

Date of first submission to ARS Central, April 16, 2013; date of final revised submission, January 30, 2014; date of acceptance, February 8, 2014.

Abbreviations Used

AKT = protein kinase B
AR = accelerated radiotherapy
ARCON = accelerated radiotherapy with carbogen and nicotinamide
bFGF = basic fibroblast growth factor
BOLD = blood oxygen level dependent
CA-IX = carbonic anhydrase IX
CBP/p300 = CREB-binding protein/E1A binding protein p300
CDS = contrast-enhanced color duplex sonography
CSC = cancer stem cell
CT = computed tomography
C-TAD = C-terminal activation domain
Cu-ATSM = copper (II) (diacetyl-bis (N4-methylthiosemicarbazone))
DAHANCA = Danish head and neck cancer group
DCE = dynamic contrast enhanced
DFS = disease-free survival
DSD = disease-specific death
DSM = disease-specific mortality
DSS = disease-specific survival
DM = distant metastasis
DPBN = dose painting by numbers
EF5 = pentafluorinated etanidazole
EPR = electron paramagnetic resonance
ERK = extracellular signal-regulated kinase
Fb = perfusion
^{18}F-EF1 = monofluorinated etanidazole
^{18}F-EF3 = trifluorinated etanidazole
^{18}F-EF5 = pentafluorinated etanidazole
^{18}F-FAZA = ^{18}F-fluoroazomycinarabinofuranoside
^{18}F-FDG = ^{18}F-fluorodeoxyglucose
^{18}F-FENI = 1-(2-[^{18}F]fluoro-1-[hydroxymethyl] ethoxy)methyl-2-nitroimidazole
^{18}F-FETA = ^{18}F-fluoroetanidazole
^{18}F-FETNIM = ^{18}F-fluoroerythronidazole
^{18}F-FMISO = ^{18}F-fluoromisonidazole
FFS = failure-free survival
FH = fumarate hydratase
FIH-1 = factor inhibiting HIF1
^{18}F-HX4 = ^{18}F-flortanidazole
FSa = fibrosarcoma
Gd = gadolinium
Gd-DTPA = gadolinium-diethylenetriaminepentaacetic acid
GI = gastrointestinal
GLUT-1 = glucose transporter 1
Gy = gray
H&NC = head and neck cancer
HR = hazard ratio
Hb = hemoglobin concentration
HbO_2 = oxy-hemoglobin
HIF = hypoxia-inducible factor
HIF-1α = hypoxia-inducible factor 1α
HIF-1β = hypoxia-inducible factor-1β
HP = hypoxic fraction
HPV = human papillomavirus
HRE = HIF-responsive element
HSV = hypoxia subvolume
IHC = immunohistochemistry
IMRT = intensity-modulated radiation therapy
K_{trans} = transfer coefficient
LOX = lysyl oxidase
LRC = locoregional control
LRF = locoregional failure
LRFF = locoregional failure-free
LRTF = locoregional tumor failure
MAPK = mitogen-activated protein kinases
MEK = MAPK/ERK kinase
MISO = misonidazole
MMP = matrix metalloproteinase
MRI = magnetic resonance imaging
MRS = magnetic resonance spectroscopy
mTOR = mammalian target of rapamycin
NF-kB = nuclear factor kappa-light-chain-enhancer of activated B cells
NIRS = near-infrared spectroscopy
NM = nimorazole
NPV = negative predictive value
NSCLC = nonsmall-cell lung cancer
N-TAD = N-terminal activation domain
OD = overall death
OMRI = Overhauser-enhanced MRI
OPN = osteopontin
OR = odds ratio
OS = overall survival
p53 = tumor protein 53
PALI = photoacoustic lifetime imaging
PAT = photoacoustic tomography

Abbreviations Used (Cont.)

PET = positron emission tomography
PFS = progression free survival
PHD = prolyl hydroxylase domain containing protein
PI3K = phosphoinositide 3 kinase
PIMO = pimonidazole
PL = placebo
pO_2 = oxygen partial pressure
PPV = positive predictive value
PS = blood volume
PSA = prostate-specific antigen
PTEN = phosphatase and tensin homolog
R = radiation
R+C = radiation plus chemotherapy
RAE = ras-activated enhancer
Raf = serine/threonin-specific protein kinase
RC = regional control
ROS = reactive oxygen species
RR = relative risk
RSI = relative signal intensity
RT = radiotherapy
SDH = succinate dehydrogenase
SI-I = signal increase over baseline
SI-I/s = slope of the time intensity curve
SNAIL1 = snail family zinc finger 1
SO_2 = oxygen saturation
STAT3 = signal transducer and activator of transcription 3
STS = soft tissue sarcomas
SUV = standard uptake value
Sv = sievert
T_1 = spin lattice relaxation time
T_2 = spin-spin relaxation time
TCP = tumor-control probability
T:B = tumor to background
T:M = tumor to muscle
TPZ = tirapazamine
TTV = total tumor volume
TWIST = class A basic helix-loop-helix protein 38
Tx = treatment
uniDE = uniform dose estimates
VEGF = vascular endothelial growth factor
VEGFA = vascular endothelial growth factor A
VEGFR = vascular endothelial growth factor receptor
VHL = von Hippel-Lindau
Ub = ubiquitylation
w/wo S = with or without surgery